

# Light Water Reactor Sustainability Program

## Interdigital Capacitance Local Non-Destructive Examination of Nuclear Power Plant Cable for Aging Management Programs



May 2018

U.S. Department of Energy

Office of Nuclear Energy

#### **DISCLAIMER**

This information was prepared as an account of work sponsored by an agency of the U.S. Government. Neither the U.S. Government nor any agency thereof, nor any of their employees, makes any warranty, expressed or implied, or assumes any legal liability or responsibility for the accuracy, completeness, or usefulness, of any information, apparatus, product, or process disclosed, or represents that its use would not infringe privately owned rights. References herein to any specific commercial product, process, or service by trade name, trade mark, manufacturer, or otherwise, does not necessarily constitute or imply its endorsement, recommendation, or favoring by the U.S. Government or any agency thereof. The views and opinions of authors expressed herein do not necessarily state or reflect those of the U.S. Government or any agency thereof.

# **Interdigital Capacitance Local Non-Destructive Examination of Nuclear Power Plant Cable for Aging Management Programs**

**Authors: S.W. Glass<sup>1</sup>, L.S. Fifield<sup>1</sup>, N. Bowler<sup>2</sup>,  
A. Sriraman<sup>2</sup>, W.C. Palmer<sup>2</sup>**

**<sup>1</sup>Pacific Northwest National Laboratory**

**<sup>2</sup>Iowa State University**

**May 2018**

**Prepared for the  
U.S. Department of Energy  
Office of Nuclear Energy**


## Light Water Reactor Sustainability Program

# Interdigital Capacitance Local Non-Destructive Examination of Nuclear Power Plant Cable for Aging Management Programs

PNNL-27546

May 18, 2018

Approved by:

  
\_\_\_\_\_  
Steve N. Schlahta  
Director, Nuclear Science Project Management Office

\_\_\_\_\_  
May 18, 2018  
Date

## SUMMARY

This Pacific Northwest National Laboratory milestone report describes progress to date on the investigation of non-destructive test methods focusing on local cable insulation and jacket testing using an interdigital capacitance (IDC) approach. Earlier studies have assessed a number of non-destructive examination (NDE) methods for bulk, distributed, and local cable tests. A typical test strategy is to perform bulk assessments of the cable response using dielectric spectroscopy,  $\tan \delta$ , or partial discharge followed by distributed tests like time domain reflectometry or frequency domain reflectometry to identify the most likely defect location followed by a local test that can include visual inspection, indenter modulus (IM) tests, or Fourier transform infrared spectroscopy (FTIR) or near infrared spectroscopy (FTNIR). If a cable is covered with an overlaying jacket, the jacket material is likely to be more severely degraded than the underlying insulation. None of the above local test approaches can be used to evaluate insulation beneath a cable jacket. Since the jacket's function is neither structural nor electrical, a degraded jacket may not have any significance regarding the cable's performance or suitability for service. IDC measurements offer a promising alternative or complement to these local test approaches including the possibility to test insulation beneath an overlaying jacket. This report addresses:

- Relevant literature coupled with a discussion of the theory of IDC measurements.
- Measurement of insulation material permittivity on flat samples with correlation to age-related degradation.
- Model-based assessment of an IDC sensor depth-of-field sensitivity as a function of sensor time gaps and other design factors.
- Correlations of IDC responses to age-related material degradations.
- An assessment of 1) the relative sensitivity of an IDC sensor to jacket and underlying insulation degradation and 2) a two-sensor scheme to determine what the IDC signal would be if the jacket were removed and the sensor were placed directly on the insulation but without removing the jacket.

The most significant conclusions of this work are:

- Material permittivity and corresponding IDC measurements do correlate with age-related material degradation on the EPR samples examined. IDC could be developed as a viable field test for local cable condition assessments as an alternate or complementary local measurement such as IM or FTIR/FTNIR.
- The IDC measurement can assess the condition of underlying insulation through an outer jacket material. This ability to assess material condition through the jacket is not possible with other local cable condition non-destructive techniques such as IM or FTIR/FTNIR.

## **ACKNOWLEDGMENTS**

Funding for this work is provided by the U.S. Department of Energy Office of Nuclear Energy's Materials Research Pathway for the Light Water Reactor Sustainability Program under the leadership of Keith Leonard and Tom Rosseel.

Pacific Northwest National Laboratory (PNNL) is a multi-program national laboratory operated for the U.S. Department of Energy by Battelle Memorial Institute.

The work performed by Iowa State University was performed under a subcontract from PNNL.

# CONTENTS

SUMMARY .....	iii
ACKNOWLEDGMENTS .....	iv
CONTENTS.....	v
FIGURES .....	vii
TABLES .....	xi
ACRONYMS AND ABBREVIATIONS .....	xiii
1. OBJECTIVES.....	1
2. INTRODUCTION AND BACKGROUND .....	3
3. CABLE DESIGN, CLASSIFICATION, AND LAYOUT .....	7
4. AGING AND ACCELERATED AGING .....	9
5. IDC THEORY AND LITERATURE REVIEW .....	11
5.1 Principles of Capacitive Testing .....	11
5.2 Permittivity of Polymers .....	12
5.3 Parallel-Plate Capacitor Measurement Setup.....	13
5.4 Interdigital Capacitors for Cable Polymer Monitoring .....	13
5.4.1 Coplanar Capacitive Sensors .....	13
5.4.2 Capacitive Sensors for Cylindrical Surfaces.....	14
5.4.3 Test Setup Considerations.....	14
6. FEM SIMULATIONS.....	17
6.1 Coplanar Interdigital Electrodes .....	17
6.2 Cylindrical Interdigital Electrodes .....	18
6.2.1 Single-Core Cable with Insulation and Jacket .....	18
6.2.2 Single Core Cable with Insulation .....	19
6.3 IDC to Characterize the Behavior of Insulation beneath Jacket .....	23
7. MEASUREMENT FIXTURE.....	27
7.1 Background .....	27
7.2 Fixture Development for NPP Cable .....	27
7.2.1 Fixture Development.....	27
7.2.2 IDC Design for NPP Cable Testing .....	28
8. MEASURED IDC INDICATIONS OF CABLE AGING.....	31
8.1 Flat-Plate Flat Sample Benchmark Measurements .....	31
8.1.1 Sample Preparation .....	31
8.1.2 Measurement Setup.....	34
8.1.3 Results.....	34

8.1.4	Flat-Plate Flat Sample Measurement Discussion.....	45
8.2	IDC Experiments on Jacketed Cable.....	46
8.2.1	Sample Preparation .....	46
8.2.2	Measurement Setup.....	48
8.2.3	Results.....	48
8.2.4	Discussion .....	55
8.2.5	Future Work .....	56
9.	CONCLUSIONS .....	57
10.	REFERENCES .....	58



## FIGURES

Figure 3-1. Configurations of typical cable designs used in NPPs. All components – particularly B, D, E, F, and G are not always present in every construction. ....	7
Figure 3-2. Typical cable layout allows access at control racks and termination junction boxes, but much of the cable is protected within cable trays and conduit thereby limiting access for local inspections. ....	8
Figure 5-1. Parallel capacitor model with dielectric sandwiched between two conductive plates. ....	11
Figure 5-2. Frequency dependence of $\epsilon'$ and $\epsilon''$ for relaxation modes in typical polymers (Bowler and Liu 2015). ....	12
Figure 5-3. Agilent E4980A precision LCR meter and Agilent 16451B test fixture connected to it. ....	13
Figure 5-4. Specific capacitance (a) and loss tangent (b) measured on tri-core, EPR-insulated cable with PVC jacket. Samples were aged thermally at 140°C for the number of hours shown in the legend (Imperatore 2017). ....	16
Figure 6-1. Perspective view of a coplanar, interdigital capacitive sensor showing geometrical parameters $g$ , the separation distance between neighboring digits, and $w$ , the digit width (Huang et al. 2017). ....	17
Figure 6-2. Schematic diagram of the design problem considered by Shao and Bowler (2017). ....	18
Figure 6-3. Sensor sensitivity $S$ as a function of the number of digits, $N$ . Other calculation parameters are given in Table 6-1 and Table 6-2. ....	19
Figure 6-4. Schematic diagram of an interdigital capacitive sensor in contact with EPR-insulated Okoguard® 15 kV Aerial Jumper Cable. ....	19
Figure 6-5. Measured real relative permittivity of Okoguard® EPR-based insulation material used in Okoguard® 15 kV Aerial Jumper Cable. ....	20
Figure 6-6. (left) COMSOL™-simulated IDC capacitance of Okoguard® Aerial Jumper Cable (Table 6-3)-type EPR material with center conductor radius varied and with varying numbers of IDC tines and gaps. (right) linear relationship between gap $g$ (mm) and penetration depth $\delta$ (mm) defined by insulation thickness for which 10% increase in capacitance is observed, as the center conductor radius increases from $r = 0$ (no center conductor). ....	21
Figure 6-7. (upper left) 7-tine, 2 mm gap ( $g$ ) IDC sensor model with voltage distribution field plot cross-section; (upper right) tine spacing $g = 0.5$ mm, (lower left) tine spacing $g = 2$ mm; (lower right) tine spacing $g = 5$ mm. ....	21
Figure 6-8. COMSOL™ calculation of sensitivity of a 7-tine IDC with varying $w$ and $g$ . ....	22
Figure 6-9. Output capacitance of the sensor calculated using AC/DC packages of COMSOL™ for digit gaps of 1, 2, 3, and 4 mm. The number of digits $N = 11$ , the width of the digits $w = 1$ mm, and the sensor length along the axial direction of the cable is 25 mm. Other sensor parameters are given in Table 6-2. Some parameters of the cable are listed in Table 6-3 and the insulation real relative permittivity as a function of frequency is plotted in Figure 6-5. ....	22
Figure 6-10. Okoguard® - Okolon® TS-CPE type MV-90 2.4kV Nonshielded power cable. ....	23

Figure 6-11. Seven (7) tine IDC model on jacketed insulation; conductor radius = 2.3 mm, insulation radius = 12 mm, jacket radius = 14 mm, $t_1 = 0.0178$ mm, substrate relative permittivity = 2.1, $t_2 = 0.0254$ mm, $w = 1.2$ mm, $g = 0.5, 2, \text{ and } 5$ mm, insulation relative permittivity = 2.48, 3.1, and 3.72, jacket relative permittivity = 2.8, 3.5, and 4.2, central conductor and sensor electrodes are copper. ....	24
Figure 6-12. Simulated IDC capacitance as insulation permittivity is varied by $\pm 10$ and 2% and jacket permittivity is varied by $\pm 20\%$ for narrow, medium, and wide gap-tined IDC sensors. ....	25
Figure 6-13. (Left) Simulated IDC measurement on jacket surface for 5 and 0.5 mm gap (Y axis) plus $C'$ for 5 different values of $C_{virt}$ where $C_{virt}$ is the virtual capacitance that would be measured on the insulation if there were no jacket present. (Right) Expanded $C'$ estimates of $C_{virt}$ based on two-variable regression using inputs from jacket measurement simulations. ....	25
Figure 7-1. Photograph of IDC described in Sheldon and Bowler (2014b). The IDC accommodates wires with diameter up to approximately 3 mm. IDC particulars: $N = 14$ , $w = 0.1$ mm, $g = 0.3$ mm, and $l = 25$ mm. ....	27
Figure 7-2. Clamp sensor setup with Agilent E4980A Precision LCR Meter, acrylic sample holder, printed interdigital capacitor electrodes, and SMA connector. Inset: (a) capacitor electrodes, two sizes; and (b) clamp setup with Okoguard® Aerial Jumper Cable sample in position. ....	28
Figure 7-3. Sensor designs 1, 2, and 3, from Table 7-1, in two lengths each (25.4 mm and 38.1 mm) laid out for printed circuit fabrication. ....	30
Figure 8-1. EPR samples aged at $140^\circ\text{C}$ in the absence of CPE. ....	31
Figure 8-2. EPR samples aged at $140^\circ\text{C}$ in the presence of CPE. ....	32
Figure 8-3. Measured mean thickness values of pink EPR samples shown in Figure 8-1. Error bars represent the standard deviation of ten measured values. ....	32
Figure 8-4. Measured mean thickness values of blackened EPR samples shown in Figure 8-2. Error bars represent the standard deviation of ten measured values. Note, the sample aged for 14 days exhibited greater curvature than others. ....	33
Figure 8-5. Measured mean thickness values of CPE samples. Error bars represent the standard deviation of ten measured values. ....	33
Figure 8-6. Mechanical measurements on witness samples that were aged under identical conditions as the IDC tested samples shown for reference. ....	34
Figure 8-7. Measured mean electrode separation during capacitance measurements on samples shown in Figure 8-1 (absence of CPE). Error bars represent the standard deviation of three measured values. ....	35
Figure 8-8. Measured capacitance of samples shown in Figure 8-1, as a function of frequency. Error bars represent the standard deviation of six measured values. ....	35
Figure 8-9. Inferred relative permittivity of EPR samples shown in Figure 8-1, as a function of frequency. Error bars represent the standard deviation of six measured values. ....	36
Figure 8-10. Inferred relative permittivity of EPR samples shown in Figure 8-1, at select frequencies, as a function of aging time at $140^\circ\text{C}$ . Error bars represent the standard deviation of six measured values. ....	36

Figure 8-11. Inferred relative permittivity of EPR samples shown in Figure 8-1, at select frequencies, versus EAB.....	37
Figure 8-12. Measured dissipation factor of EPR samples shown in Figure 8-1, as a function of frequency. Error bars represent the standard deviation of four measured values. The discontinuity at $10^5$ Hz corresponds to internal switching in the LCR meter circuitry.....	37
Figure 8-13. Measured dissipation factor of EPR samples shown in Figure 8-1, at select frequencies, as a function of aging time at $140^\circ\text{C}$ . Error bars (smaller than the symbol size) represent the standard deviation ( $\sim 10^{-5}$ ) of six measured values.....	38
Figure 8-14. Measured mean electrode separation during capacitance measurements on blackened (in presence of CPE) EPR samples shown in Figure 8-2. Error bars represent the standard deviation of four measured values. Note, the sample aged for >14 days exhibited greater curvature than others. ....	39
Figure 8-15. Measured capacitance of blackened (in presence of CPE) EPR samples shown in Figure 8-2, as a function of frequency. Error bars represent the standard deviation of four measured values. ....	39
Figure 8-16. Inferred relative permittivity of blackened (in presence of CPE) EPR samples shown in Figure 8-2, as a function of frequency. Error bars represent the standard deviation of four measured values. ....	40
Figure 8-17. Inferred relative permittivity of blackened (in presence of CPE) EPR samples shown in Figure 8-2, at select frequencies, as a function of aging time at $140^\circ\text{C}$ . Error bars represent the standard deviation of four measured values. ....	40
Figure 8-18. Inferred relative permittivity of blackened (in presence of CPE) EPR samples shown in Figure 8-2, at select frequencies, versus EAB.....	41
Figure 8-19. Measured dissipation factor of blackened (in presence of CPE) EPR samples shown in Figure 8-2, as a function of frequency. Error bars represent the standard deviation of four measured values. The discontinuity at $10^5$ Hz corresponds to internal switching in the LCR meter circuitry. ....	41
Figure 8-20. Measured dissipation factor of blackened (in presence of CPE) EPR samples shown in Figure 8-2, at select frequencies, as a function of aging time at $140^\circ\text{C}$ . Error bars (smaller than the symbol size) represent the standard deviation ( $\sim 10^{-5}$ ) of four measured values.....	42
Figure 8-21. Measured mean electrode separation during capacitance measurements on CPE samples whose direct thickness measurements are plotted in Figure 8-5. Error bars represent the standard deviation of six measured values.....	42
Figure 8-22. Measured capacitance of CPE samples aged at $165^\circ\text{C}$ , as a function of frequency. Error bars represent the standard deviation of six measured values.....	43
Figure 8-23. Inferred relative permittivity of CPE samples aged at $165^\circ\text{C}$ , as a function of frequency. Error bars represent the standard deviation of six measured values. ....	43
Figure 8-24. Inferred relative permittivity of CPE samples aged at $165^\circ\text{C}$ , at select frequencies, as a function of aging time. Error bars represent the standard deviation of six measured values.....	44

Figure 8-25. Measured dissipation factor of CPE samples aged at 165°C, as a function of frequency. Error bars represent the standard deviation of four measured values. The discontinuity at 10 <sup>5</sup> Hz corresponds to internal switching in the LCR meter circuitry. ....	44
Figure 8-26. Measured dissipation factor of CPE samples aged at 165°C, at select frequencies, as a function of aging time. Error bars (smaller than the symbol size) represent the standard deviation (~10 <sup>-5</sup> ) of six measured values.....	45
Figure 8-27. EPR/TS-CPE cable samples aged at 140°C for various durations up to 63 d in 7 d increments. The sample ends were sealed with foil during aging. ....	46
Figure 8-28. Measured mean outer diameter values of samples shown in Figure 8-27. Error bars represent the standard deviation of ten measured values.....	46
Figure 8-29. EPR/TS-CPE cable samples aged at 140°C for up to 35 d in 7 d increments. After aging, part of the jacket was removed. ....	47
Figure 8-30. Measured mean outer diameter values (jacketed region) of samples shown in Figure 8-29. Error bars represent the standard deviation of ten measured values. ....	47
Figure 8-31. Measured mean diameter values (non-jacketed region) of samples shown in Figure 8-29. Error bars represent the standard deviation of ten measured values. ....	48
Figure 8-32. Measured capacitance of the CPE jacket of Okoguard® -Okolon® TS-CPE Type MV-90 2.4kV Nonshielded Power Cable samples, as a function of frequency.....	49
Figure 8-33. Inferred relative permittivity of the CPE jacket of Okoguard® -Okolon® TS-CPE Type MV-90 2.4kV Nonshielded Power Cable samples, as a function of frequency. ....	49
Figure 8-34. Inferred relative permittivity of CPE jacket of Okoguard® -Okolon® TS-CPE Type MV-90 2.4kV Nonshielded Power Cable samples normalized with respect to data for the pristine sample, at select frequencies, as a function of aging time.....	50
Figure 8-35. Dissipation factor of the CPE jacket of Okoguard® -Okolon® TS-CPE Type MV-90 2.4kV Nonshielded Power Cable samples, as a function of frequency. ....	50
Figure 8-36. Dissipation factor of CPE jacket of Okoguard® -Okolon® TS-CPE Type MV-90 2.4kV Nonshielded Power Cable samples normalized with respect to data for the pristine sample, at select frequencies, as a function of aging time. ....	51
Figure 8-37. Measured capacitance of the CPE jacket of Okoguard® -Okolon® TS-CPE Type MV-90 2.4kV Nonshielded Power Cable samples, as a function of frequency.....	52
Figure 8-38. Inferred relative permittivity of the CPE jacket of Okoguard® -Okolon® TS-CPE Type MV-90 2.4kV Nonshielded Power Cable samples, as a function of frequency. ....	52
Figure 8-39. Inferred relative permittivity of CPE jacket of Okoguard® -Okolon® TS-CPE Type MV-90 2.4kV Nonshielded Power Cable samples normalized with respect to data for the pristine sample, at select frequencies, as a function of aging time.....	53
Figure 8-40. Measured capacitance of Okoguard® -Okolon® TS-CPE Type MV-90 2.4kV Nonshielded Power Cable samples insulation, as a function of frequency. ....	53
Figure 8-41. Inferred relative permittivity of the EPR insulation of Okoguard® -Okolon® TS-CPE Type MV-90 2.4kV Nonshielded Power Cable samples, as a function of frequency. ....	54

Figure 8-42. Inferred relative permittivity of EPR insulation of Okoguard® -Okolon® TS-CPE Type MV-90 2.4kV Nonshielded Power Cable samples normalized with respect to data for the pristine sample, at select frequencies, as a function of aging time. ....	54
Figure 8-43. % change of dissipation factor (D) and relative permittivity and similarly capacitance (C/P) for EPR and CPE material of this study between initial and extreme aging points for the materials. ....	55

## TABLES

Table 3-1. A Sort of Insulation Material for U.S. NPPs (from EPRI 1994) .....	7
Table 3-2. Categories of Cable Grouping .....	8
Table 6-1. Cable parameters used in the simulations whose results are presented in Figure 6-2 .....	18
Table 6-2. Fixed parameters of the sensor for the simulations whose results are presented in Figure 6-3.....	18
Table 6-3. Cable parameters used in the simulations whose results are presented in Figure 6-6 .....	20
Table 6-4. Design parameters for Okoguard® - Okolon® TS-CPE Type MV-90 2.4kV Nonshielded Power Cable.....	24
Table 7-1. Designed parameters of sensors for monitoring Okoguard®-Okolon® TS-CPE Type MV-90 2.4kV Nonshielded Power Cable. ....	29



## ACRONYMS AND ABBREVIATIONS

AMP	aging management program
C	capacitance
CM	condition monitoring
CPE	chlorinated polyethylene
CSPE	chlorosulphonated polyethylene (Hypalon)
DBE	design-basis events
DOE	U.S. Department of Energy
EAB	elongation-at-break
EPR	ethylene propylene rubber
EPRI	Electric Power Research Institute
ETFE	Ethylene - tetrafluoroethylene copolymer
F	Farad - SI unit of capacitance
$f$	frequency
FEM	finite-element model or modeling
FTIR	Fourier Transform Infrared Spectroscopy
FTNIR	Fourier Transform Near Infrared Spectroscopy
$g$	IDC electrode gap
Gy	Gray (unit measure of ionizing radiation)
IDC	interdigital capacitance
IM	indenter modulus
LCR	inductance-capacitance-resistance
LOCA	loss-of-coolant accident
$N$	Number of IDC digits
NDE	non-destructive evaluation
NPP	nuclear power plant
NRC	U.S. Nuclear Regulatory Commission
PNNL	Pacific Northwest National Laboratory
PVC	polyvinyl chloride
$S$	sensitivity
SLR	subsequent license renewal
SMA	SubMiniature version A
$w$	IDC electrode width
XLPE	cross-linked polyethylene
$\delta$	penetration depth
$\varepsilon$	complex permittivity

# **1. OBJECTIVES**

This Pacific Northwest National Laboratory (PNNL) milestone report describes progress to-date on the investigation of non-destructive test methods focusing particularly on interdigital capacitance (IDC) testing of cable jackets and insulation that provide key indicators of cable aging and degradation.

The overall objectives of this program are to develop the technical basis for assessing existing and emerging non-destructive evaluation (NDE) methods for cable insulation aging and degradation in nuclear power plants (NPPs). In July 2012, a workshop (Simmons et al. 2012) was held to lay the groundwork for a research and development roadmap to address aging cable management in NPPs, including methods for nondestructively measuring the condition of aging cables. This roadmap addresses the overall gaps that were identified at that workshop using a phased approach and covering three areas:

1. Determination of key indicators of cable aging. This has largely been addressed in earlier reports (Ramuhalli et al. 2015; Simmons et al. 2014; Fifield et al. 2015).
2. Characterize and advance current NDE methods and develop new NDE methods by using insights from the determination of key indicators. This activity was generally addressed by Glass et al. (2015) describing the overall state-of-the-art for both bulk electrical tests and local tests. A more focused report was prepared to address local NDE cable tests (Glass et al. 2016). This separate 2016 report addresses bulk electrical tests.
3. Develop models that use the advances in key indicators and NDE methods to assist in predicting remaining life of cables. Modeling has been and continues to be essential to understand the relevance and aid in interpretation of NDE results. Examples of this include Fifield et al. (2017) and Glass et al. (2017).

This report is submitted in fulfillment of deliverable M3LW-18OR0404022 –Interdigital Capacitance Local Non-Destructive Examination of Nuclear Power Plant Cable for Aging Management Programs.





## 2. INTRODUCTION AND BACKGROUND

As NPPs consider applying for second, or subsequent, license renewal (SLR) to extend their operating period from 60 years to 80 years, it is important to understand how the materials installed in plant systems and components will age during that time and develop aging management programs (AMPs) to assure continued safe operation under normal and design-basis events (DBE).

Degradation of the cable jacket, electrical insulation, and other cable components of installed cables within NPPs is known to occur as a function of age, temperature, radiation, and other environmental factors. Although system tests verify cable function under normal loads, concern remains over cable performance under exceptional loads associated with DBEs. The cable's ability to perform safely over the initial 40-year planned and licensed life has generally been demonstrated and there have been very few age-related cable failures (EPRI 2015; Mantey 2015). With greater than 1000 km of power, control, instrumentation, and other cables typically found in an NPP, replacing all the cables would be a severe cost burden. License renewal to 60 years and subsequent license renewal to 80 years, therefore, requires a cable AMP in accordance with regulatory guidance (NRC 2012) to justify cable performance under normal operation as well as accident conditions.

The aging of insulation and jacketing material in electrical and instrumentation cables is considered to be one of the factors that may limit the ability of light water reactors to continue operations beyond their licensed period (up to 60 and 80 years, depending on the specific plant). The focus for cable SLR qualification is the continued ability to withstand a DBE. Aging and subsequent degradation of insulation will impair the ability of cables to perform their function under all environmental conditions. Methods to nondestructively assess the level of aging and degradation in cable insulation and jacketing materials are therefore needed. In addition to providing an estimate of the level of aging and degradation, such condition assessment or condition monitoring (CM) methods for cable insulation can also provide critical inputs into condition-based qualification approaches, assess corresponding remaining useful qualified life of the cable, and ensure that the cables do not exceed a qualified level of degradation.

The U.S. Nuclear Regulatory Commission (NRC) commissioned the U.S. Department of Energy (DOE) to perform a detailed analysis of NPP material aging in this context. The results of this analysis, the Expanded Materials Degradation Assessment, have been published in five volumes. The first provides a summary of the analysis process and results. The second through fourth volumes focus on the aging of individual systems of concern including core internals and piping systems, reactor pressure vessels, and concrete and civil structures. The fifth volume (NRC 2013) considers the aging of cable and cable systems. It identifies age-related degradation scenarios that could be important to the use of NPP electrical cable components over an 80-year timeframe and identifies issues for which enhanced aging management guidance may be warranted.

In July 2012, a workshop (Simmons et al. 2012) was held to lay the groundwork for a research and development roadmap to address aging cable management in NPPs, including methods for nondestructively measuring the condition of aging cables. This workshop brought together subject matter experts from the NRC, DOE national laboratories, the Electric Power Research Institute (EPRI), universities, and cable manufacturers and inspectors. The workshop focused on identifying key research needs in the NDE of aging cable insulation in NPPs and the associated technical gaps. Identifying measurable quantities due to changes in chemical structure of insulating materials that would be a precursor to eventual failure of an aging cable, and the current state-of-the-art in NDE methods that could be applied to estimate the remaining life of the cable, were determined to be key to addressing the aging management challenge for nuclear cables. The development of new NDE methods or development of new measurement techniques using existing NDE methods that target these types of changes is of significant interest. Further, the ability to perform non-destructive tests to determine chemical, physical, mechanical, and electrical properties of the cable jackets and insulation without significant disturbance of the cables and connectors as they lay in situ is essential. This cable research program is sponsored by DOE under the

Light Water Reactor Sustainability program to address knowledge and technique gaps to support the evolution of industry cable AMPs. Cable NDE methods comprise one topic of ongoing coordination and communication efforts on aging NPP cable research between the DOE, NRC, EPRI, and Iowa State University. Coordination of efforts helps to minimize duplication in research and to ensure that prioritized knowledge gaps are addressed.

Acceptance criteria that define the threshold for degradation below which cables may continue to be used are a challenge, because it is impractical to subject each cable system to loss-of-coolant accident (LOCA) or seismic simulation events following 40+ years of service. The report *Initial Acceptance Criteria Concepts and Data for Assessing Longevity of Low-Voltage Cable Insulations and Jackets* (EPRI 2005) develops a basis for acceptance criteria and evaluates the aging profiles for many commonly used cable jackets and polymers. The report describes 50 percent elongation-at-break (EAB) as a conservative practical end-of-life threshold for cables that may be stressed during maintenance or subjected to LOCA exposure. The report also discusses the basis for cautious continued use of cables beyond the 50-percent EAB threshold. EAB measurement inherently compromises the in-service cable use as it is a destructive ex situ test so the challenge is to develop NDE methods that can reasonably be correlated with EAB. Reliable NDE in situ approaches are needed to objectively determine the suitability of installed cables for continued service. A variety of tests are available to assess various aspects of electrical and mechanical cable performance, but none of the available tests are suitable for all cable configurations nor does any single test assess all features of interest. Nevertheless, the complete collection of test possibilities offers a powerful range of tools to assure the integrity of critical cables.

Cable test technologies may generally be divided into:

- Bulk/distributed electrical measurements [resistance or impedance measurements, high voltage withstand tests,  $\tan \delta$  (dissipation factor), time domain reflectometry, frequency domain reflectometry, partial discharge, and other techniques]. These tests are administered in situ from the cable termination ends and test the full length of the cable. Normally both ends of the cable are isolated from the supply or from the indicating instrument and from the motor, actuator, or sensor to perform the test. Bulk tests (withstand,  $\tan \delta$ , partial discharge) simply provide an overall indication of the cable's impedance or leakage current. Distributed tests (TDR, FDR) also provide information regarding the location of cable conductor or insulation degradation.
- Local insulation measurements include visual or optical inspection, indenter, infrared, or near infrared spectral measurement, and IDC. Local tests may be impractical to apply if cables are inaccessible because they are buried, enclosed in conduit, or require expensive scaffolding to access; however, such local tests can be important to justify continued service or repair rather than replacement. Visual tests provide subjective indications of the cable condition. Indenter tests evaluate mechanical properties of the insulation which are shown to correlate well with EAB (Glass et al. 2016). Fourier transform infrared (FTIR) and Fourier transform near infrared (FTNIR) optical methods show promise as a practical way to quickly test accessible cable insulation or jacket material particularly if there is a calibration baseline library of the specific material's aging behavior (Fifield et al. 2017; Glass et al. 2016). None of these tests however address electrical characteristics of interest. Moreover, neither indenter, visual, FTIR nor FTNIR support interrogation of insulation covered by an overlaying jacket. The primary promising technology for local testing of electrical characteristics of the insulation is the IDC testing that is the primary subject of this report.
- Laboratory sample tests – Virtually all local and bulk and distributed electrical NDE tests may be applied in a laboratory environment if the cable can be moved to that environment; however, the laboratory environment offers some additional test possibilities that are not practical to perform on in situ cables. In order for these tests to aid the utilities in evaluating in-service cables, these tests require samples from surrogate cables that may have been left in place but are no longer in service (rare) or a section of the actual in-service cable may be sampled, followed by a splice or termination repair. Such tests include EAB, oxidation induction time and temperature (evaluates loss of anti-oxidant

compounds), insulation density measurement, temperature at maximum rate of weight loss and activation energy measurements using a thermogravimetric analyzer, swelling ratio and gel fraction measurements, atomic force microscope for micro-scale viscoelastic properties, nuclear magnetic resonance, and FTIR. These tests are mentioned but are not addressed further in this report. Such tests can be useful to characterize general plant cable aging behavior, but their destructive nature and impracticality for field application make them unsuitable as methods for justifying continued use of in-service cables.

Cable test motivations may be grouped as follows:

- Factory in-process and post manufacture acceptance test. These tests are designed to confirm the quality of the manufactured cable and catch any quality issues prior to releasing the cable to the ultimate customer.
- Post-installation tests that prove the cable is fit for service and has not been damaged during installation.
- CM associated with the cable AMP. The primary focus here is to determine if the cable is currently acceptable and is expected to continue to be acceptable for a period of time. Usually the units or increments of time of interest are the number of operating/refueling cycle periods (typically 2 years).
- Troubleshooting tests to determine the nature and location of degradation and to assess whether repair is possible or if replacement is necessary.
- Failure and forensic assessments to identify reasons for failure or degradation and to recommend mitigation or corrective action on similar applications and circuits.



### 3. CABLE DESIGN, CLASSIFICATION, AND LAYOUT

NPP cable designs typically include a conductor to carry power, instrumentation or control signals, and an insulating cover layer to isolate the conductor (Figure 3-1). They may include more than one insulated conductor within a bundle. Other components typically associated with the overall cable design include a semiconductor screen, a shield over each conductor, and/or over all conductors, binder tape, and a jacket. While the insulation provides electrical isolation, in jacketed cable configurations the jacket mainly serves to provide mechanical protection during installation and sometimes fire or moisture resistance depending on the cable construction. The materials for cable components are chosen based on the use environment, such as wet, dry, radiation, or sunlit conditions, and the application such as for power or instrumentation. Conductors, made from copper, aluminum, or tin, are relatively insensitive to age and related damage. Cross-linked polyethylene (XLPE) and ethylene-propylene rubber (EPR) compose the vast majority of insulation materials in the nuclear industry, with silicone rubber also being of interest. The most significant jacket materials are chlorosulphonated polyethylene (CSPE – also known as Hypalon® [registered trademark of DuPont]), chlorinated polyethylene (CPE), polychloroprene, and polyvinyl chloride (PVC). While installed cables with intact insulation may well be able to continue to provide safe operation with degraded jacket material, the tendency of jacketing materials to degrade more readily than insulation materials enables their use as lead indicators for local stress prior to insulation degradation and failure.

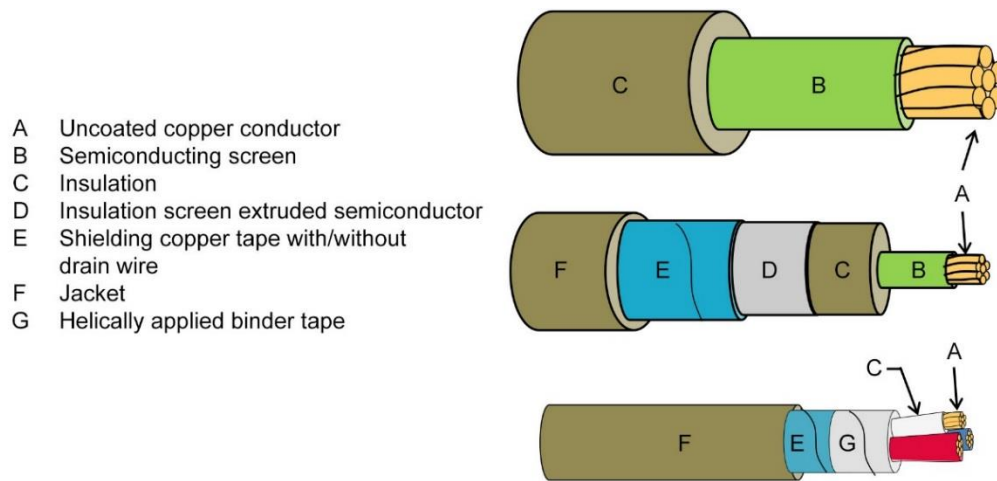


Figure 3-1. Configurations of typical cable designs used in NPPs. All components – particularly B, D, E, F, and G are not always present in every construction.

A survey performed by EPRI in the mid-1990s established a representative distribution of insulation materials within the U.S. nuclear fleet (EPRI 1994) (see Table 3-1). Note that over 70 percent of the materials are XLPE or EPR.

Table 3-1. A Sort of Insulation Material for U.S. NPPs (from EPRI 1994)

Insulation Material	Database Entries	Percent of Total (%)	Insulation Material	Database Entries	Percent of Total (%)
XLPE	439	36	ETFE	39	3
EPR	434	36	Flame retardant EPR	36	3
Silicone Rubber	63	5	CSPE	28	2
Kerite®	61	5	Butyl rubber	20	2
Polyethylene	52	5	All others		Each ≤ 1%

Numerous standards have been developed over the years to group and categorize cables based on application, voltage, environment, and basic design type (Table 3-2). Exactly what grouping is used depends on the application but for cable aging management, generally the nuclear industry has focused on medium- and low-voltage cables. Low-voltage cables constitute the majority of NPP cables but many safety-critical cables exposed to moisture are medium-voltage cables. Most plants have a rigorous program to test and verify performance of safety-critical medium-voltage cables. Cable CM programs are encouraged through NRC's Draft Regulatory Guide 1240 (NRC 2010) with particular emphasis on medium-voltage cables. Examples are cited of cable failures particularly for wet-environment cables. Although this is not currently a required program, it is encouraged by the NRC *to promote discussion between staff and licensees when a facility's operating experience indicates cable failure or degraded cable performance as a causal factor. The NRC staff will use this guidance to evaluate compliance with the Maintenance Rule.*

Table 3-2. Categories of Cable Grouping

Application	Voltage	Environment	Design
Power	Low ( $\leq 2$ KV)	Normal operating temperature	Single/multi-conductor
Control	Medium ( $\leq 2$ –46 KV)		Triplex
Instrument	High ( $> 46$ KV)	High temperature	Thermocouple alloys
Thermocouple		Fire/flame retardant	Coaxial
Communication		High radiation	Shielded/unshielded (and shield type – tape, braid, ...)
Specialty Configuration		Submerged – water	Special jacket
Safety Related		Aggressive solvents	Conductor/shield material (copper, tinned copper, aluminum, ...)
Non-Safety Related			Insulation/jacket material (XLPE, EPR, PVC, ...)

Cable layout in typical plants is not designed to facilitate access and inspection of significant portions of the cable lengths. Cable trays and conduits are designed to protect the cables from environmental stresses as well as accidental damage from workers and equipment that may be moving either inside containment, auxiliary buildings, or control buildings. While cable ends are generally accessible at termination boxes and control panels, many cables are grouped together with other cables in trays that do not necessarily follow personnel access pathways, pass-through penetration pipes and conduits that may be buried in concrete, under-ground, or even passing through areas that may be flooded (Figure 3-2).

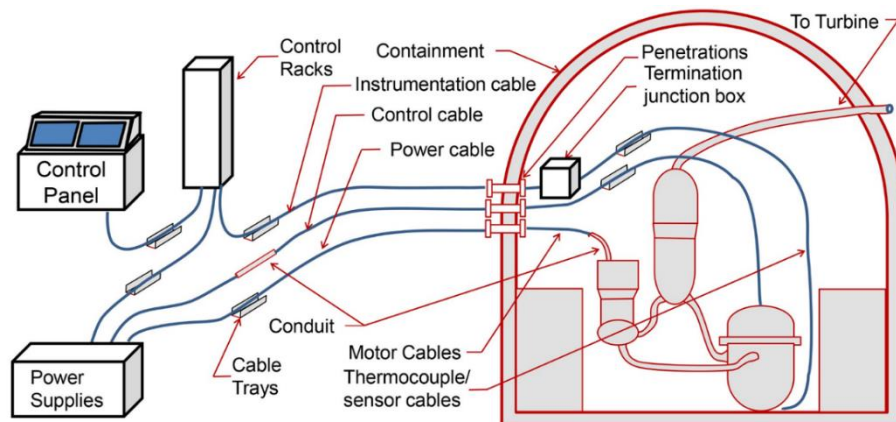


Figure 3-2. Typical cable layout allows access at control racks and termination junction boxes, but much of the cable is protected within cable trays and conduit thereby limiting access for local inspections.

## 4. AGING AND ACCELERATED AGING

Stressors leading to cable degradation can generally be divided into three groups (Lindsay and Benson 2012):

- Environmental: radiation, heat, moisture, chemical, etc.
- Operational: high voltage, electrical transients, ohmic heating, flexing/vibration, mechanical damage, etc.
- Error-induced damage: from inappropriate design/selection for the given environmental or operational stressors above, manufacturing, or maintenance deficiencies.

When CM techniques are being applied to evaluate cable condition, consideration of the stressors can be important to indicate where to look and what to look for. Tests look for changes in the cable material characteristics. These changes can generally be considered as follows:

- Various insulation and jacket polymers (XLPE, EPR, PVC) subject to elevated temperature from ohmic heating of the conductor, radiant or ambient heat acting on the outside of the insulation and jacket, water or chemical attack from the cable exterior, and/or radiation are prone to embrittlement, cracking, decrease in dielectric strength, increased leakage current, reduction in structural integrity, and susceptibility to intrusion of moisture or contaminants.
- PVCs (mostly related to jackets) are also subject to hydrogen chloride evolution and salt formation resulting from wet environments that can reduce dielectric strength and increase leakage currents. Because PVCs are rarely used for insulation, however, this may be only a cosmetic issue limited to the jacket.
- Various insulation and jacket polymers are also subject to wetting and moisture intrusion in the form of “water trees” resulting in decreased dielectric strength and increased leakage currents.
- Copper conductors subjected to wetting may experience corrosion resulting in increased electrical resistance and corresponding ohmic heating that may accentuate the corrosion process.
- Various insulation and jacket polymers are subject to handling, physical contact abuse during installation, maintenance, operation, or testing that may result in crushing, cracking, scuffing, cutting, bending deformation, etc. and may result in visually observed damage, reduced dielectric strength, and increased leakage current.

PNNL (Glass et al. 2015) has developed:

- extensive capabilities for controlled accelerated aging of cable samples
- laboratory measurements of cable and particularly insulation characteristics, and
- a collection of laboratory and in situ techniques that may be applied to cable CM assessment.

The principal concerns for adverse environments experienced by polymer insulated/jacketed electrical cables in the NPPs are elevated temperature, gamma radiation exposure, and the presence of moisture or other chemical environmental stress. Typical NPP temperatures and dose environments allow the cable to operate for 40+ years before material degradation is of sufficient concern to warrant specific tests and repair or replacement if necessary. Because it is not practical to wait 40+ years for suitably aged samples to be available for study, the ability to accelerate aging is essential to the program. A series of aging ovens has been acquired with room to house either racks of samples inside or to support pass-through, intact cables. In addition, PNNL has a Co-60 gamma radiation facility that can subject samples to up to 1 kGy/hr. The facility can also combine the ovens and the radiation test source for combined thermal and radiation aging. The capability to specify both temperature and dose rate during sample preparation enables PNNL to address knowledge gaps in the understanding of degradation from combined exposure including synergistic effects and inverse temperature effects. These facilities have been used to generate the representative aged samples where PNNL and PNNL collaborators have performed verification or demonstration CM measurements.





## 5. IDC THEORY AND LITERATURE REVIEW

### 5.1 Principles of Capacitive Testing

Capacitive sensors are utilized in the area of materials characterization known as *dielectrometry* (Nassr and El-Dakhkhni 2009; Sheldon and Bowler 2014a). The output capacitance of a capacitive sensor placed in the vicinity of a test-material is sensitive to the dielectric properties of that material. Capacitance can be measured using a typical inductance-capacitance-resistance (LCR) meter, connected to a capacitive probe.

Generally familiar is the parallel-plate capacitor configuration with a dielectric wafer sandwiched between charged (+/-Q) conductive plates (Figure 5-1) whose complex capacitance  $C^*$  [F] is given by

$$C^*(f) = \varepsilon^*(f) A/d \quad (5.1)$$

wherein  $\varepsilon^* = \varepsilon' - j\varepsilon''$  [F/m] is the complex permittivity of the material that fills the space between the capacitor plates,  $A$  [m<sup>2</sup>] is the area of one of the two identical capacitor electrodes,  $d$  [m] is the uniform separation between them, and  $f$  [Hz] is frequency. Parallel-plate electrodes are suitable for dielectrometry on flat specimens of uniform thickness that are somewhat thinner than the diameter of the electrodes, and can be accessed on both sides. For other sample shapes, and in the case of samples that can be accessed from only one side, custom capacitive electrodes can be designed according to various considerations (Sheldon and Bowler 2014b; Chen and Bowler 2013; Chen and Bowler 2009) (These design considerations usually involve a trade-off between signal amplitude and measurement sensitivity.

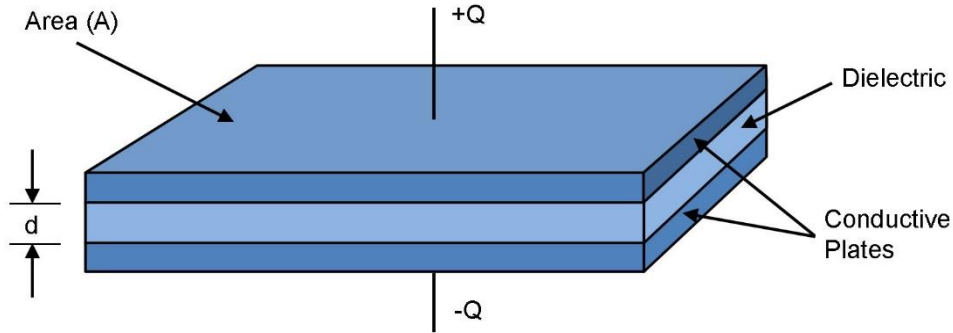


Figure 5-1. Parallel capacitor model with dielectric sandwiched between two conductive plates.

A typical LCR meter measures  $C$  as the real part and  $D$  as the loss factor of the complex capacitance, where

$$C^*(f) = C(f)[1 - jD(f)] \quad (5.2)$$

Thus, for the parallel-plate geometry,  $C = \varepsilon' A/d$  and  $D = \varepsilon''/\varepsilon'$ . A typical LCR meter covers frequency range ~1 Hz to ~1 MHz, although specialized dielectric spectrometers can access ~1 mHz to ~1 GHz (Novocontrol). Permittivity measurements up to potentially hundreds of GHz can be accessed using waveguide approaches, and at even higher frequencies using optical test methods.

## 5.2 Permittivity of Polymers

The permittivity of any material, measured at a particular frequency, likely involves the sum of several types of dipolar contributions. In polymers, the particular contributions depend on the composition of the material and the frequency of the measurement. Dipolar contributions to permittivity may be from dipoles induced by an applied electric field or from dipoles permanently present in the material. All materials exhibit electronic polarization that arises as a consequence of relative displacement of electronic and nuclear charge in the presence of an applied electric field. Since the electron cloud in a hydrocarbon polymer is relatively light and responsive to the presence of an applied electric field, this polarization mechanism persists up to  $\sim 10^{15}$  Hz. Permanent dipole moments in the polymer itself also contribute to the permittivity of the material. These may be associated with side groups attached to the polymer main chain, or with the polymer main chain itself. Those dipole moments associated with the polymer chain tend to become active in their polarization contribution at temperatures above the glass transition temperature  $T_g$  of the polymer, and the observance of this contribution to polarization can indeed be used as a measure of  $T_g$ . Contributions from side groups may be observable at temperatures both above and below  $T_g$ , with relaxation frequency higher than that of any relaxation associated with the polymer main chain. For further information see, for example, (Menczel and Prime 2009, Chapter 6).

Each dipole has associated with it a polarizability,  $\alpha$ , and dipole moment  $p = \alpha E$ . The extent to which each dipole may contribute to the overall polarization of the material depends on the strength of the individual contribution, represented by its polarizability. The polarizability of a dipole is a function of frequency, giving rise to frequency dependence of the permittivity. Each type of contribution has a characteristic relaxation frequency associated with it, above which its contribution to the overall polarization of the material falls off. This behavior is illustrated in Figure 5-2, which shows the frequency dependence of permittivity for a typical polymer. Three relaxations are illustrated—interfacial polarization relaxation that can occur when free charges in a semi-crystalline polymer become trapped at the crystal-amorphous boundary, for example; the alpha relaxation associated with the glass transition mentioned before; and a beta relaxation associated with polarization of a side group. The strength of each relaxation and its frequency depends on the particulars of the material. Notice that each relaxation is characterized by a decline in  $\epsilon'$  and a peak in  $\epsilon''$ . These real and imaginary parts of the same complex number are related mathematically by the Kramers-Kronig relations that are rooted in the causal nature of the relaxation process (Landau and Lifshitz 1960).

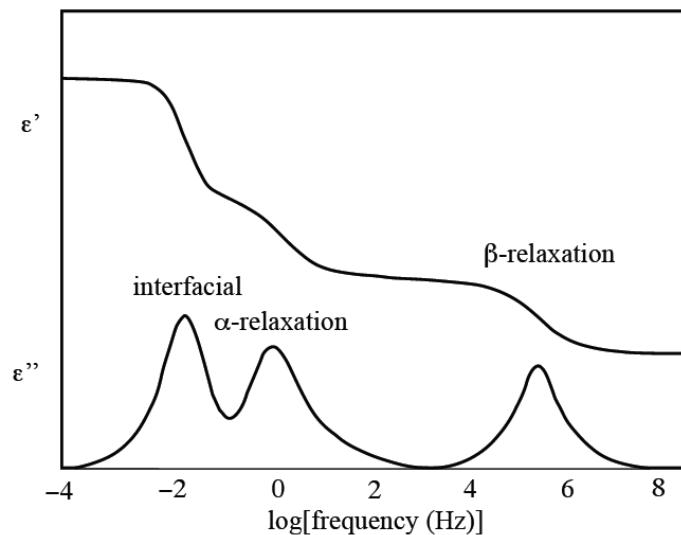


Figure 5-2. Frequency dependence of  $\epsilon'$  and  $\epsilon''$  for relaxation modes in typical polymers (Bowler and Liu 2015).

## 5.3 Parallel-Plate Capacitor Measurement Setup

The parallel-plate capacitor offers a low-uncertainty approach to obtaining dielectric spectra, if flat specimens with uniform thickness are available. As a rule of thumb, uncertainties due to fringing field effects (non-uniform electric fields at the edges of the electrodes) are controlled by maintaining a ratio of greater than ten between the electrode diameter and the sample thickness. Many electrode set-ups also employ guard electrodes to maintain the uniformity of the electric field between the sensing electrodes. Uniformity of the electric field between the electrode plates allows equation (5.1) to be employed in the conversion from measured capacitance to the material property, permittivity.

An Agilent E4980A precision LCR meter, or other spectrometer/impedance analyzer may be employed in measuring capacitance, ( $C^*$ ) and inferring permittivity ( $\epsilon^*$ ). An Agilent 16451B fixture, employing a 56-mm-diameter unguarded electrode and a 5-mm-diameter guarded electrode, may be connected to the LCR meter as shown in Figure 5-3. Examples of data measured using this setup are found in Section 8.1.



Figure 5-3. Agilent E4980A precision LCR meter and Agilent 16451B test fixture connected to it.

## 5.4 Interdigital Capacitors for Cable Polymer Monitoring

### 5.4.1 Coplanar Capacitive Sensors

Early work investigating coplanar capacitive sensors for defect detection in dielectric materials, both at and below the surface, and for surface flaw detection in metals, showed promise and noted the high lift-off sensitivity of capacitive sensors (Shull et al. 1990). Rectangular, coplanar, interdigital dielectrometry sensors, and a semi-analytical model for inferring the permittivity of a dielectric plate from the measured capacitance, were presented (Shay and Zahn 2005). Rectangular coplanar capacitive sensors were also applied to detect water intrusion in composite structures (Nassr et al. 2008) and evanescent field dielectrometry was used to monitor fresco degradation due to moisture and soluble salts (Olmi et al. 2006). Building upon these works, a concentric coplanar capacitive sensor was analyzed for quantitative

dielectrometry, motivated by the need to detect ingressed water or excessive inhomogeneity due to improper repair of modern radome structures (Chen and Bowler 2009; Chen et al. 2011). The concentric coplanar capacitive sensor consists of a charged disc and coplanar annular ring that exhibit a measurable transcapacitance  $C_T$ . The effectiveness of the sensor for detecting water ingression in glass fiber-honeycomb-glass fiber sandwich panels was demonstrated (Chen and Bowler 2010).

Recognizing that the sensing area of the concentric coplanar capacitive sensor is limited to the vicinity of the circular gap between the two electrodes, and that the magnitude of  $C_T$  is essentially proportional to the length of this gap, concentric interdigital electrodes were introduced to increase the sensing area of the sensor and the measured capacitance (Chen and Bowler 2013).

#### 5.4.2 Capacitive Sensors for Cylindrical Surfaces

Motivated by the need to inspect wire insulation in air- and spacecraft, a capacitive sensor whose two electrodes conform to the cylindrical surface of the insulated wire was developed (Chen et al. 2012). By means of a semi-analytical model developed through a Green's function analysis of the electric field distribution in the wire due to a point charge on its surface, with a method-of-moments calculation to determine the charge distribution upon the curved electrodes, the permittivity of the wire insulation was inferred from measured capacitance. In an accelerated aging experiment, differences between wire insulation thermally exposed at various temperatures were observed (Chen and Bowler 2012a). Again recognizing the advantages of interdigital electrodes for increasing the measured capacitance and the sensing area of the sensor, a clamp fixture with interdigital capacitive sensor was developed for in situ evaluation of wire insulation (Sheldon and Bowler 2013, 2014a; Sheldon and Bowler 2014b). It was demonstrated that the sensor was capable of detecting differences between aircraft wires exposed to various types of aviation fluids (Sheldon and Bowler 2014b).

The interdigital capacitive sensor was applied to nuclear-related wires and cables beginning in 2014. EPR-insulated wires of various colors that had been exposed to thermal- and radiation-induced oxidative aging were tested and very good correlations were observed between measured  $C$  and  $D$  at 1 kHz and 1 MHz, EAB and indenter modulus measurements (Arvia et al. 2014; Bowler et al. 2015). These encouraging results provided significant momentum for continuing development of interdigital capacitive sensing for monitoring polymer components (jacket and insulation) in NPP cables. Correlation magnitudes of around 0.85 were found between measured  $C$  at 1 kHz and EAB in thermally-aged EPR and cross-linked polyolefin cable jacket materials; for example, Sun et al. (2016).

#### 5.4.3 Test Setup Considerations

Non-destructive testing of dielectrics using interdigital capacitors offers various design parameters that can be adjusted to improve signal strength, sensitivity, or sensing area. As mentioned above, increase in signal strength and sensing area can often be accomplished by increasing the number of sensor digits. Sensitivity to a particular depth of the sample can be increased by adjusting the separation of the digits, and sensitivity to material property changes in a particular polymer can be increased by selecting a frequency at which the expected changes are large.

##### 5.4.3.1 Electrode design

In a relatively lossy material the penetration depth of the dynamic electromagnetic field, commonly known as the skin depth, is defined as the depth at which the field magnitude falls to  $1/e$  (about 37%) of its surface value. In a low-loss (dielectric) material, a different definition is needed. Following Nassr and El-Dakhkhni (2009) and Li et al. (2006), Chen and Bowler (2012b) defined the penetration depth of the fringing field of a concentric coplanar capacitive sensor as “the thickness of a dielectric layer that results in a 10% decrease from the capacitance measured for a half-space of the same medium” (Chen and Bowler 2012b). This definition was adapted by Sheldon and Bowler (2013) to describe sensing depth for

an interdigital capacitive electrode situated on the curved surface of a cylindrical dielectric medium with a coaxial conductive core. In this case, penetration depth  $\delta$  is given by

$$\delta = b - a_{10}$$

wherein  $b$  is the radius from the cylinder axis to the exterior surface of the dielectric layer and  $a_{10}$  is the radius of a conductor that generates a 10% increase in capacitance compared with that for the case in which there is no conductor.

In Sheldon and Bowler (2014b), the above definition was used to explore the variation in capacitance of an interdigital sensor as a function of the parameter  $g$ , the gap length between neighboring digits, and the number of digits (Figure 6-2). The parameter  $g$  has the strongest influence on  $\delta$  of all the sensor parameters.

A similar idea was exploited in the context of samples with planar geometry for measuring permittivity and determining thickness of dielectric plates and shells (Matiss 2014). In this work, the electrode digits were excited selectively with the effect of varying  $g$  electronically without physically changing the separation of the electrode digits.

More recently, a finite-element modeling (FEM) approach has been employed to investigate the question of how to optimize the design of the interdigital sensor for various purposes (Huang et al. 2017; Shao and Bowler 2017). Subject to certain constraints, such as available dimensions of the sensor for a certain type of cable application, the need to achieve a value of  $C$  that is above the instrument noise floor, and the limitations of sensor fabrication approaches, the sensor sensitivity to expected changes in the material permittivity as a function of its aging has been modeled and used as a metric by which to seek an optimal sensor design. The adjustable parameters in the design process are taken to be the number of electrode digits, the width of those digits, and the separation between them—although these are not completely independent of one another. In the planar geometry treated by Huang et al. (2017), it was shown that there is a design trade-off between the sensor's sensitivity and the penetration depth of the fringing field into the test piece. In other words, the sensor sensitivity to permittivity changes is better for electrodes whose digits are close together, but the penetration depth of the electric field is smaller in this case. Shao and Bowler (2017) studied the case of a cylindrical test piece (RSCC cable type P62-3902, diameter 14.49 mm) and sensor constrained to 37.5% of the cable circumference (135 degrees of arc) with the goal of maximizing sensor sensitivity to property changes in the XLPE insulation layer concealed beneath the CSPE jacket. In this case, optimal design parameters were found to be  $N = 3$ ,  $w = 4$  mm, and  $g = 1$  mm, yielding a sensitivity of 4.66 pF/m and output capacitance of 2.09 nF/m when the insulation relative permittivity was assumed to be 2.5.

#### **5.4.3.2 Inspection frequency**

In solid dielectric materials, the dielectric relaxations are often broad and overlapping but, nonetheless, judicious selection of inspection frequency can help to increase measurement sensitivity to the particular polymer of interest, in the case of a cable with different polymer components, or to the particular aging mechanism of interest. An excellent illustration of this point can be found in Figure 5-4, which shows broadband permittivity data measured from 0.01 Hz to 1 MHz on thermally-aged cable samples with EPR insulation and PVC jacket (Imperatore 2017). It can be seen that there are two peaks in the loss tangent of the new cable, Figure 5-4(b), corresponding to the decline in specific capacitance plotted in Figure 5-4(a). The pronounced peak observable at around 0.2 Hz corresponds to a relaxation process occurring in EPR (Verardi 2013). The lower-amplitude peak at around 100 kHz corresponds to a relaxation process occurring in PVC (Orrit-Prat et al. 2011). For this cable, then, it should be possible to separate the influences of the two different materials by selecting the appropriate frequency range in which to work. To access property changes occurring in the insulation, therefore, it would be appropriate to work in a frequency range below 1 Hz.

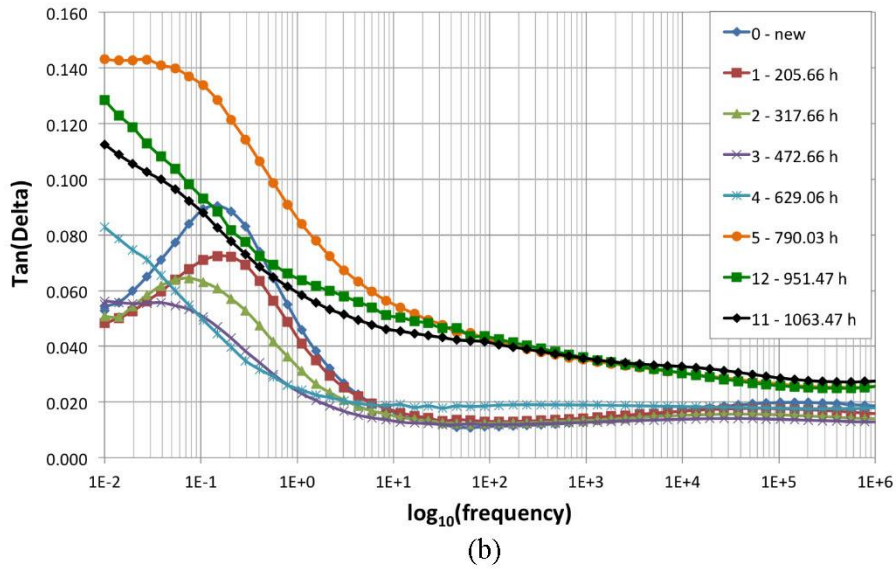
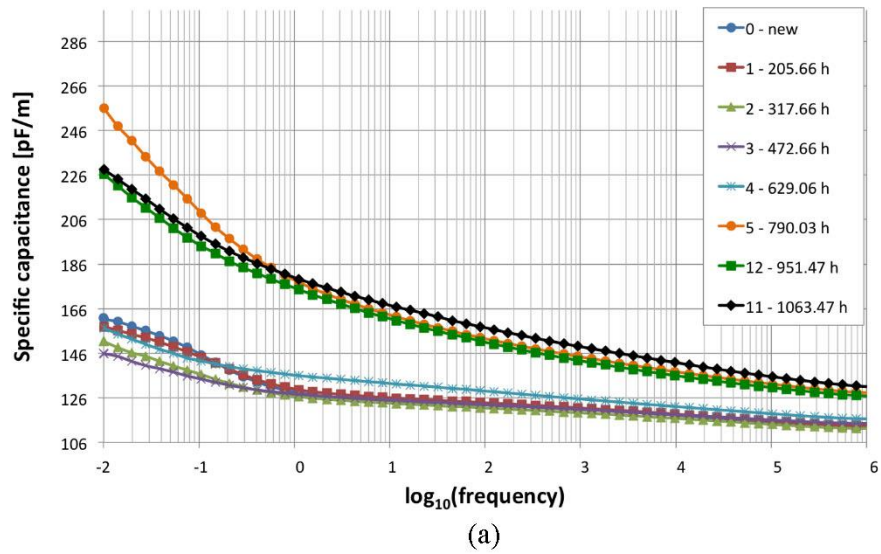


Figure 5-4. Specific capacitance (a) and loss tangent (b) measured on tri-core, EPR-insulated cable with PVC jacket. Samples were aged thermally at 140°C for the number of hours shown in the legend (Imperatore 2017).



## 6. FEM SIMULATIONS

FEM has been used to explore the design space associated with interdigital electrodes with the aim of optimizing the sensor design for certain inspection tasks. Generally speaking, a modeling or simulation tool can assist with sensor design and optimization in a design process that avoids a large number of laboratory trials. For this effort, commercially available simulation packages from ANSYS and COMSOL™ have been used to predict the capacitance and electric field distributions associated with interdigital sensor configurations. PNNL has used ANSYS Maxwell® while Iowa State University has used COMSOL™ Multiphysics. Both tools include electrostatic field solvers for 2D and 3D geometries.

### 6.1 Coplanar Interdigital Electrodes

Huang et al. (2017) investigated the effect of varying the geometrical parameters  $g$ ,  $w$  (and consequently the number of digits,  $N$ ) of a coplanar, interdigitated sensor with fixed overall dimensions upon its output capacitance and sensitivity. A schematic diagram of the sensor is given in Figure 6-1 (Huang et al. 2017). The sensor is comprised of fork-like electrodes whose tines of width  $w$  are separated by a gap  $g$ . The driven and sensing electrodes may be connected to an impedance analyzer capable of sweeping from 1 Hz or below to more than 1 MHz and where the measurement of interest is the complex capacitance  $C^*$  [F] expressed at a particular frequency or as a plot over the frequency range.

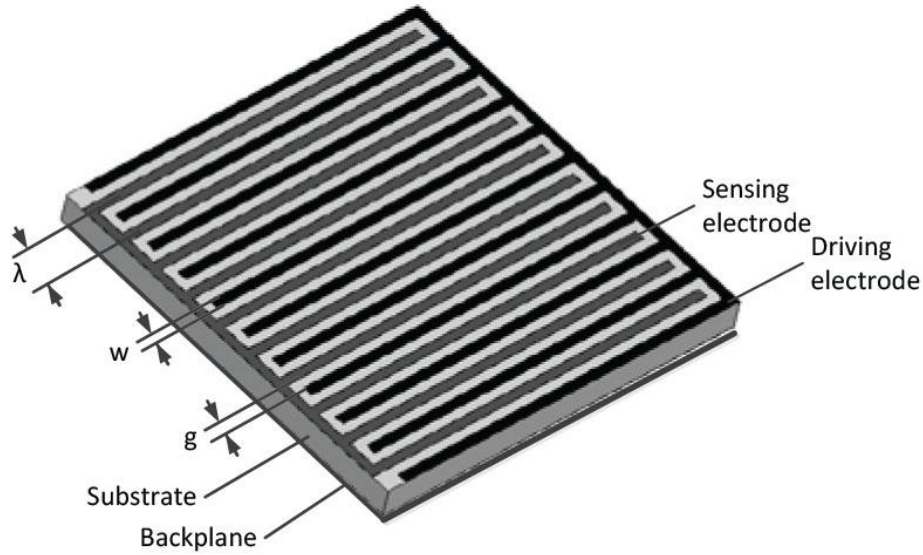


Figure 6-1. Perspective view of a coplanar, interdigital capacitive sensor showing geometrical parameters  $g$ , the separation distance between neighboring digits, and  $w$ , the digit width (Huang et al. 2017).

It was shown that there is a design trade-off between sensitivity  $S$ , defined as the rate of change of capacitance as a function of test piece permittivity,

$$S = \frac{\partial C}{\partial \epsilon}$$

and the depth of penetration of the electric fringing field into the test piece.



## 6.2 Cylindrical Interdigital Electrodes

### 6.2.1 Single-Core Cable with Insulation and Jacket

Shao and Bowler (2017) addressed the problem of designing curved interdigital capacitive electrodes for maximal sensitivity to permittivity changes in second-layer dielectric material. Given certain geometrical constraints, the sensor's geometrical parameters  $g$  and  $w$  were varied with the goal of determining the electrode design with best sensitivity to permittivity changes in the insulation layer of an unshielded, single-core cable, when the sensor was applied to the exterior surface of the cable jacket, (Figure 6-2). Recognizing that the penetration depth  $\delta$  increases as the separation of the digits  $w$  increases, but that increasing  $w$  causes the output capacitance of the sensor  $C$  to drop, this design exercise deals with the trade-off between the need for a large depth of penetration while maintaining an output capacitance well above the noise floor.

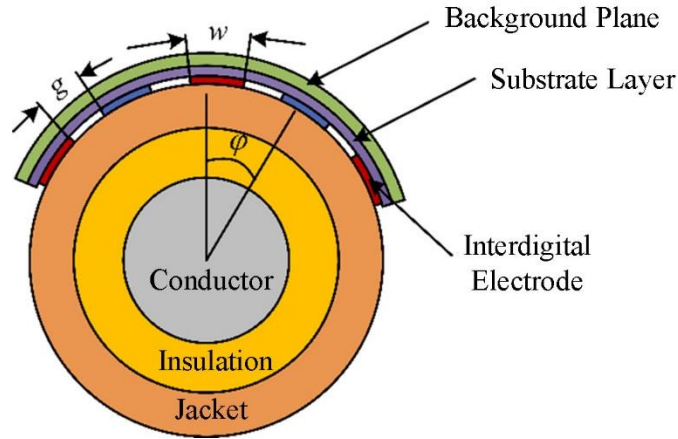


Figure 6-2. Schematic diagram of the design problem considered by Shao and Bowler (2017).

For cable type P62-3092 supplied by RSCC company whose parameters are given in Table 6-1, and for certain fixed parameters of the sensor given in Table 6-2, sensor sensitivity and output capacitance were computed using AC/DC packages of COMSOL<sup>TM</sup> as functions of parameters  $g$  and  $w$  (Figure 6-3) Shao and Bowler (2017).

Table 6-1. Cable parameters used in the simulations whose results are presented in Figure 6-2

Company	Cable Type	Total Diameter (mm)	Jacket		Insulation	
			Thickness (mm)	Material	Thickness (mm)	Material
RSCC	P62-3902	14.49	1.143	CSPE	1.4	XLPE

Table 6-2. Fixed parameters of the sensor for the simulations whose results are presented in Figure 6-3.

	Thickness, $t_e$ ( $\mu\text{m}$ )	Material	Relative Permittivity
Electrode	17.8	Copper	n/a
Substrate	25.4	PTFE	2.1
Back Plane	17.8	Copper	n/a

Optimal design parameters for non-destructive evaluation of the XLPE insulation layer for the cable configuration were found to be  $N = 3$ ,  $w = 4$  mm, and  $g = 1$  mm when the cable surface available for inspection is assumed to be 37.5% of the full circumference. With these assumptions, a sensitivity of 4.66 pF/m and output capacitance of 2.09 nF/m were determined for the sensor when the insulation relative permittivity was assumed to be  $\epsilon_1 = 2.5$ .

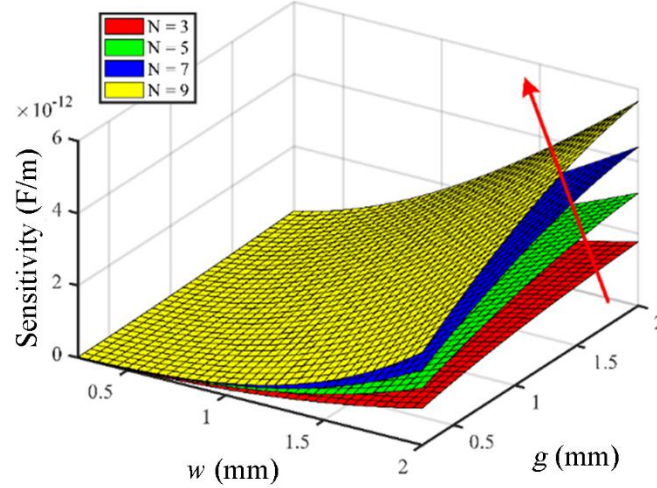


Figure 6-3. Sensor sensitivity  $S$  as a function of the number of digits,  $N$ . Other calculation parameters are given in Table 6-1 and Table 6-2.

### 6.2.2 Single Core Cable with Insulation

In more recent work associated with this project, an interdigital capacitive sensor with curved electrodes conforming to the surface of Okoguard® 15 kV Aerial Jumper Cable (The Okonite Company N.D.) was modeled (Figure 6-4) to explore the influence of IDC design parameters such as tine gap ( $g$ ), width ( $w$ ), and number ( $n$ ). Parameters of the cable are listed in Table 6-3 and the insulation real relative permittivity as a function of frequency is plotted in Figure 6-5. This data was measured on a flat sample of the material with thickness  $0.8145 \pm 0.0004$  mm using parallel-plate capacitive electrodes with diameter 31.75 mm. Fixed parameters of the sensor are listed in Table 6-2.

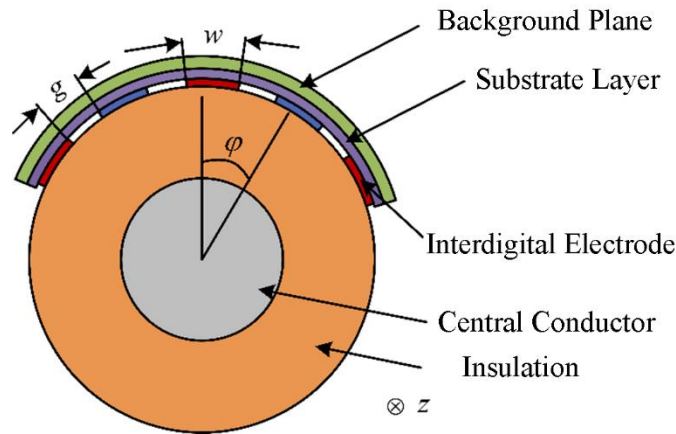


Figure 6-4. Schematic diagram of an interdigital capacitive sensor in contact with EPR-insulated Okoguard® 15 kV Aerial Jumper Cable.

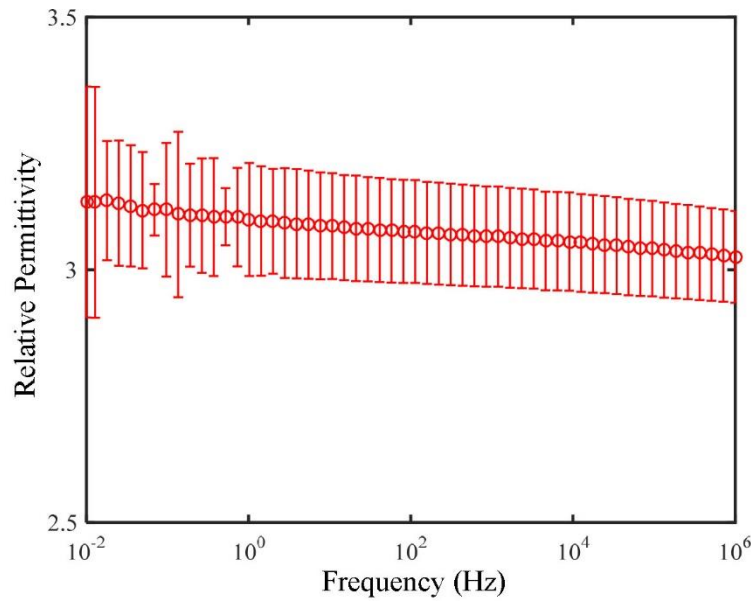


Figure 6-5. Measured real relative permittivity of Okoguard® EPR-based insulation material used in Okoguard® 15 kV Aerial Jumper Cable.

Table 6-3. Cable parameters used in the simulations whose results are presented in Figure 6-6

Company	Cable Type	Total Diameter (mm)	Conductor		Insulation	
			Diameter (mm)	Material	Thickness (mm)	Material
Okonite	Okoguard® Aerial Jumper Cable 15kV-90°C Rating	27.2	11.68	Coated, stranded copper	7.76	Okoguard® (EPR- based): Nominal permittivity=3.1

The influence of the IDC gap ( $g$ ), and penetration depth ( $\delta$ ) was explored using COMSOL™ by varying the diameter of the center conductor and noting the influence on the simulated IDC capacitance measurement for a sensor placed on the outside cable insulation (Figure 6-6). The linear relationship and strong correlation between the  $g$  and  $\delta$  is encouraging for using a wide gap-tined sensor and a narrow gap-tined sensor to compensate for jacket influences on a measurement of the underlying insulation condition. This influence of  $g$  on the voltage distribution can be visually appreciated from the ANSYS FEM model of an IDC field simulation image shown in Figure 6-7.

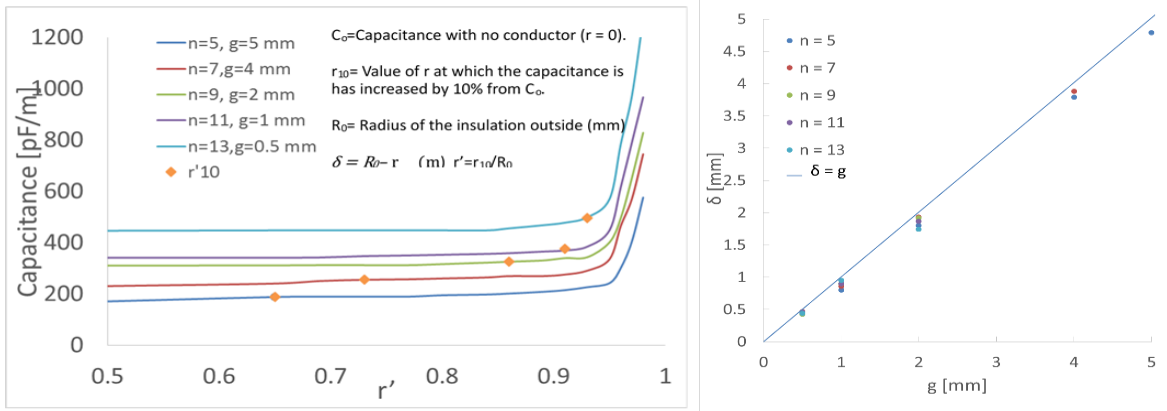


Figure 6-6. (left) COMSOL™-simulated IDC capacitance of Okoguard® Aerial Jumper Cable (Table 6-3)-type EPR material with center conductor radius varied and with varying numbers of IDC tines and gaps. (right) linear relationship between gap  $g$  (mm) and penetration depth  $\delta$  (mm) defined by insulation thickness for which 10% increase in capacitance is observed, as the center conductor radius increases from  $r = 0$  (no center conductor).

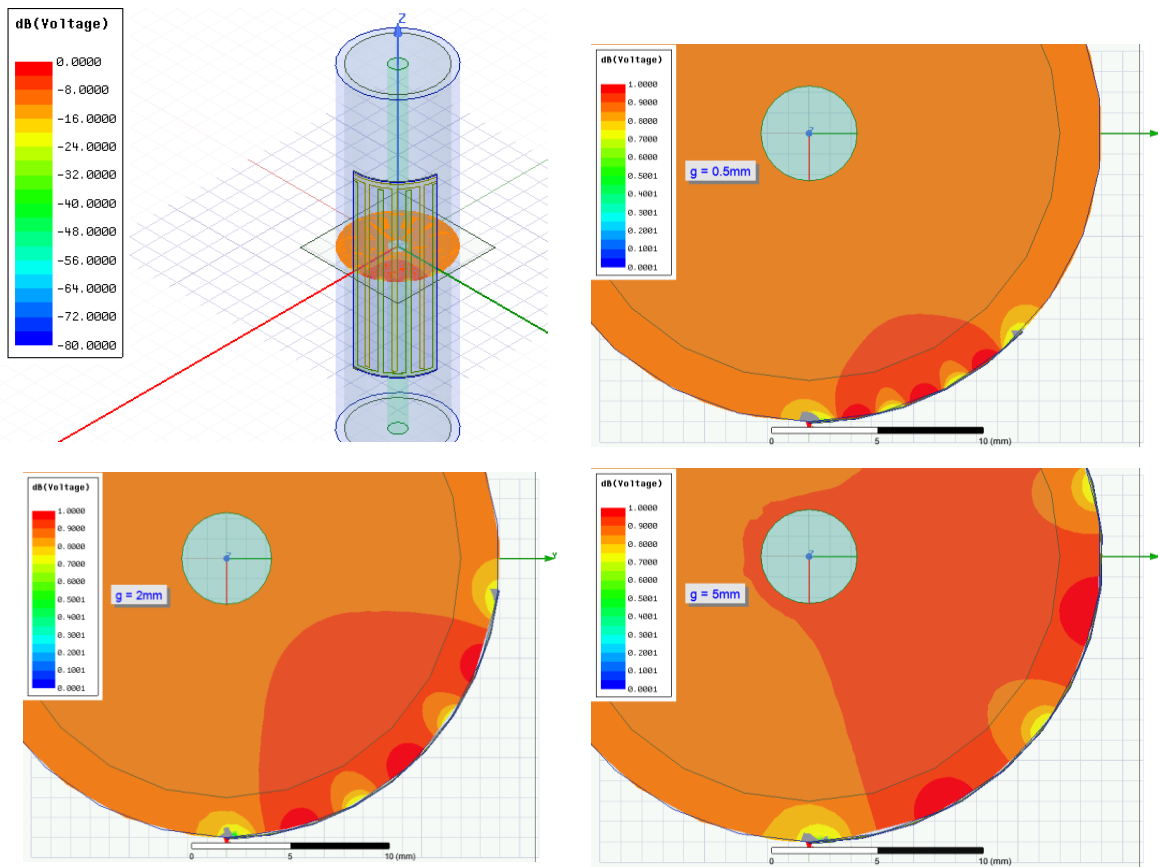


Figure 6-7. (upper left) 7-tine, 2 mm gap ( $g$ ) IDC sensor model with voltage distribution field plot cross-section; (upper right) tine spacing  $g = 0.5$  mm, (lower left) tine spacing  $g = 2$  mm; (lower right) tine spacing  $g = 5$  mm.

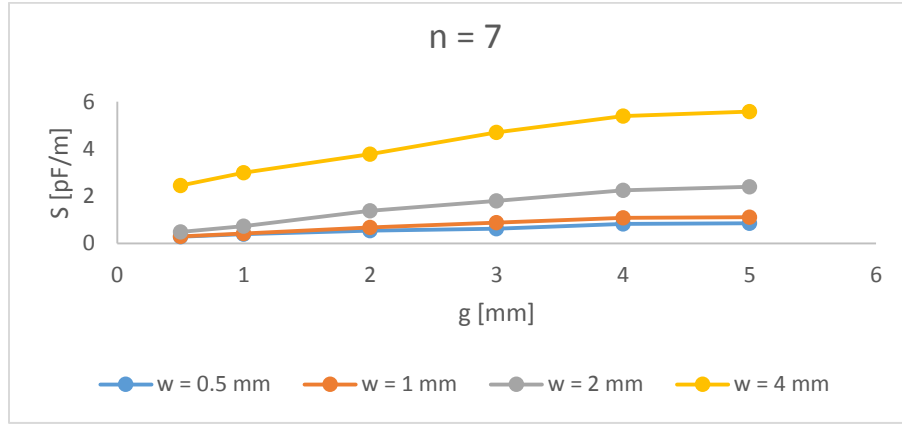


Figure 6-8. COMSOL<sup>TM</sup> calculation of sensitivity of a 7-tine IDC with varying  $w$  and  $g$ .

The effect of varying the width-to-gap ratio  $w/g$  has been examined by (Huang et al. 2017) for a flat IDC, Figure 6-1. It was found that there is a design trade-off between the sensor's sensitivity and the penetration depth of the fringing field into the test piece. As the gap increases, the penetration depth also increases, but the sensor sensitivity declines. Similar behavior is observed for an IDC in contact with the exterior of a cylindrical sample, as follows.

The simulated frequency sweep of capacitance, predicted for various IDC configurations, is shown in Figure 6-9. Fixing the number of digits  $N = 11$ , the width of the digits  $w = 1$  mm, and the sensor length along the axial direction of the cable to be 25 mm, the separation between the digits  $g$  was allowed to take values 1, 2, 3, and 4 mm. The output capacitance of the sensor calculated using AC/DC packages of COMSOL<sup>TM</sup> for these conditions is plotted as a function of frequency in Figure 6-9. Noting that the number of digits and their width are constant in this comparison, it is intuitively reasonable that the calculated capacitance decreases as the parameter  $g$  increases, but the overall change in output capacitance is not very large—around 0.7%. What changes more dramatically is the penetration or sensing depth for these different configurations, a point that is explored in the following.

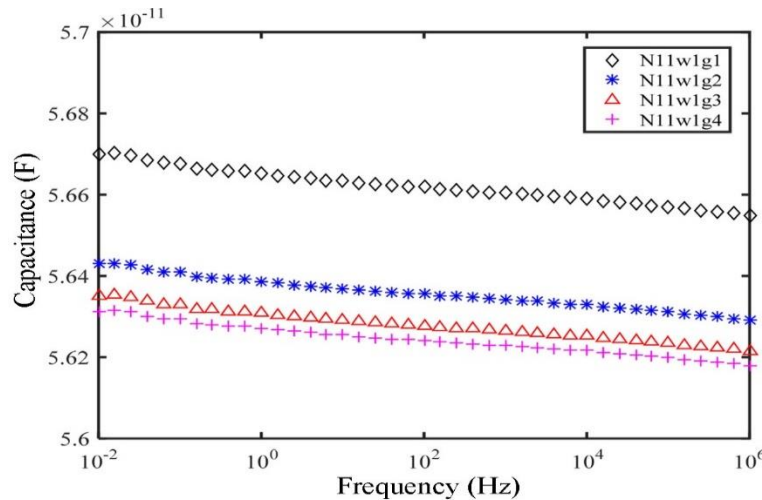


Figure 6-9. Output capacitance of the sensor calculated using AC/DC packages of COMSOL<sup>TM</sup> for digit gaps of 1, 2, 3, and 4 mm. The number of digits  $N = 11$ , the width of the digits  $w = 1$  mm, and the sensor length along the axial direction of the cable is 25 mm. Other sensor parameters are given in Table 6-2. Some parameters of the cable are listed in Table 6-3 and the insulation real relative permittivity as a function of frequency is plotted in Figure 6-5.

The thickness of the EPR insulation layer in the Okoguard® 15 kV Aerial Jumper Cable is almost 8 mm (Table 6-3). It is possible that, in some service environments, the exterior of this relatively thick polymer layer may age differently than the interior. In the same way that the study by Shao and Bowler (2017) considered sensitivity of the designed sensor in relation to sensing depth, it is interesting to consider developing a sensor for this aerial jumper cable that may be able to assess the polymer dielectric properties as a function of depth. One way that this may be achieved is by sequential excitation of different combinations of electrode digits or sequential measurements using narrow gap and wide gap-tined sensors thereby varying the effective gap between the digits,  $g$ . This idea has also been proposed by Matiss (2014) in the planar electrode configuration.

### 6.3 IDC to Characterize the Behavior of Insulation beneath Jacket

The feasibility of using a narrow gap tine and wide gap tine IDC sensor to characterize insulation beneath jacket was investigated using an ANSYS IDC simulation. The model parameters are identified in Table 6-4. The tine gap width  $g$  was varied from 0.5 to 2.0 to 5 mm and the permittivity of both the insulation and jacket was varied by  $\pm 20\%$  from a nominal value postulated to be representative of the Okoguard® -Okolon® TS-CPE Type MV-90 2.4kV Nonshielded Power Cable (Table 6-4)(Figure 6-10). The model output is the simulated IDC electrostatic capacitance (single value expected from a low-voltage, very low frequency impedance meter).

The first simulation showed the variations among the three sensor types for the range of permittivity values in both the insulation and the jacket (Figure 6-13). Observations are as follows:

- Sensitivity to jacket permittivity change (near IDC) is far greater than insulation permittivity sensitivity in all cases.
- Slope / sensitivity to insulation permittivity change is 6 x greater for 5 mm spacing IDC than for 0.5 mm spacing IDC (5 mm  $g$  slope = 0.133; 0.5 mm  $g$  slope = 0.022 i.e., a factor of six higher).
- Vertical separation as a function of jacket permittivity is least with 5 mm gap and most with 0.5 mm gap.



Figure 6-10. Okoguard® - Okolon® TS-CPE type MV-90 2.4kV Nonshielded power cable.

Table 6-4. Design parameters for Okoguard® - Okolon® TS-CPE Type MV-90 2.4kV Nonshielded Power Cable

Service	Total Diameter (mm)	Conductor		Insulation		Jacket	
		Diameter (mm)	Material	Thickness (mm)	Material	Thickness (mm)	Material
Type MV-90 2.4kV Nonshielded Power Cable (90°C, wet or dry) – manufactured by Okonite	22.4	12.0	Coated, stranded copper	3.2	Okoguard® (EPR-based) Nominal Permittivity =3.1	2.0	CPE: Nominal Permittivity = 3.5

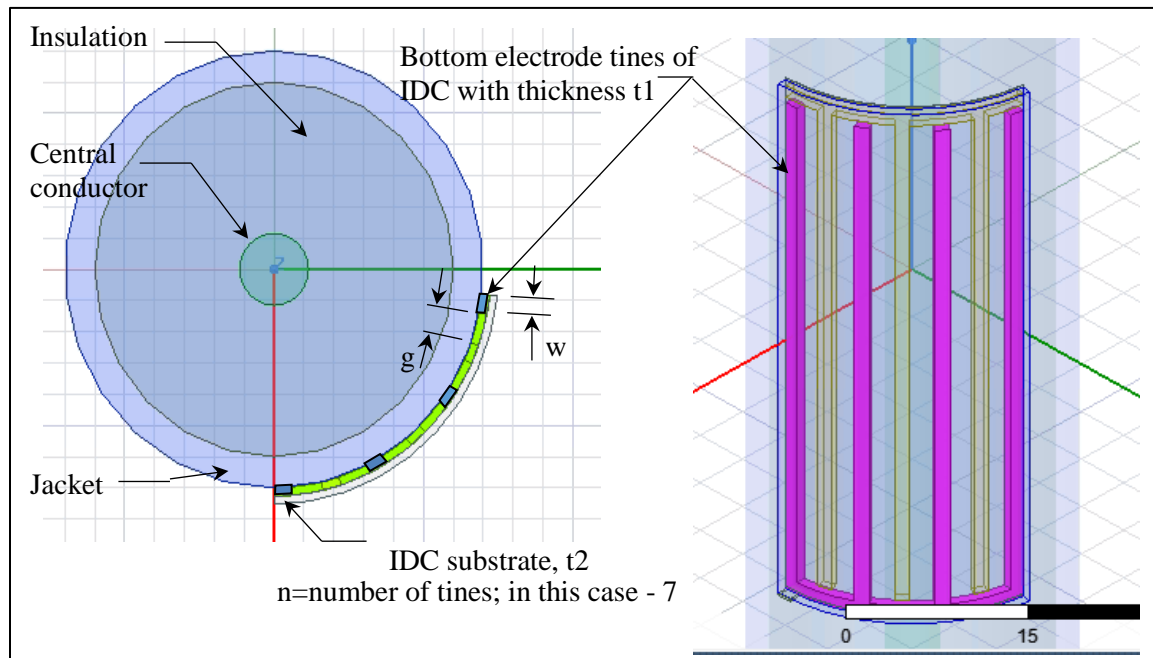


Figure 6-11. Seven (7) tine IDC model on jacketed insulation; conductor radius = 2.3 mm, insulation radius = 12 mm, jacket radius = 14 mm,  $t_1 = 0.0178$  mm, substrate relative permittivity = 2.1,  $t_2 = 0.0254$  mm,  $w = 1.2$  mm,  $g = 0.5, 2$ , and  $5$  mm, insulation relative permittivity = 2.48, 3.1, and 3.72, jacket relative permittivity = 2.8, 3.5, and 4.2, central conductor and sensor electrodes are copper.



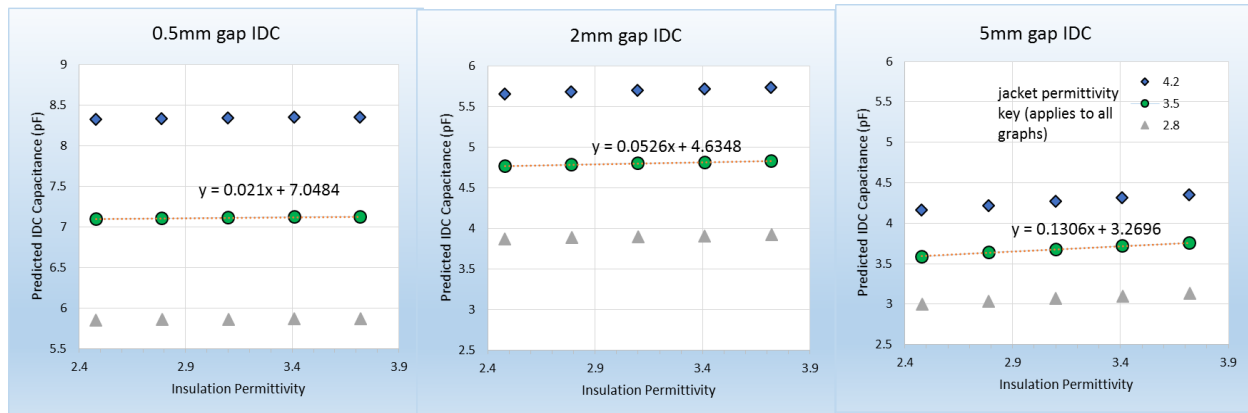


Figure 6-12. Simulated IDC capacitance as insulation permittivity is varied by +/- 10 and 2% and jacket permittivity is varied by +/- 20% for narrow, medium, and wide gap-tined IDC sensors.

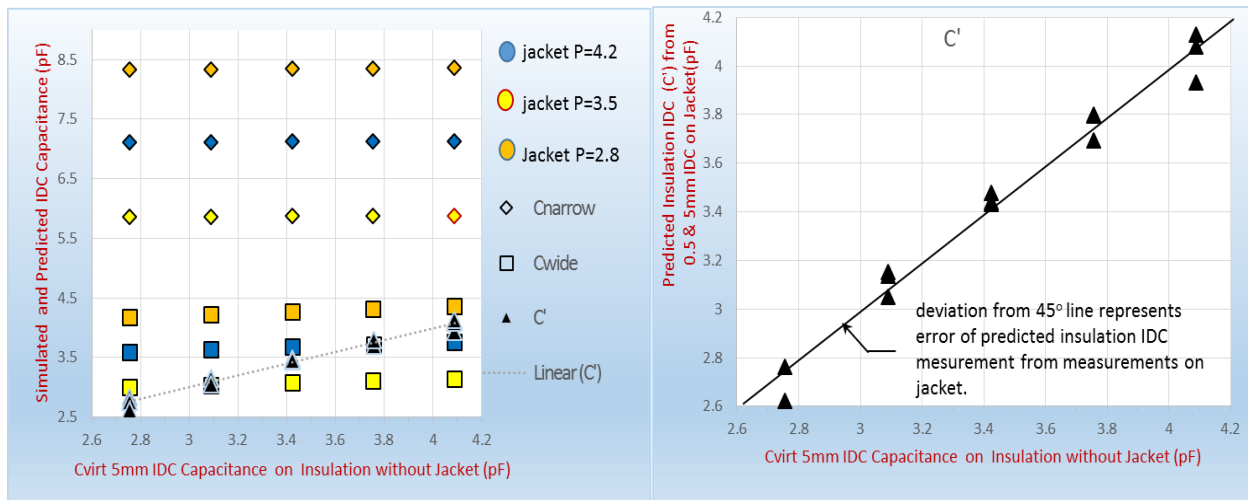


Figure 6-13. (Left) Simulated IDC measurement on jacket surface for 5 and 0.5 mm gap (Y axis) plus  $C'$  for 5 different values of  $C_{virt}$  where  $C_{virt}$  is the virtual capacitance that would be measured on the insulation if there were no jacket present. (Right) Expanded  $C'$  estimates of  $C_{virt}$  based on two-variable regression using inputs from jacket measurement simulations.

During field measurements, only the outside of the jacket is accessible for measurement. Using the FEM simulation however, the model can estimate what the measurement would be on the insulation if the jacket were not present. This estimate is designated as  $C_{virt}$ . Knowing  $C_{virt}$  coupled with the estimate of measurements with the wide gap tine and narrow tine IDCs ( $C_{wide}$  gap tine and  $C_{narrow}$  gap tine) can be used to develop the relationship between measurements that can be made on the outside of the jacket to the virtual measurement –  $C_{virt}$  that would be possible to measure if there were no jacket. This estimate of  $C_{virt}$  is designated as  $C'$ . The general form of the estimate is:

$$C' = A * C_{wide} \text{ gap tine} - B * C_{narrow} \text{ gap tine} + D$$

Solving for A, B, and D conforms to a classical two-variable linear regression analysis that is supported as a function call within Excel. The simulations of  $C_{virt}$ ,  $C_{wide}$  gap tine, and  $C_{narrow}$  gap tine were determined using the FEM model and  $C'$  was then estimated based on the two-variable regression as shown below.

$$C' = 8.8 * C_{tine} - 4.3 * C_{narrow} \text{ gap tine} + 1.4$$



The error between  $C'$  and  $C_{vert}$  is shown in Figure 6-13 right.

Note that the error from this simulated estimate of  $C_{vert}$  is quite small compared to the change of  $C_{wide\ gap\ line}$  and  $C_{narrow\ gap\ line}$  associated with change in permittivity. This tends to support the feasibility of assessing the insulation condition under the jacket.

The approach can be verified by testing the jacketed cable then trimming off the jacket and testing the underlying insulation directly to compare the measurement and estimate of  $C'$  based on measurements taken on the jacket to the measured Capacitance taken directly on the insulation with the jacket removed.

## 7. MEASUREMENT FIXTURE

### 7.1 Background

A flexible clamp-on fixture to position the IDC sensors on wires with diameter in the range 1 mm to 3 mm was developed by (Arvia et al. 2014). Development of a fixture for nominally one-inch-diameter cables has been discussed in (Glass SW 2017).



Figure 7-1. Photograph of IDC described in Sheldon and Bowler (2014b). The IDC accommodates wires with diameter up to approximately 3 mm. IDC particulars:  $N = 14$ ,  $w = 0.1$  mm,  $g = 0.3$  mm, and  $l = 25$  mm.

### 7.2 Fixture Development for NPP Cable

#### 7.2.1 Fixture Development

To accommodate the dimensions of the MV NPP power cables of interest to this study, with diameter 20 to 25 mm, a new clamp arrangement was developed, Figure 7-3. Such a clamping assembly is helpful to minimize measurement variability as a function of uncontrolled lift-off of the electrodes from the insulation or jacket surface.

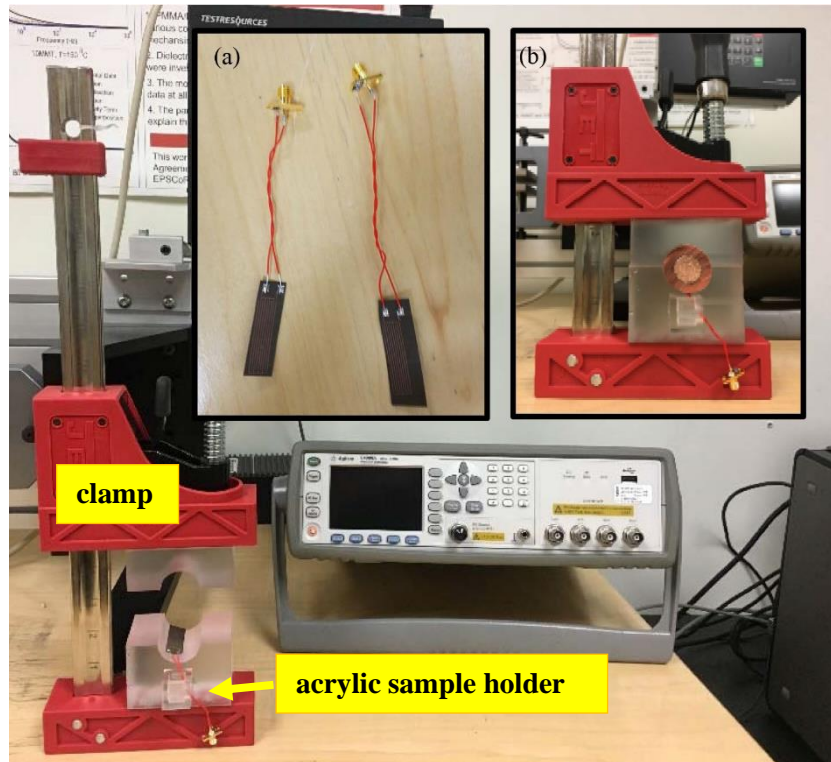


Figure 7-2. Clamp sensor setup with Agilent E4980A Precision LCR Meter, acrylic sample holder, printed interdigital capacitor electrodes, and SMA connector. Inset: (a) capacitor electrodes, two sizes; and (b) clamp setup with Okoguard® Aerial Jumper Cable sample in position.

## 7.2.2 IDC Design for NPP Cable Testing

In the context of designing a sensor for capacitive testing of Okoguard®-Okolon® TS-CPE Type MV-90 2.4kV Nonshielded Power Cable, Figure 6-10, the dimensions provided in Table 6-4 are important. Coupled with the findings presented in Figure 6-6, that the depth of penetration of the fringing electric field into the polymer sample,  $\delta$ , is approximately the same as the separation of the electrode digits,  $g$ , it is clear that a sensor for monitoring changes in insulation properties through the cable jacket requires a sensor with  $g$  sufficiently large that  $\delta$  is greater than the jacket thickness (2.0 mm).

### 7.2.2.1 Sensor design constraints

- **Cable geometry:** The maximum digit separation achievable is constrained by the cable geometry (the maximum digit separation is accomplished by the minimum number of digits located at opposite poles of the cable circumference).
- **Instrument noise floor:** The signal strength (measured capacitance) declines as the digit separation increases. In other words, if the jacket is “thick” then the digits must be well-separated in order for the measured capacitance to be sensitive to the underlying insulation, but if the digits are too far apart then the measured capacitance may be of such low magnitude that it becomes unacceptably noisy and information cannot be deduced from the measurement. In practice it is acceptable to keep the capacitance of the sensor above 10 pF because, for example, the error listed in the operating manual of an Agilent E4980A Precision LCR meter operating at 1 MHz, for a 10 pF measurement, is the minimum achievable (approximately 0.3%).

- *Sensor arc*: Keeping in mind the importance of making measurements repeatedly and, in a field environment and appreciating that only one side of the cable may be accessible for measurement, the target sensing area is limited to ~133 degrees of arc.
- *Sensor length*: Cable samples often exhibit mild curvature that makes it difficult to achieve consistent contact between the cable surface and the sensor electrodes, if the electrodes are too long. To avoid this problem the sensor length is limited to 25 mm, a choice based upon typical curvatures observed for samples studied here.
- *Printed circuit technology*: The lithographic techniques employed in patterning printed circuitry on flexible polymer substrate, as employed in fabricating the sensors used here, imposes a minimum dimension of 100  $\mu\text{m}$  on digit width ( $w$ ) and separation ( $g$ ).

### 7.2.2.2 Sensor designs

The radius of Okoguard®-Okolon® TS-CPE Type MV-90 2.4kV Nonshielded Power Cable is 11.2 mm. On this basis there is approximately 26 mm of available arc to be populated with sensor digits. Imposing that the number of digits  $n$  on the positive (or negative) electrode is odd, with  $n = 3, 5, 7, \dots$ , and that the number of digits on the opposing electrode is  $n - 1$ , the number of electrodes is constrained by

$$nw + (n - 1)g < 26 \text{ mm}$$

wherein  $w$  (mm) is the width of each digit and  $g$  (mm) is the gap between neighboring digits.

Accounting for the constraints laid out in Section 7.2.2.1, and the inequality above, three types of electrodes were designed for fabrication. The parameters for these are provide in Table 6-2, along with the parameters of a pre-existing electrode that was also used for sample characterization. The electrodes were laid out in design for printed circuit patterning as shown in Figure 7-3.

Table 7-1. Designed parameters of sensors for monitoring Okoguard®-Okolon® TS-CPE Type MV-90 2.4kV Nonshielded Power Cable.

Sensor	$n$	$w$ (mm)	$g$ (mm)	$C$ (pF/m)
0	9	0.1	0.1	760
1	7	1.2	0.5	500
2	7	2.0	2.0	460
3	5	3.5	5.0	375

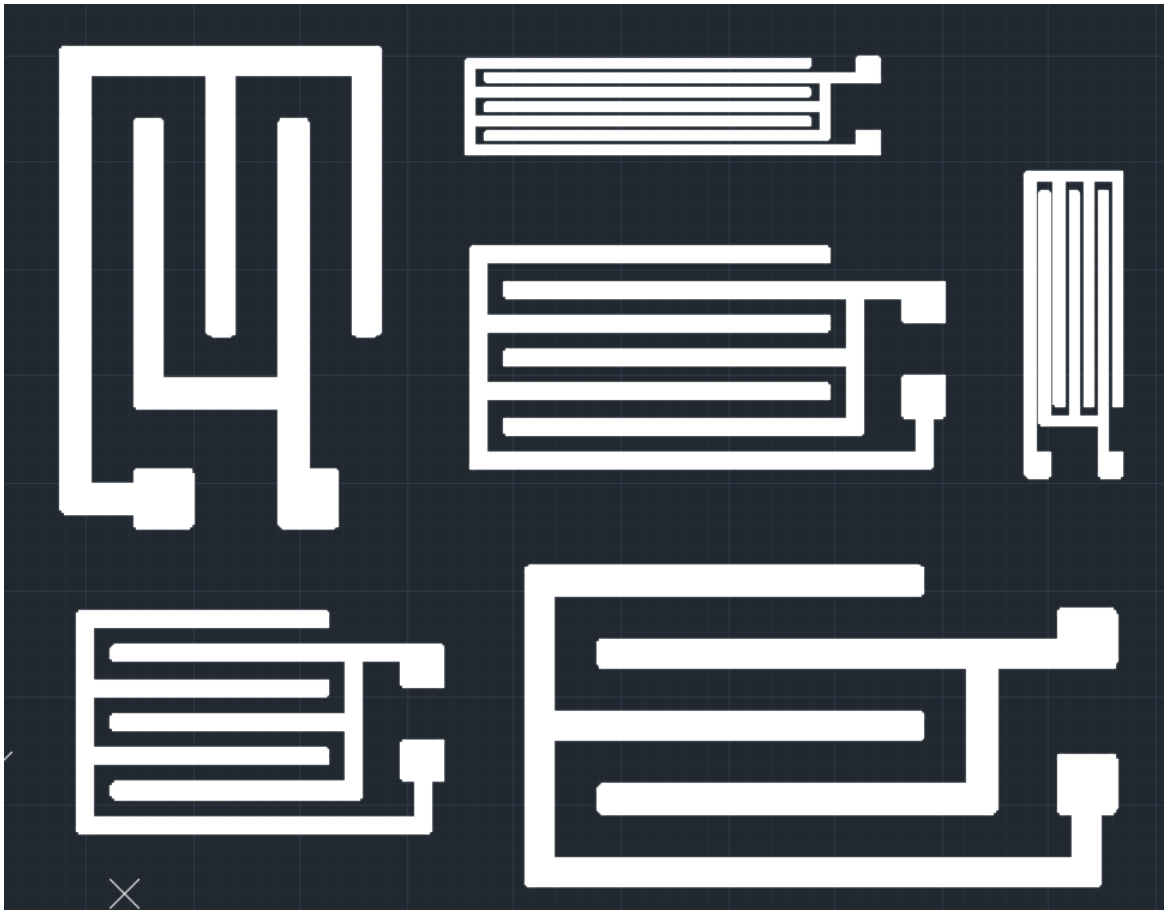


Figure 7-3. Sensor designs 1, 2, and 3, from Table 7-1, in two lengths each (25.4 mm and 38.1 mm) laid out for printed circuit fabrication.

## 8. MEASURED IDC INDICATIONS OF CABLE AGING

In this section, several sets of capacitive measurements are presented that show sensitivity to changes in polymer electrical properties, both insulation and jacket materials, in response to thermal aging. The results are presented in order of increasing sample complexity, beginning with benchmark experiments on flat “witness” specimens, from which baseline property information can be obtained. Then, results of measurements taken on single-core, two-polymer (jacketed) Okoguard® -Okolon® TS-CPE Type MV-90 2.4kV Nonshielded Power Cable (Table 6-4) are presented.

### 8.1 Flat-Plate Flat Sample Benchmark Measurements

Benchmark experiments were conducted on flat mat samples of EPR and CPE insulation and jacket polymers, respectively. Dielectric properties were measured as a function of frequency on these samples according to the method described in Section 5.3.

#### 8.1.1 Sample Preparation

Flat polymer samples with approximate dimensions  $50 \times 50 \times 1.5 \text{ mm}^3$  were prepared by suspending them from a rack inside an air-circulating oven that was maintained at a pre-selected accelerated aging temperature, with the goal of inducing aging representative of longer-term aging in normal service environment. Sample thickness was measured at ten locations on each sample, using a Fowler Ultra Digit Mark IV micrometer with systematic uncertainty of  $1 \mu\text{m}$ , and the mean thickness values with standard deviation computed. Accurate thickness values are important for obtaining permittivity from measured capacitance using equation (5.1).

##### 8.1.1.1 EPR mats

Two sets of EPR mats were aged at  $140^\circ\text{C}$ , one set in the absence of CPE jacket polymers for up to 70 days, Figure 8-1, and one in the presence of CPE that caused surface blackening of the EPR, Figure 8-2. Mean thickness values with standard deviation (error bars) are plotted in Figure 8-3 and Figure 8-4 for these two sample sets.



Figure 8-1. EPR samples aged at  $140^\circ\text{C}$  in the absence of CPE.



Figure 8-2. EPR samples aged at 140°C in the presence of CPE.

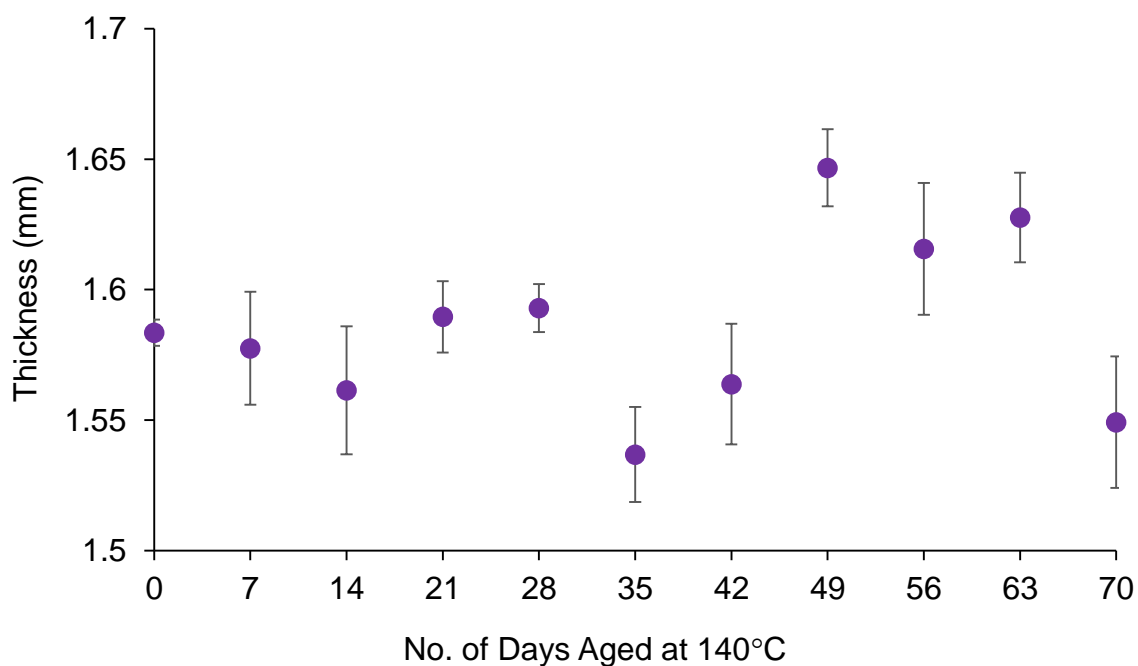


Figure 8-3. Measured mean thickness values of pink EPR samples shown in Figure 8-1. Error bars represent the standard deviation of ten measured values.

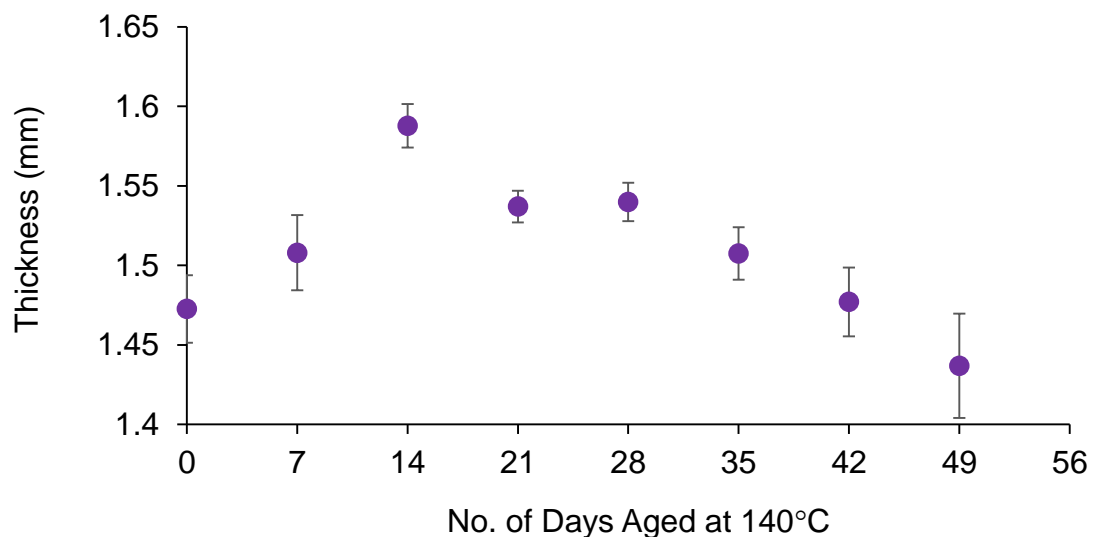


Figure 8-4. Measured mean thickness values of blackened EPR samples shown in Figure 8-2. Error bars represent the standard deviation of ten measured values. Note, the sample aged for 14 days exhibited greater curvature than others.

#### 8.1.1.2 CPE mats

CPE mats were aged at 165°C for up to 4.5 days. In appearance, they are all black. Mean thickness values with standard deviation (error bars) are plotted in Figure 8-5 for samples aged at 165°C.

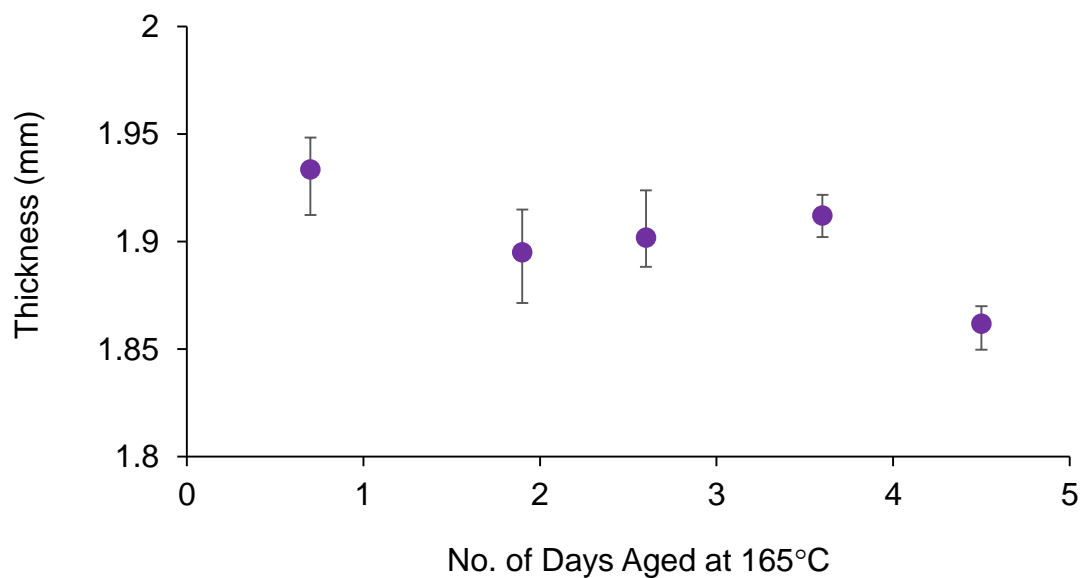


Figure 8-5. Measured mean thickness values of CPE samples. Error bars represent the standard deviation of ten measured values.



## 8.1.2 Measurement Setup

Dielectric properties were measured as a function of frequency on these samples according to the method discussed in Section 5.3. Frequency was swept from 1 Hz to 1 MHz and capacitance  $C$  and dissipation factor  $D$ , both defined in equation (5.2), recorded. The data plotted in Section 8.1.3 represents the average of several recorded sets of data with  $\pm 1$  standard deviation error bar except where sample size or setup constraints limited the number of measurements and consequently no error bars can be shown. Mechanical measurements (EAB and IM) on actual cable samples or of stamped dog-bones from witness sample material having undergone identical aging for the dielectric samples are also shown for reference Figure 8-6.

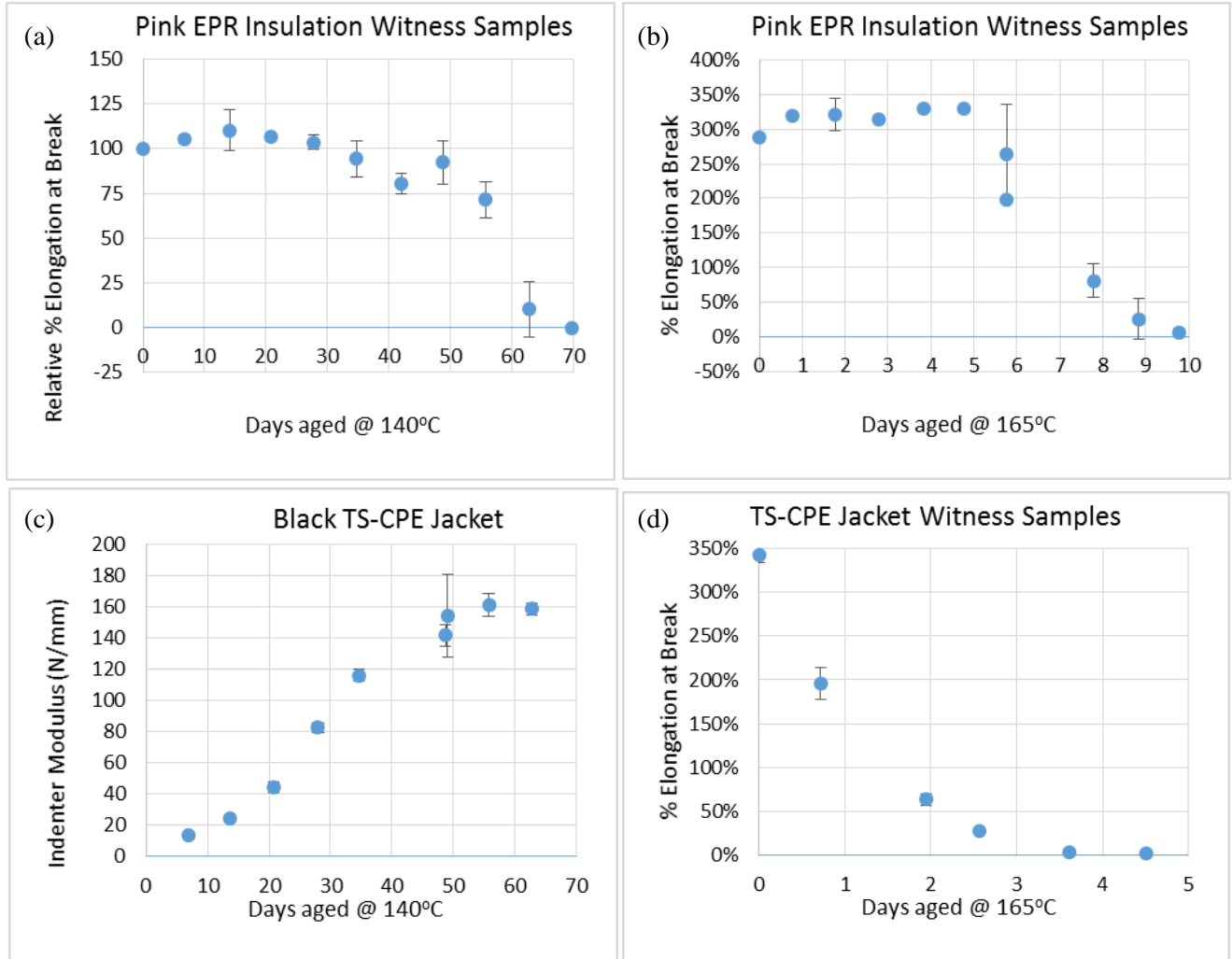


Figure 8-6. Mechanical measurements on witness samples that were aged under identical conditions as the IDC tested samples shown for reference.

## 8.1.3 Results

### 8.1.3.1 EPR mats

In situ electrode separation values of the EPR mats shown in Figure 8-1 are presented in Figure 8-7. Measured capacitance is presented in Figure 8-8. The in situ separation values presented in Figure 8-7 were used in converting measured capacitance to relative permittivity via equation (5.1). Relative

permittivity inferred from those measurements is presented in Figure 8-9 as a function of frequency, in Figure 8-10 as a function of aging time and in Figure 8-11 versus EAB. Measured dissipation factor of the same EPR mats is presented in Figure 8-12 as a function of frequency and in Figure 8-13 as a function of aging time.

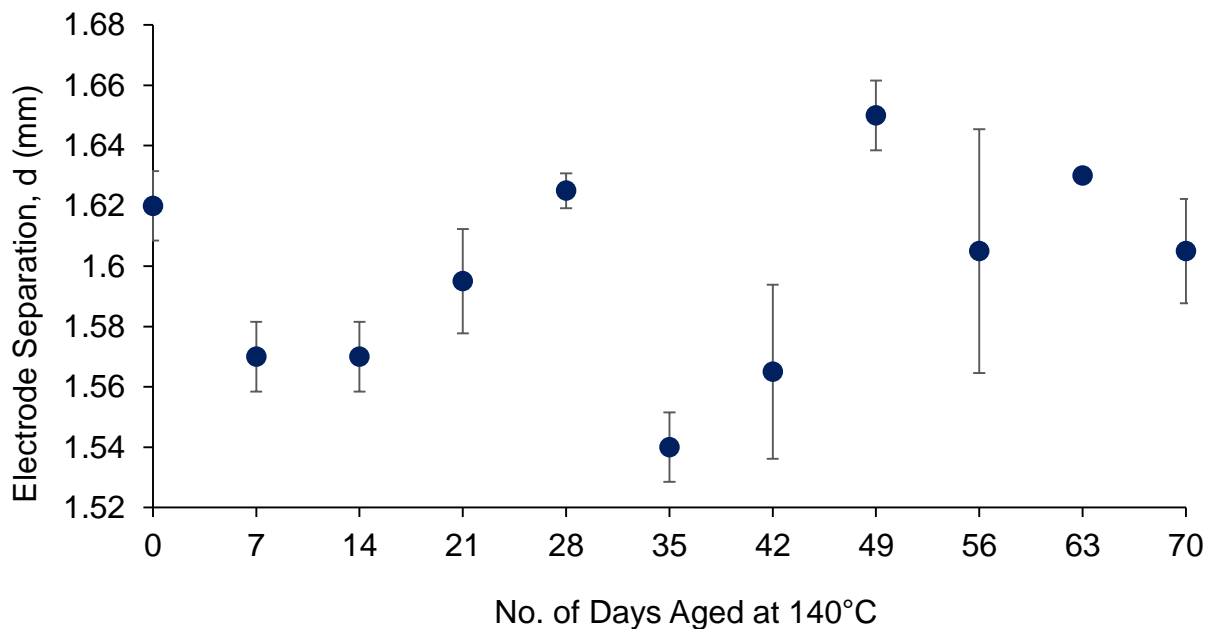


Figure 8-7. Measured mean electrode separation during capacitance measurements on samples shown in Figure 8-1 (absence of CPE). Error bars represent the standard deviation of three measured values.

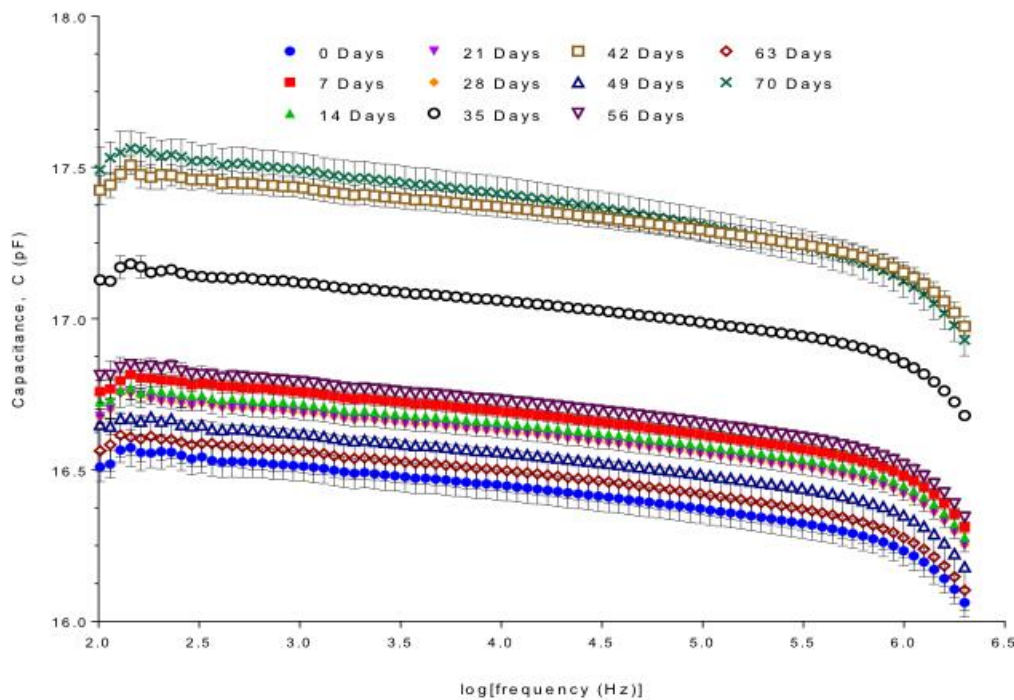


Figure 8-8. Measured capacitance of samples shown in Figure 8-1, as a function of frequency. Error bars represent the standard deviation of six measured values.

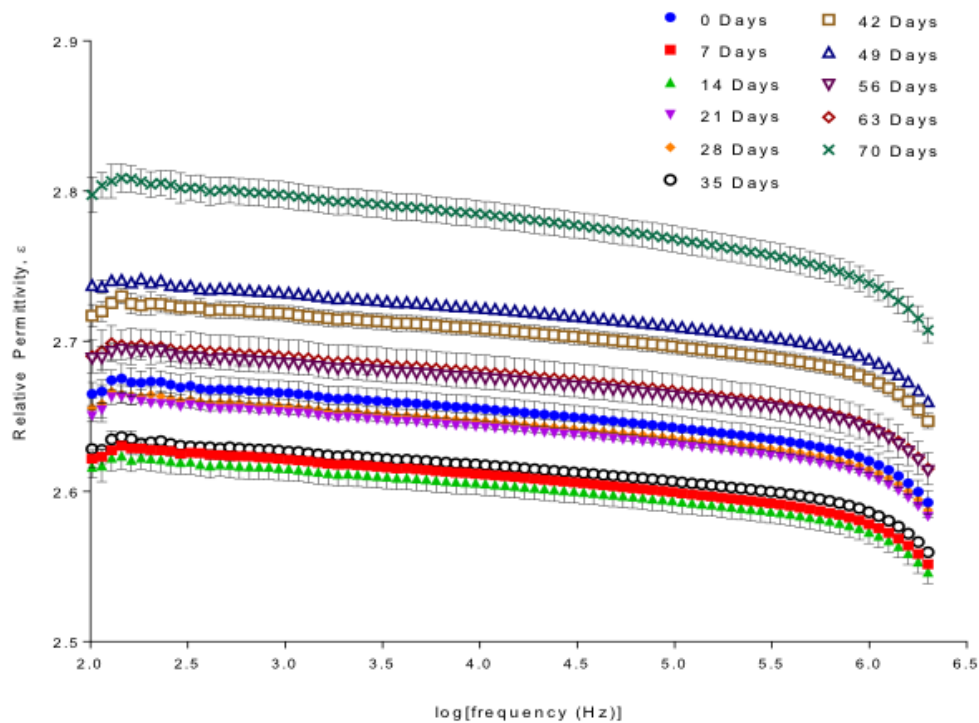


Figure 8-9. Inferred relative permittivity of EPR samples shown in Figure 8-1, as a function of frequency. Error bars represent the standard deviation of six measured values.

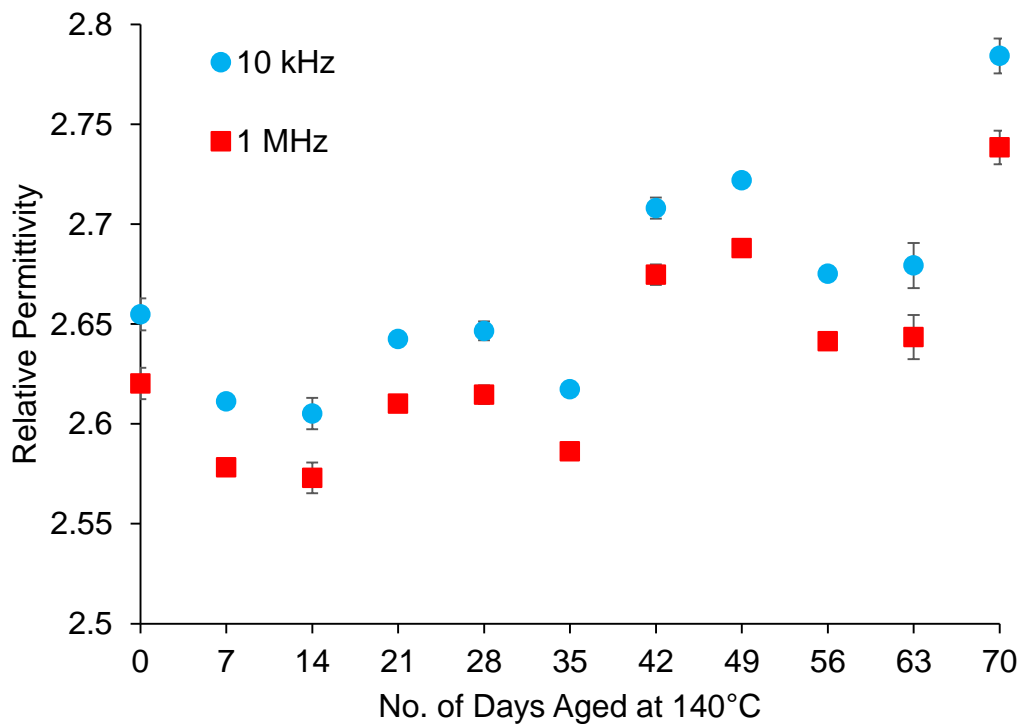


Figure 8-10. Inferred relative permittivity of EPR samples shown in Figure 8-1, at select frequencies, as a function of aging time at 140°C. Error bars represent the standard deviation of six measured values.

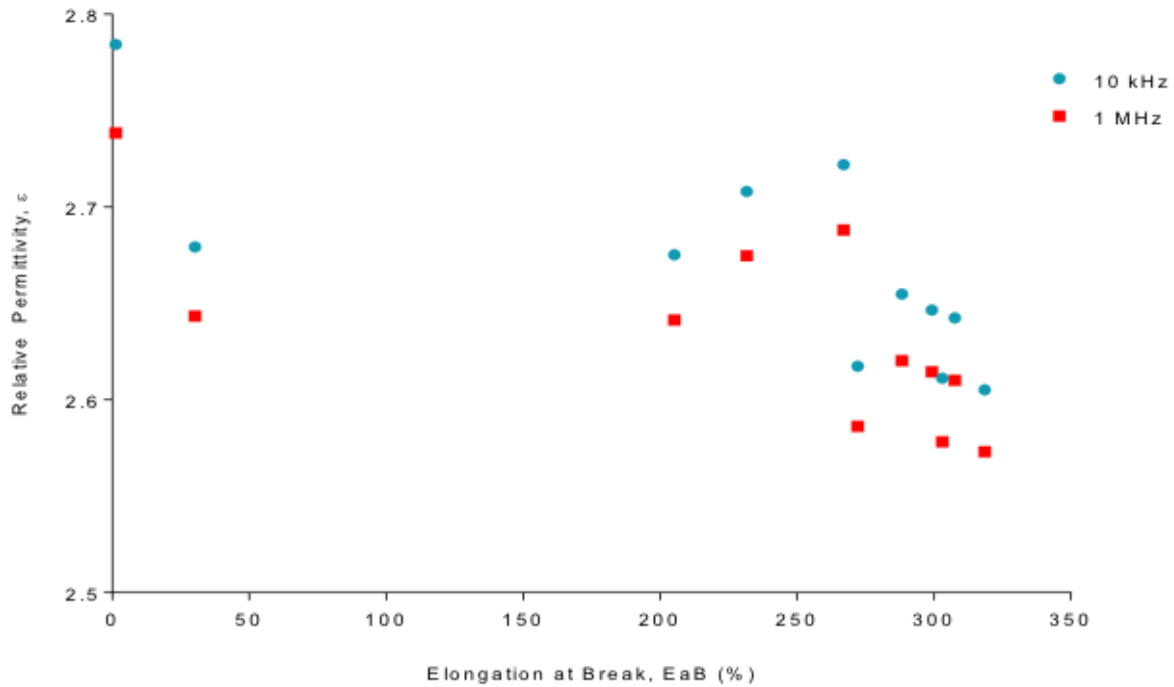


Figure 8-11. Inferred relative permittivity of EPR samples shown in Figure 8-1, at select frequencies, versus EAB.

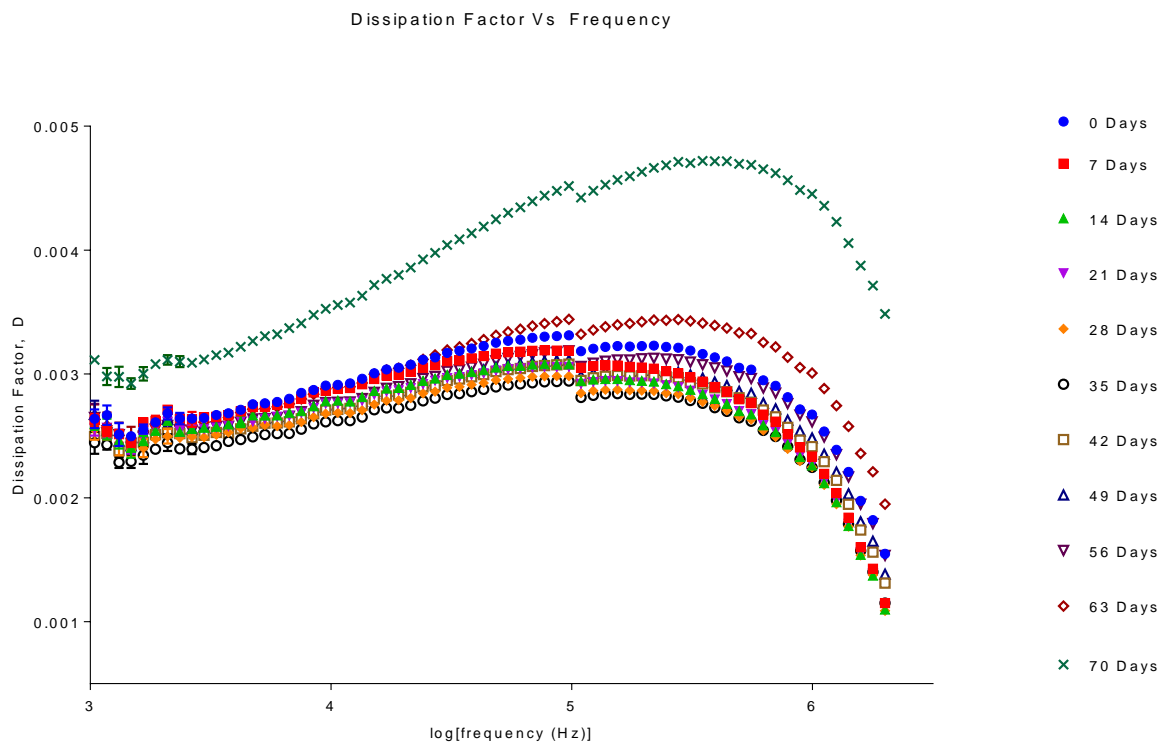


Figure 8-12. Measured dissipation factor of EPR samples shown in Figure 8-1, as a function of frequency. Error bars represent the standard deviation of four measured values. The discontinuity at  $10^5$  Hz corresponds to internal switching in the LCR meter circuitry.

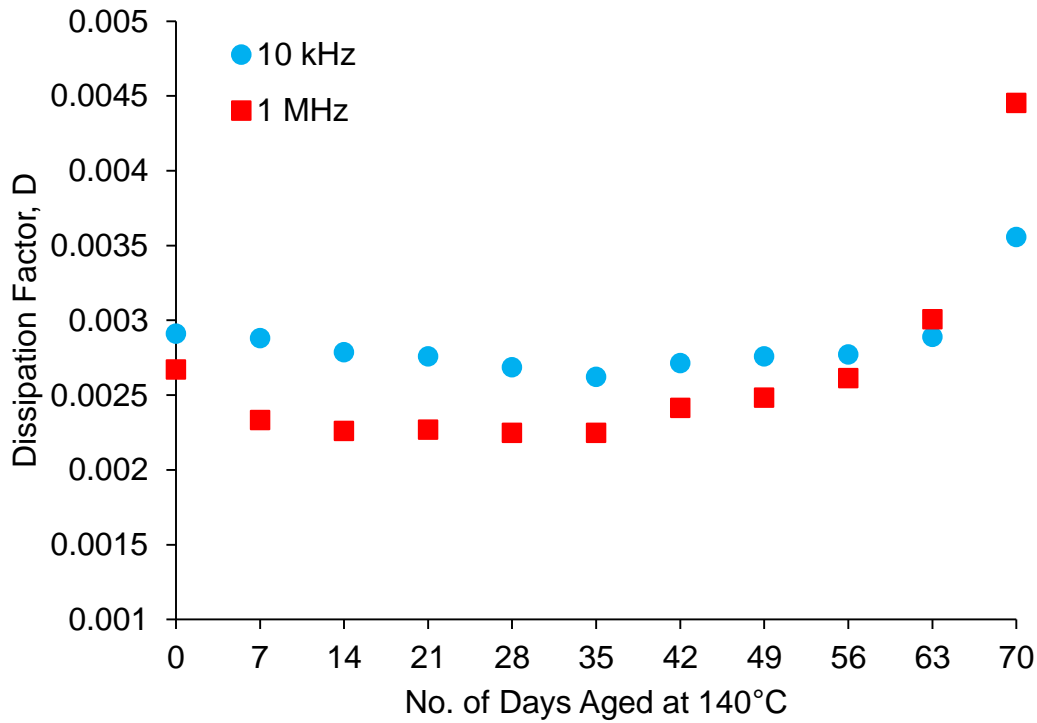


Figure 8-13. Measured dissipation factor of EPR samples shown in Figure 8-1, at select frequencies, as a function of aging time at 140°C. Error bars (smaller than the symbol size) represent the standard deviation ( $\sim 10^{-5}$ ) of six measured values.

In situ electrode separation values of the blackened EPR mats shown in Figure 8-1 are presented in Figure 8-14. Measured capacitance is presented in Figure 8-13. The in situ separation values were used in converting measured capacitance to relative permittivity via equation (5.1). Relative permittivity inferred from those measurements is presented in Figure 8-14 and Figure 8-15 as a function of frequency, in Figure 8-16 and Figure 8-15 as a function of aging time, and in Figure 8-16 and Figure 8-17 as a function of EAB. Measured dissipation factor of the same blackened EPR mats is presented in Figure 8-19 as a function of frequency and in Figure 8-20 as a function of aging time.

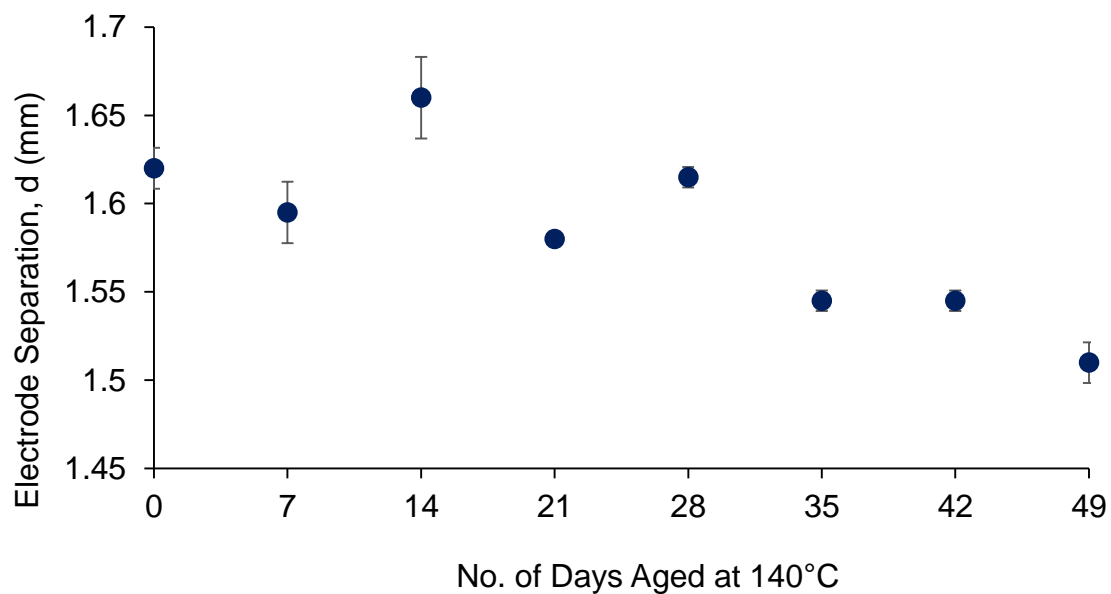


Figure 8-14. Measured mean electrode separation during capacitance measurements on blackened (in presence of CPE) EPR samples shown in Figure 8-2. Error bars represent the standard deviation of four measured values. Note, the sample aged for >14 days exhibited greater curvature than others.

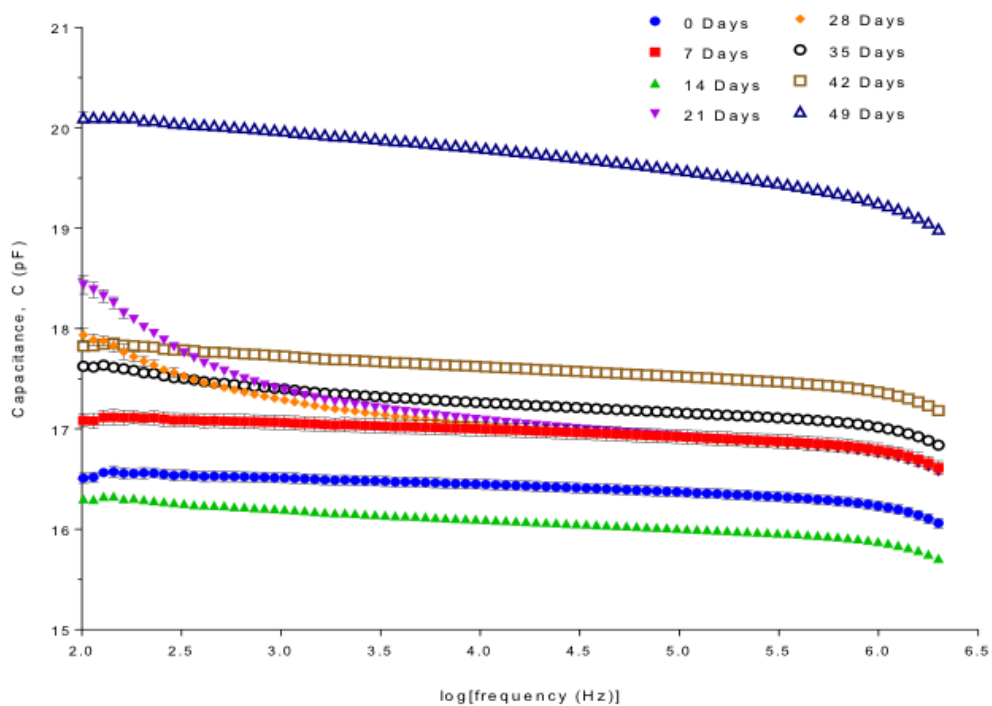


Figure 8-15. Measured capacitance of blackened (in presence of CPE) EPR samples shown in Figure 8-2, as a function of frequency. Error bars represent the standard deviation of four measured values.

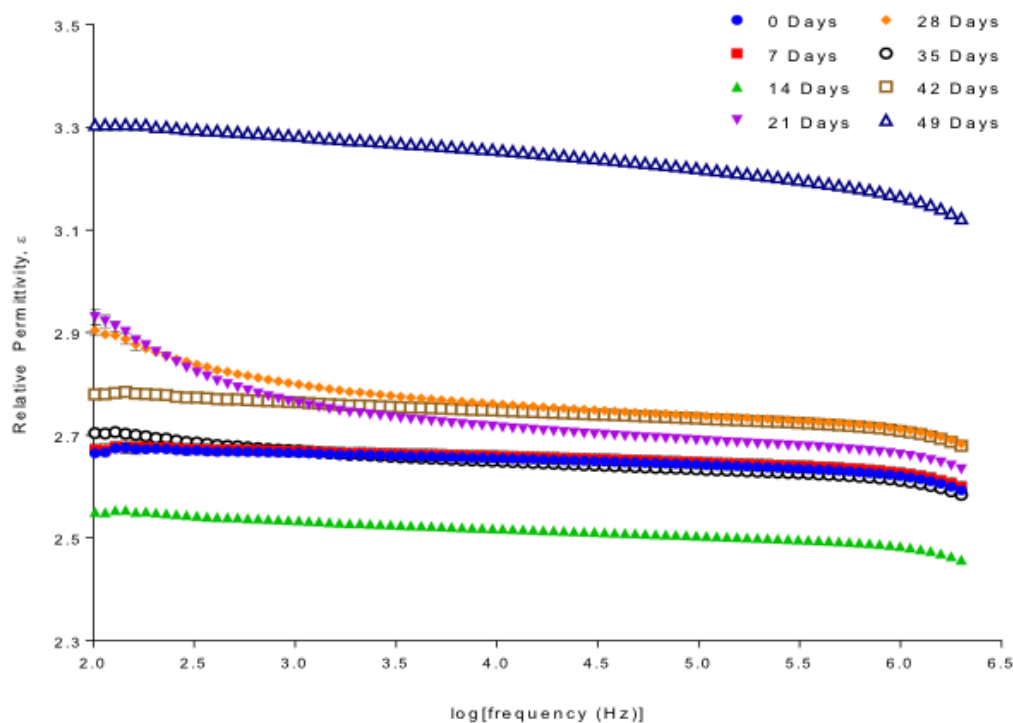


Figure 8-16. Inferred relative permittivity of blackened (in presence of CPE) EPR samples shown in Figure 8-2, as a function of frequency. Error bars represent the standard deviation of four measured values.

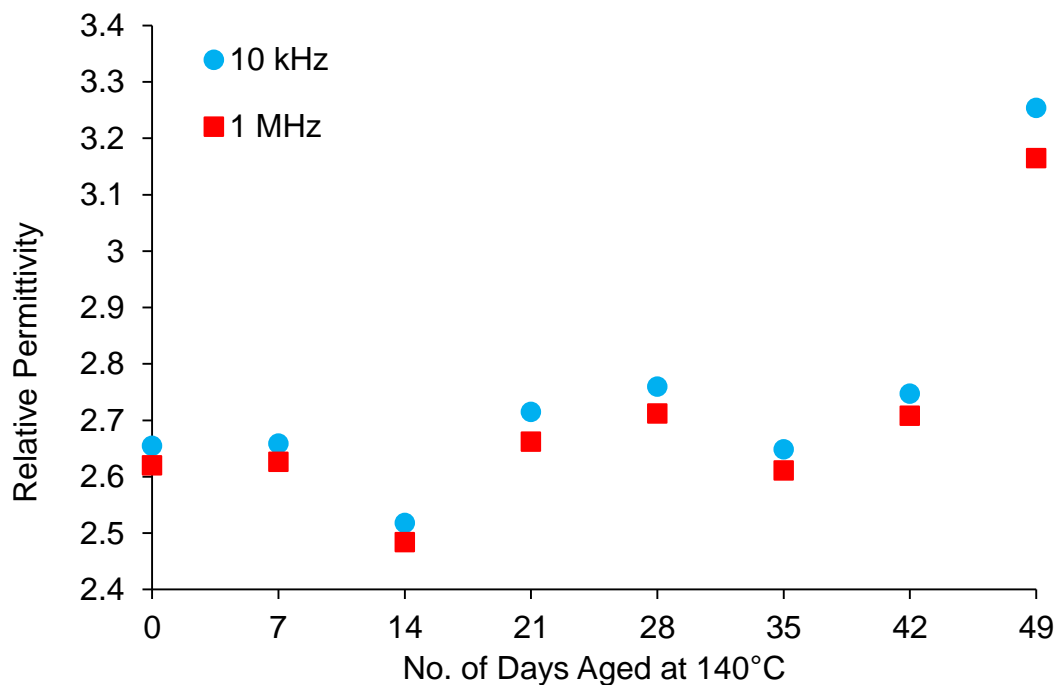


Figure 8-17. Inferred relative permittivity of blackened (in presence of CPE) EPR samples shown in Figure 8-2, at select frequencies, as a function of aging time at 140°C. Error bars represent the standard deviation of four measured values.

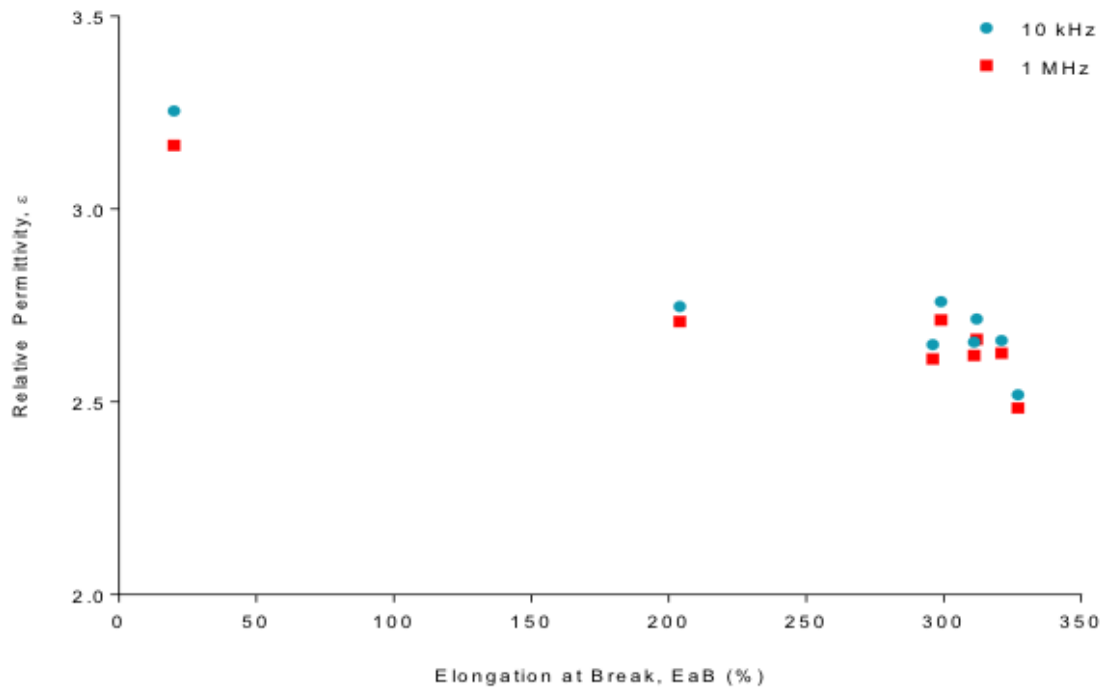


Figure 8-18. Inferred relative permittivity of blackened (in presence of CPE) EPR samples shown in Figure 8-2, at select frequencies, versus EAB.

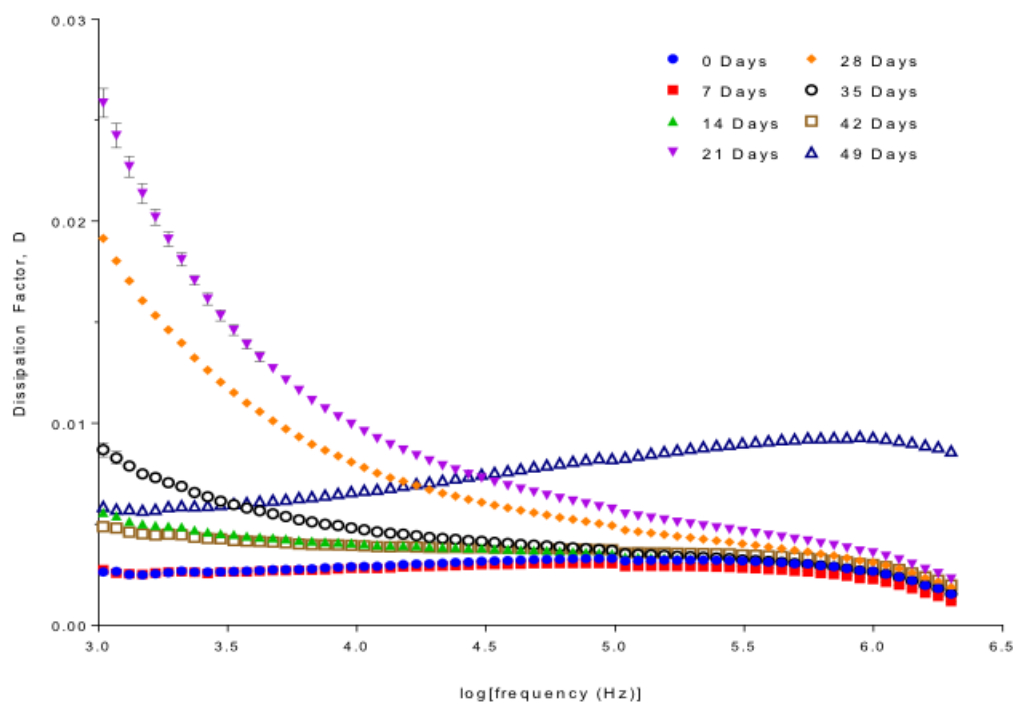


Figure 8-19. Measured dissipation factor of blackened (in presence of CPE) EPR samples shown in Figure 8-2, as a function of frequency. Error bars represent the standard deviation of four measured values. The discontinuity at  $10^5$  Hz corresponds to internal switching in the LCR meter circuitry.



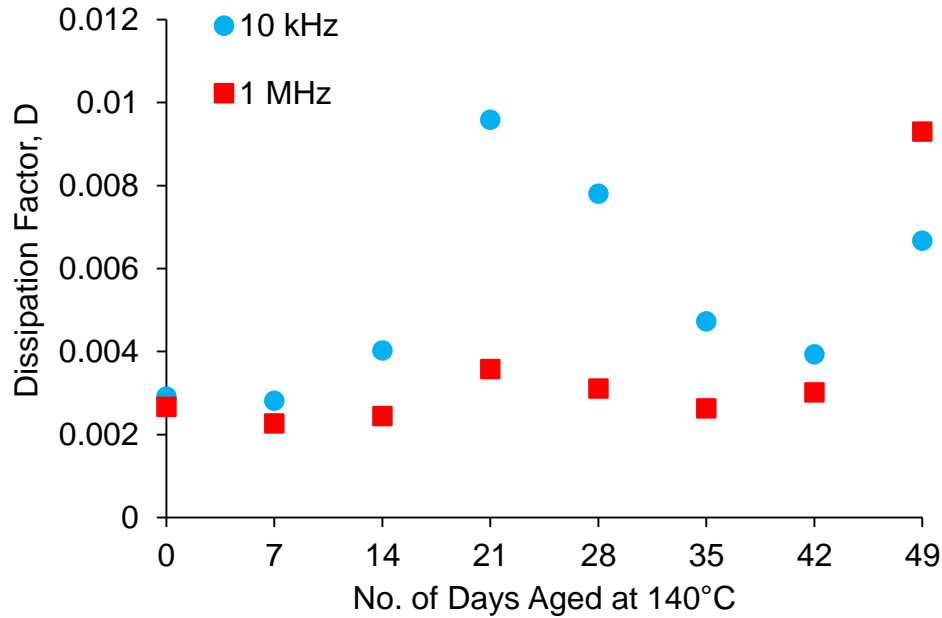


Figure 8-20. Measured dissipation factor of blackened (in presence of CPE) EPR samples shown in Figure 8-2, at select frequencies, as a function of aging time at 140°C. Error bars (smaller than the symbol size) represent the standard deviation ( $\sim 10^{-5}$ ) of four measured values.

### 8.1.3.2 CPE mats

In situ electrode separation values of the CPE mats whose direct thickness measurements are plotted in Figure 8-5 are presented in Figure 8-21. Measured capacitance is presented in Figure 8-22. The in situ separation values presented in Figure 8-21 were used in converting measured capacitance to relative permittivity via equation (5.1). Relative permittivity inferred from those measurements is presented in Figure 8-23 as a function of frequency and in Figure 8-24 as a function of aging time. Measured dissipation factor of the same CPE mats is presented in Figure 8-25 as a function of frequency and in Figure 8-26 as a function of aging time.

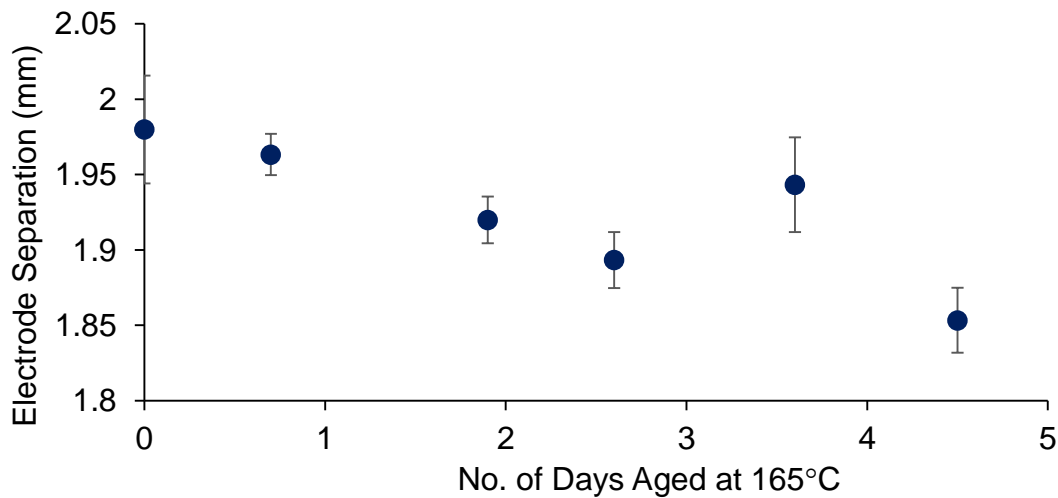


Figure 8-21. Measured mean electrode separation during capacitance measurements on CPE samples whose direct thickness measurements are plotted in Figure 8-5. Error bars represent the standard deviation of six measured values.

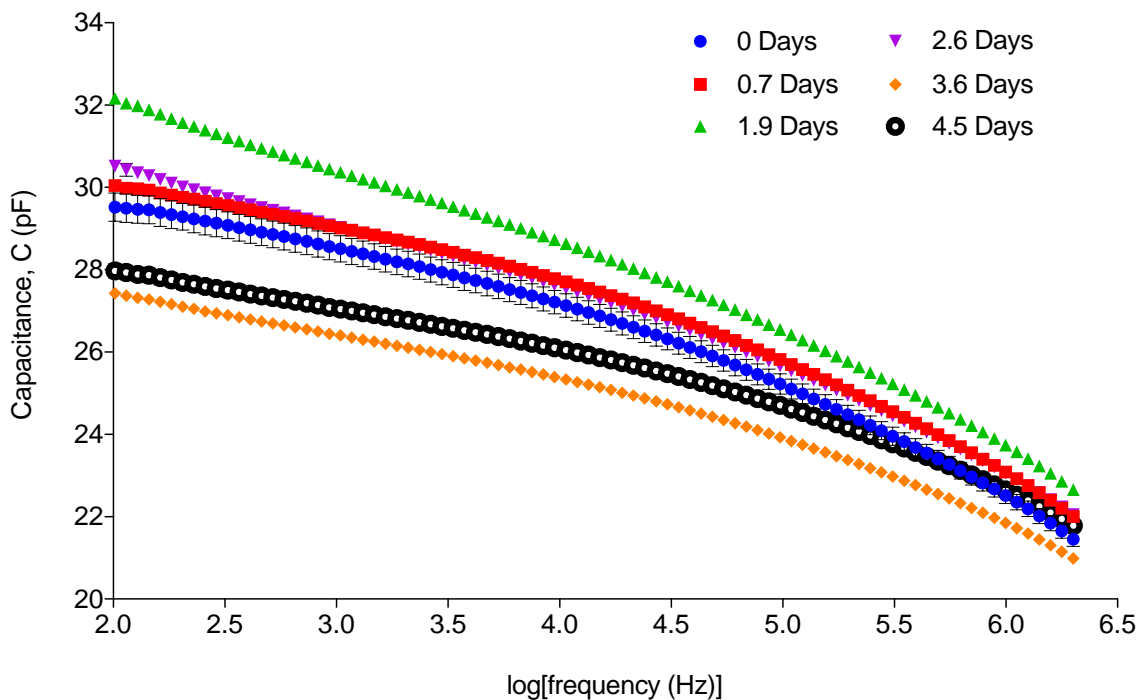


Figure 8-22. Measured capacitance of CPE samples aged at 165°C, as a function of frequency. Error bars represent the standard deviation of six measured values.

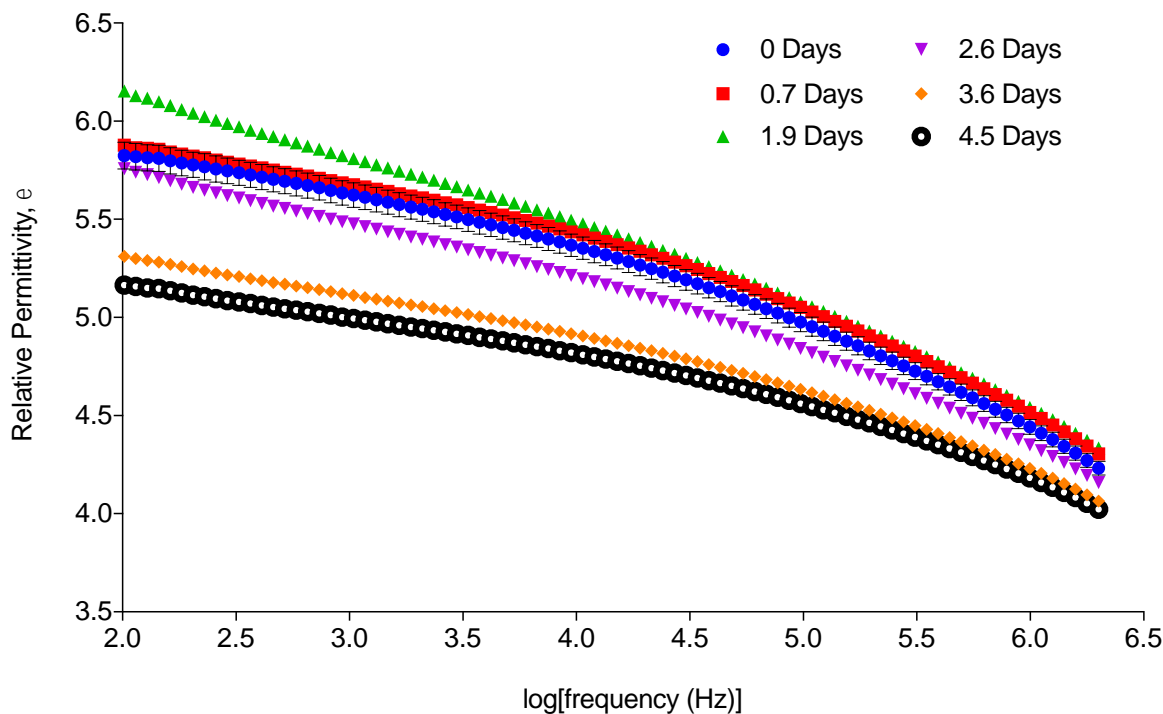


Figure 8-23. Inferred relative permittivity of CPE samples aged at 165°C, as a function of frequency. Error bars represent the standard deviation of six measured values.

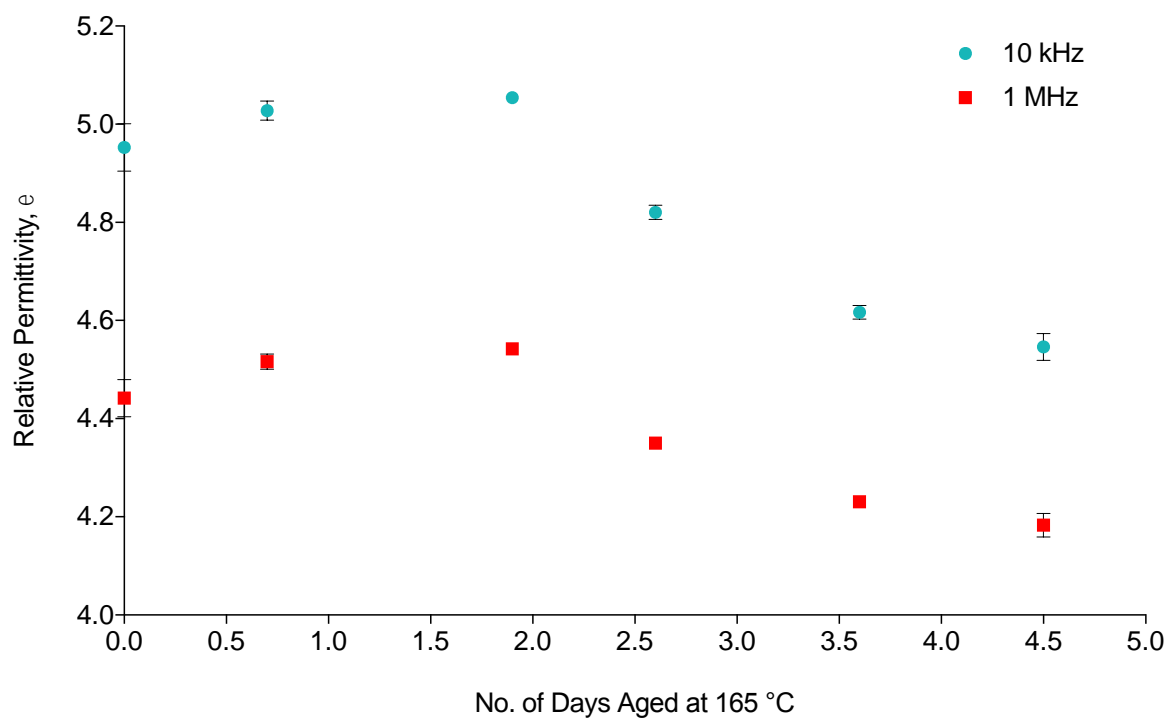


Figure 8-24. Inferred relative permittivity of CPE samples aged at 165°C, at select frequencies, as a function of aging time. Error bars represent the standard deviation of six measured values.

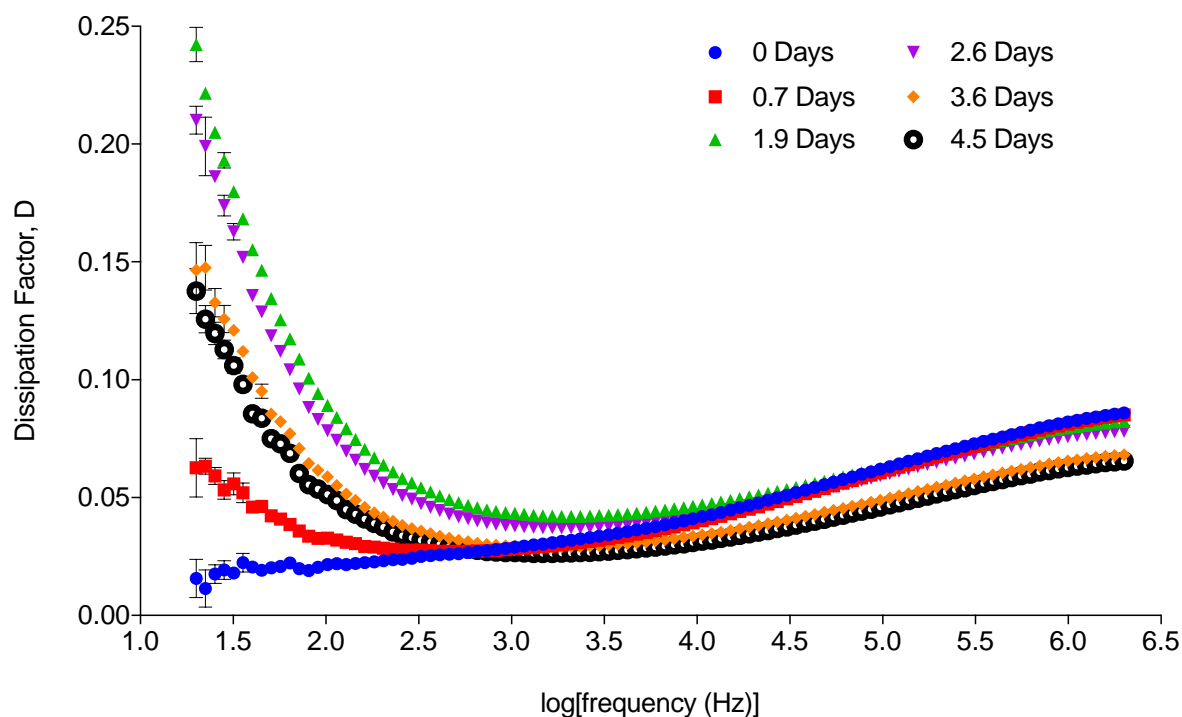


Figure 8-25. Measured dissipation factor of CPE samples aged at 165°C, as a function of frequency. Error bars represent the standard deviation of four measured values. The discontinuity at  $10^5$  Hz corresponds to internal switching in the LCR meter circuitry.

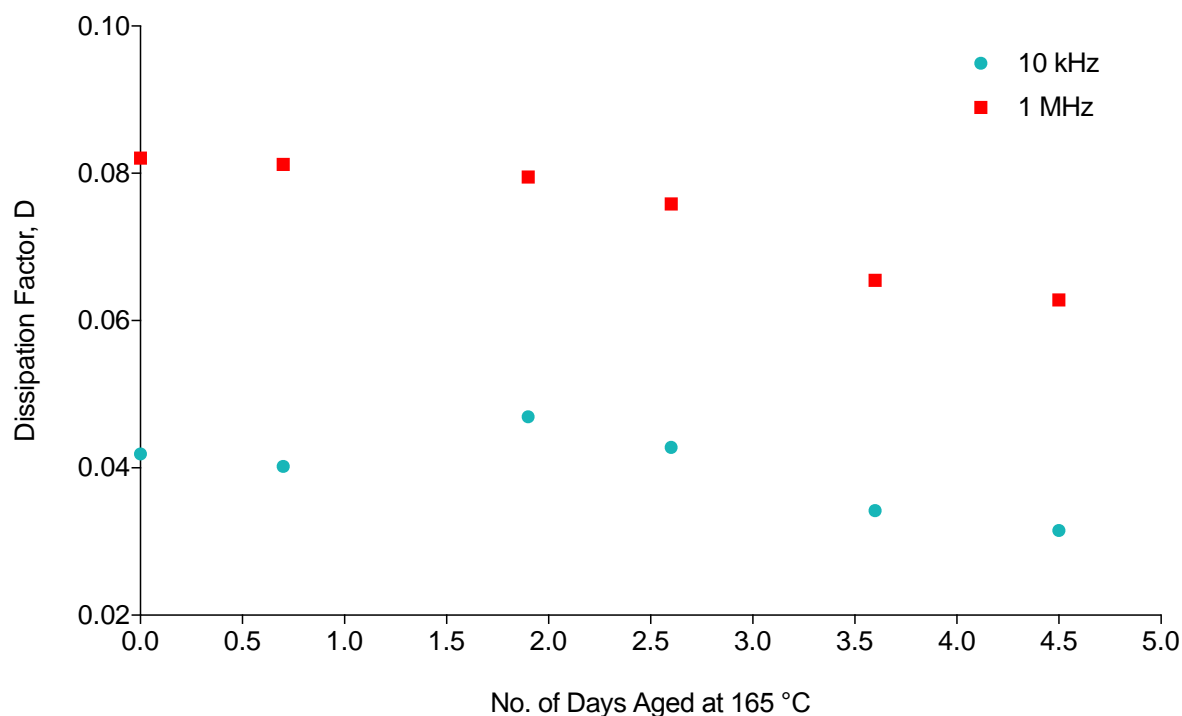


Figure 8-26. Measured dissipation factor of CPE samples aged at 165°C, at select frequencies, as a function of aging time. Error bars (smaller than the symbol size) represent the standard deviation ( $\sim 10^{-5}$ ) of six measured values.

#### 8.1.4 Flat-Plate Flat Sample Measurement Discussion

Comparing sample thickness values, measured directly (Figure 8-3, Figure 8-4, and Figure 8-5, with those measured in situ as electrode separation while capacitance was being measured, Figure 8-7, Figure 8-14, and Figure 8-21, it is found that electrode separation and sample thickness follow a similar trend but the values measured during in situ capacitance measurement are approximately 0.02 mm (1%) and 0.05 mm (3%) larger than those measured by the micrometer, on EPR and blackened EPR mats, respectively. One reason for this may be the spring loading of the micrometer and its relatively small tip (approximately 2 mm radius) causing some compression or indentation of the EPR sample surface during the thickness measurement. In the case of CPE, the sample thickness values measured directly and those measured as electrode separation are similar. Electrode separation was used in equation (5.1) to infer permittivity from measured capacitance.

Comparing, for example, Figure 8-8 and Figure 8-9 it can be seen that converting from capacitance (a measured parameter) to relative permittivity (a material parameter) serves to show that the material changes with aging time increase somewhat linearly for non-blackened EPR, as shown in Figure 8-10. Smoother trends are observed in dissipation factor, plotted as a function of aging time in Figure 8-13. Note also that the dissipation factor of non-blackened EPR is low, Figure 8-13, on the order of 0.001. This contrasts strongly with the dissipation factor of CPE, Figure 8-26, which is on the order of 0.05 for the same frequencies. Relative permittivity of blackened EPR samples also increases with aging time, Figure 8-17.

## 8.2 IDC Experiments on Jacketed Cable

### 8.2.1 Sample Preparation

Two sets of Okoguard®-Okolon® TS-CPE Type MV-90 2.4kV Nonshielded Power Cable samples with nominal outer diameter 22.4 mm, fully jacketed (Section 8.2.1.1) and part-jacketed (Section 8.2.1.2), were aged by laying them on a rack inside an air-circulating oven that was maintained at a pre-selected accelerated aging temperature, with the goal of inducing aging representative of longer-term aging in normal service environment (jacketing was removed after aging, not before). As described in Section 8.1.2, sample diameters were measured at ten locations on each sample, using digital calipers with systematic uncertainty of 0.1 mm, and the mean diameter values with standard deviation computed. Accurate dimensions are important for obtaining permittivity from measured capacitance. For cable samples, permittivity was inferred from measured capacitance by inserting known geometrical and material parameters into a COMSOL™ model and adjusting permittivity in the model until the measured capacitance was matched.

#### 8.2.1.1 Fully-jacketed sample set

Okoguard®-Okolon® TS-CPE Type MV-90 2.4kV Nonshielded Power Cable samples, Figure 8-27, were aged at 140°C for up to 63 days in seven-day increments. Mean diameter values with standard deviation (error bars) are plotted in Figure 8-28.



Figure 8-27. EPR/TS-CPE cable samples aged at 140°C for various durations up to 63 d in 7 d increments. The sample ends were sealed with foil during aging.

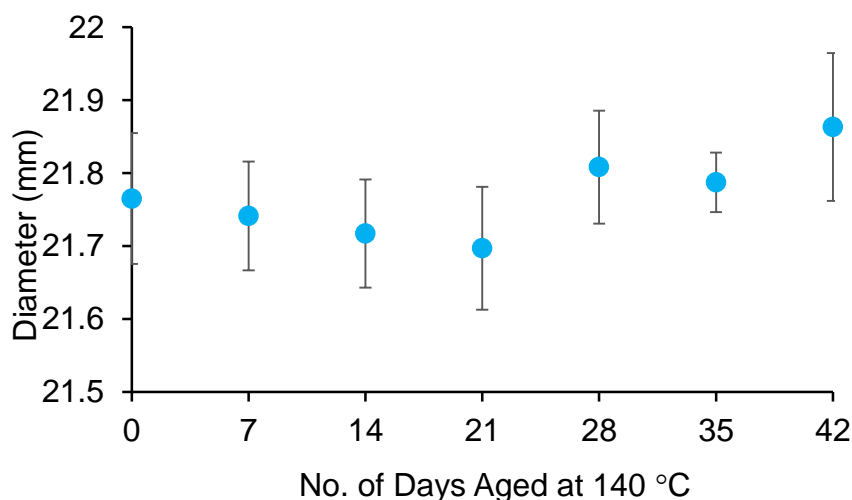


Figure 8-28. Measured mean outer diameter values of samples shown in Figure 8-27. Error bars represent the standard deviation of ten measured values.

### 8.2.1.2 Part-jacketed sample set

Okoguard®-Okolon® TS-CPE Type MV-90 2.4kV Nonshielded Power Cable samples, Figure 8-29, were aged at 140°C for up to 35 days in seven-day increments. Mean diameter values with standard deviation (error bars) are plotted in Figure 8-30 and Figure 8-31 for the jacketed and non-jacketed regions, respectively.



Figure 8-29. EPR/TS-CPE cable samples aged at 140°C for up to 35 d in 7 d increments. After aging, part of the jacket was removed.

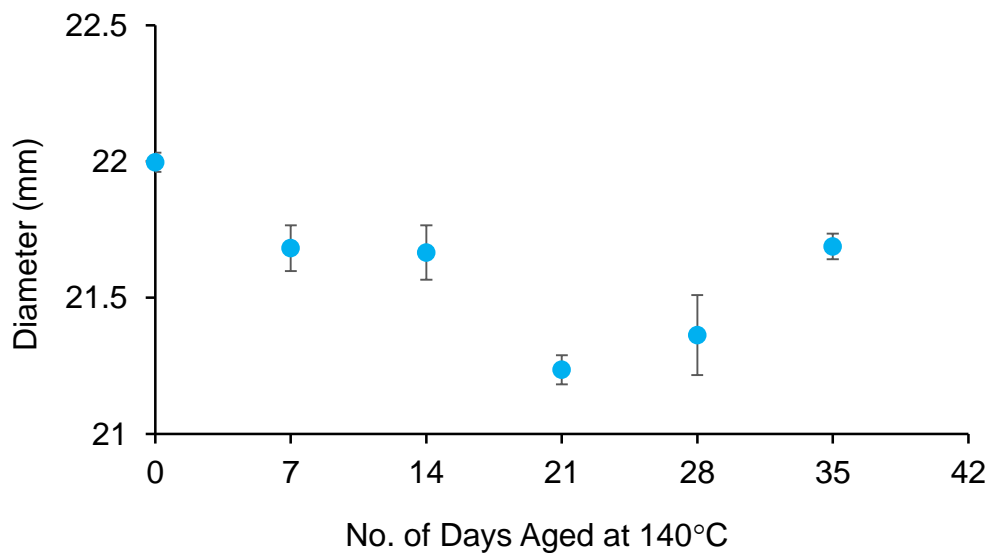


Figure 8-30. Measured mean outer diameter values (jacketed region) of samples shown in Figure 8-29. Error bars represent the standard deviation of ten measured values.

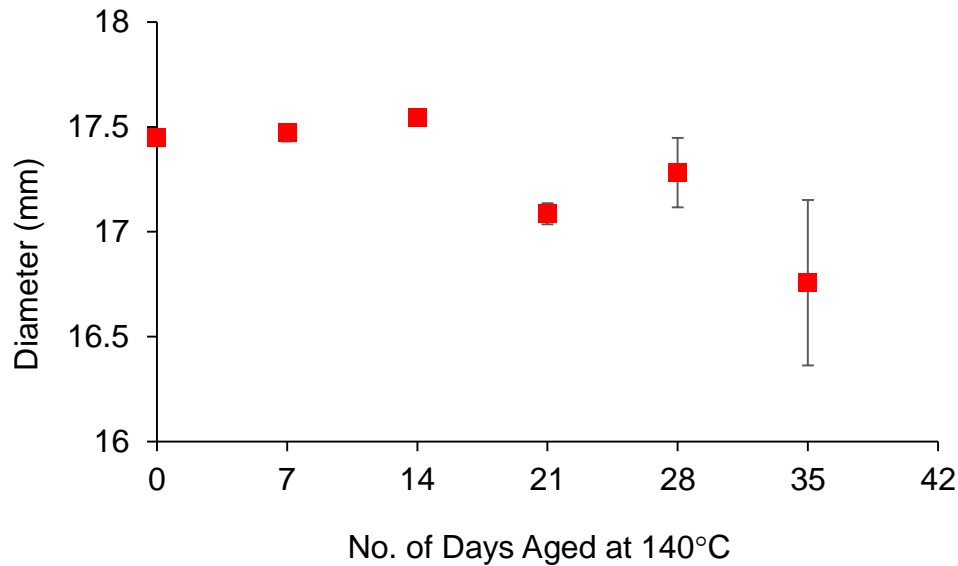


Figure 8-31. Measured mean diameter values (non-jacketed region) of samples shown in Figure 8-29. Error bars represent the standard deviation of ten measured values.

## 8.2.2 Measurement Setup

A first set of measurements was taken with “Sensor 0”,  $g = 0.1$  mm, described in Table 7-1, in order to establish permittivity of the material close to the electrodes without introducing errors from the influence of underlying material. Measurements were performed on the fully-jacketed sample set, Figure 8-27, and, in the case of the part-jacketed sample set, on both the CPE jacket and the EPR insulation from which the jacket had been removed.

## 8.2.3 Results

### 8.2.3.1 Fully-jacketed sample set

Measured capacitance of the CPE jacket, for the fully-jacketed sample set, is presented in Figure 8-32 and permittivity inferred from those measurements (obtained by COMSOL™ modeling using appropriate dimensions for each sample) is presented in Figure 8-33. Differential permittivity where the value measured on the pristine sample has been subtracted is shown as a function of aging time, for select frequencies, in Figure 8-34. Measured dissipation factor of the CPE jacket, for the fully-jacketed sample set, is presented in Figure 8-35. Differential dissipation factor, from which the values measured on the pristine sample have been subtracted, is presented as a function of aging time in Figure 8-36.

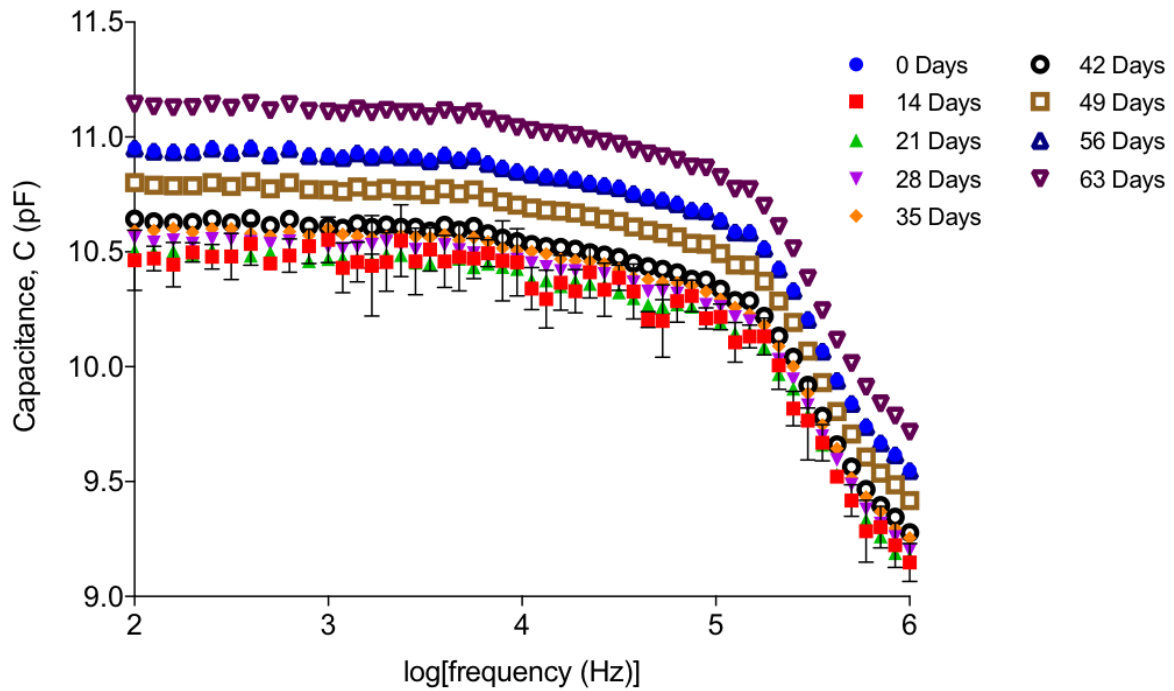


Figure 8-32. Measured capacitance of the CPE jacket of Okoguard® -Okolon® TS-CPE Type MV-90 2.4kV Nonshielded Power Cable samples, as a function of frequency.

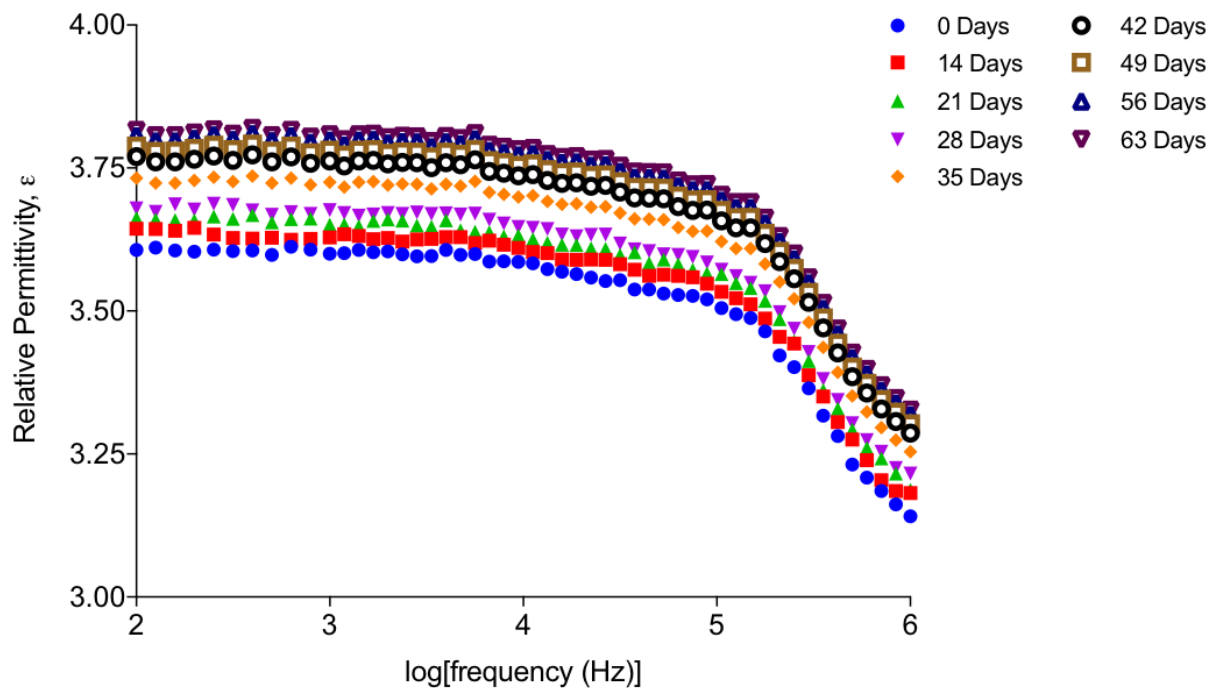


Figure 8-33. Inferred relative permittivity of the CPE jacket of Okoguard® -Okolon® TS-CPE Type MV-90 2.4kV Nonshielded Power Cable samples, as a function of frequency.



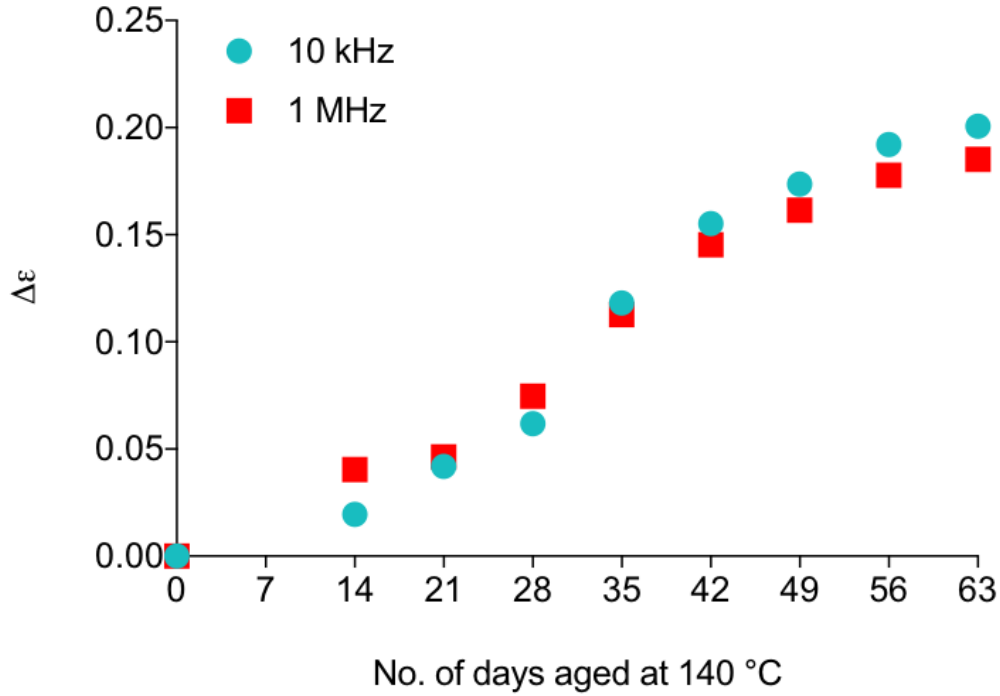


Figure 8-34. Inferred relative permittivity of CPE jacket of Okoguard® -Okolon® TS-CPE Type MV-90 2.4kV Nonshielded Power Cable samples normalized with respect to data for the pristine sample, at select frequencies, as a function of aging time.

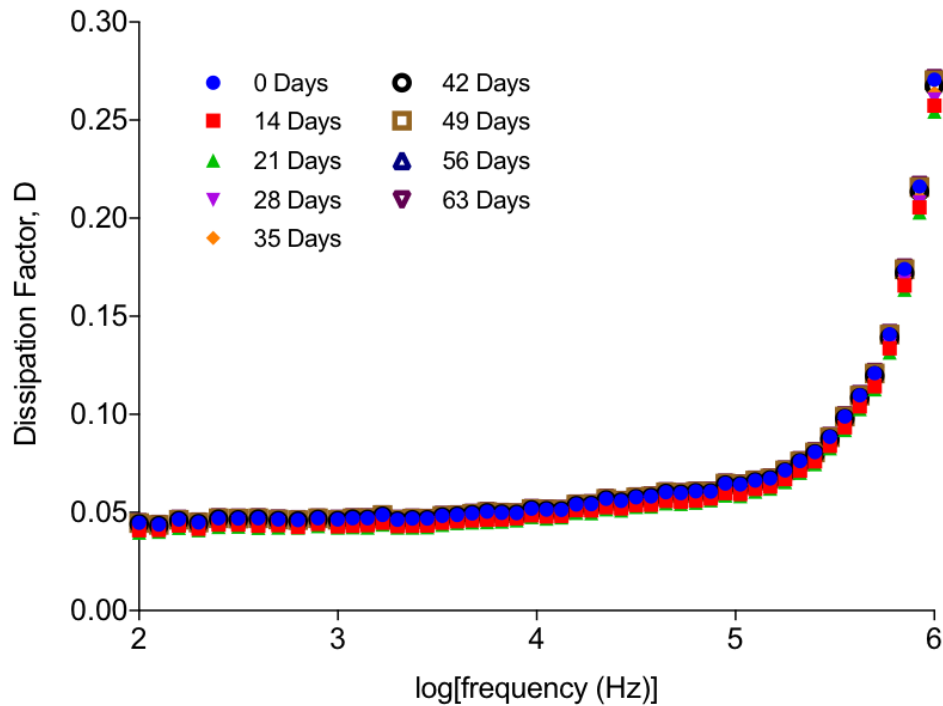


Figure 8-35. Dissipation factor of the CPE jacket of Okoguard® -Okolon® TS-CPE Type MV-90 2.4kV Nonshielded Power Cable samples, as a function of frequency.

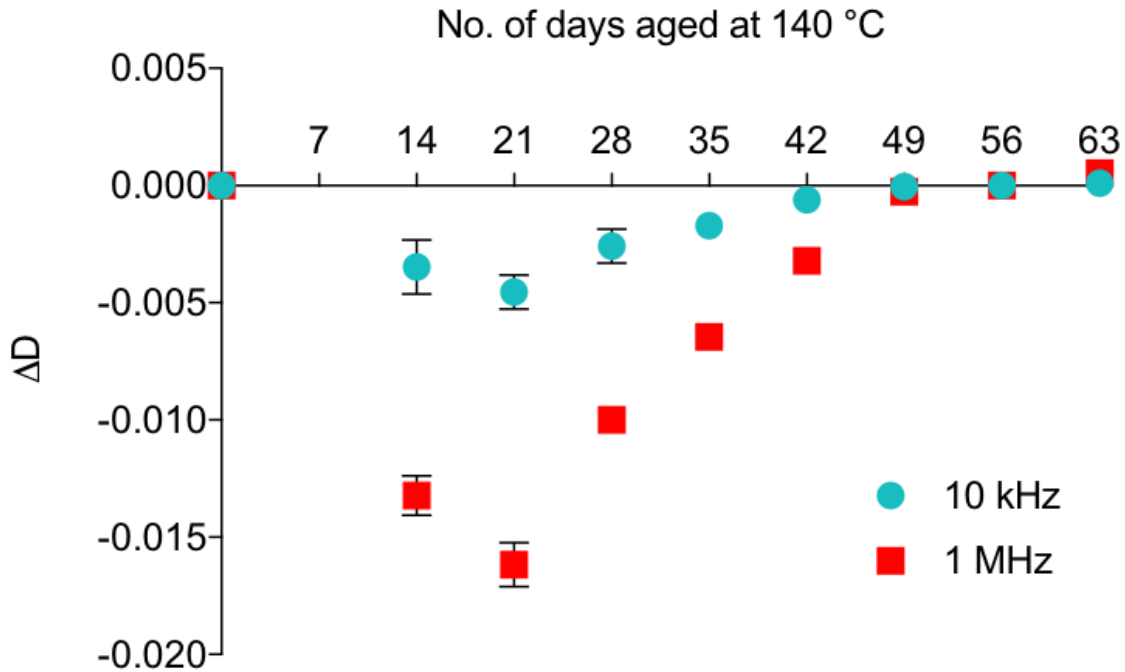


Figure 8-36. Dissipation factor of CPE jacket of Okoguard® -Okolon® TS-CPE Type MV-90 2.4kV Nonshielded Power Cable samples normalized with respect to data for the pristine sample, at select frequencies, as a function of aging time.

### 8.2.3.2 Part-jacketed sample set

Measured capacitance of the CPE jacket is presented in Figure 8-37 and permittivity inferred from those measurements (obtained by COMSOL™ modeling using appropriate dimensions for each sample) is presented in Figure 8-38. Differential permittivity where the value measured on the pristine sample has been subtracted is shown on an expanded scale Figure 8-39.

Measured capacitance of the EPR insulation is presented in Figure 8-40 and permittivity inferred from those measurements (obtained by COMSOL™ modeling using appropriate dimensions for each sample) is presented in Figure 8-41. Differential permittivity, from which the values measured on the pristine sample have been subtracted, is presented in Figure 8-42.

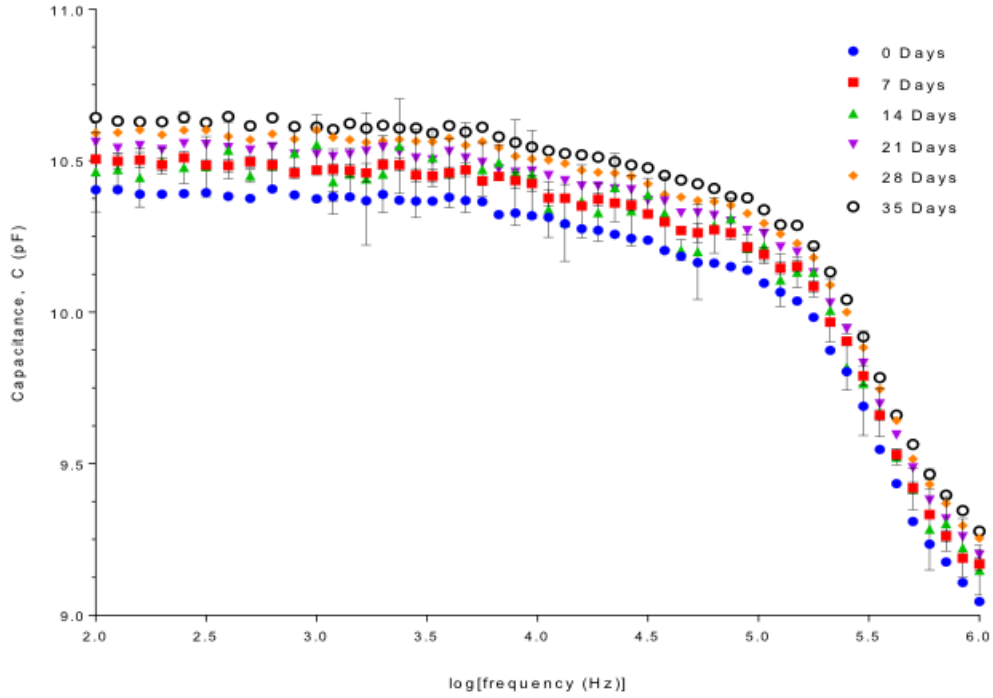


Figure 8-37. Measured capacitance of the CPE jacket of Okoguard® -Okolon® TS-CPE Type MV-90 2.4kV Nonshielded Power Cable samples, as a function of frequency.

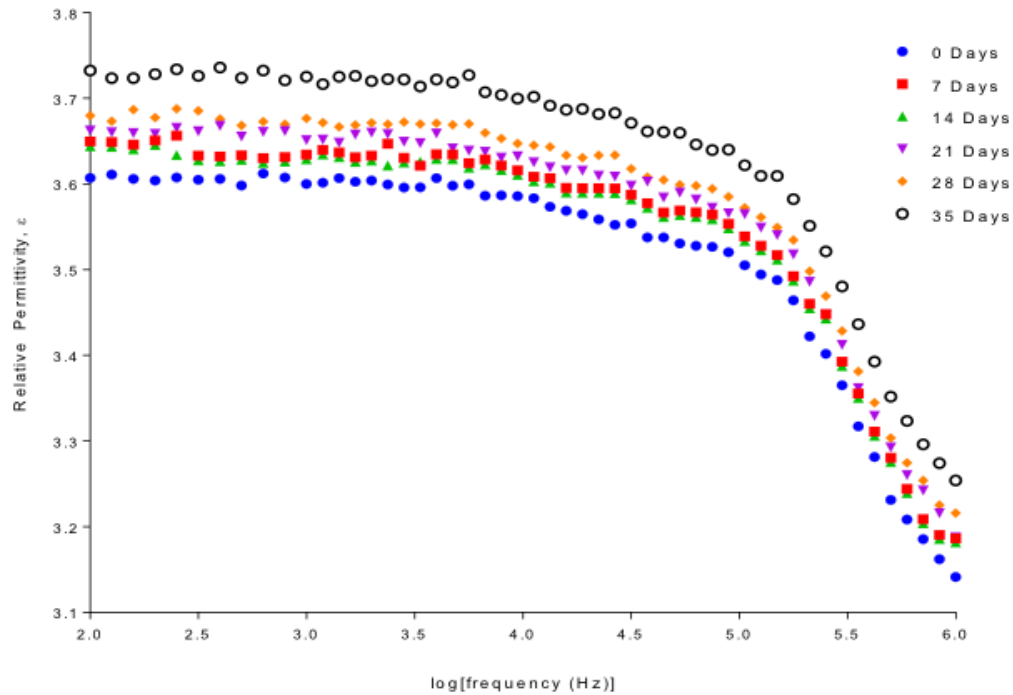


Figure 8-38. Inferred relative permittivity of the CPE jacket of Okoguard® -Okolon® TS-CPE Type MV-90 2.4kV Nonshielded Power Cable samples, as a function of frequency.

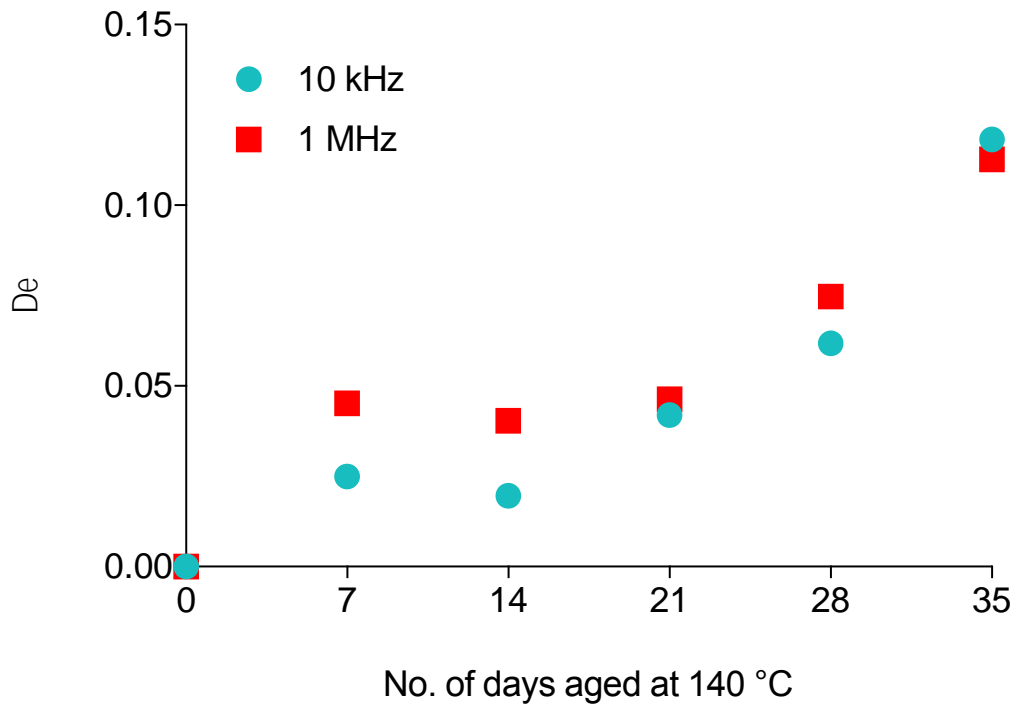


Figure 8-39. Inferred relative permittivity of CPE jacket of Okoguard® -Okolon® TS-CPE Type MV-90 2.4kV Nonshielded Power Cable samples normalized with respect to data for the pristine sample, at select frequencies, as a function of aging time.

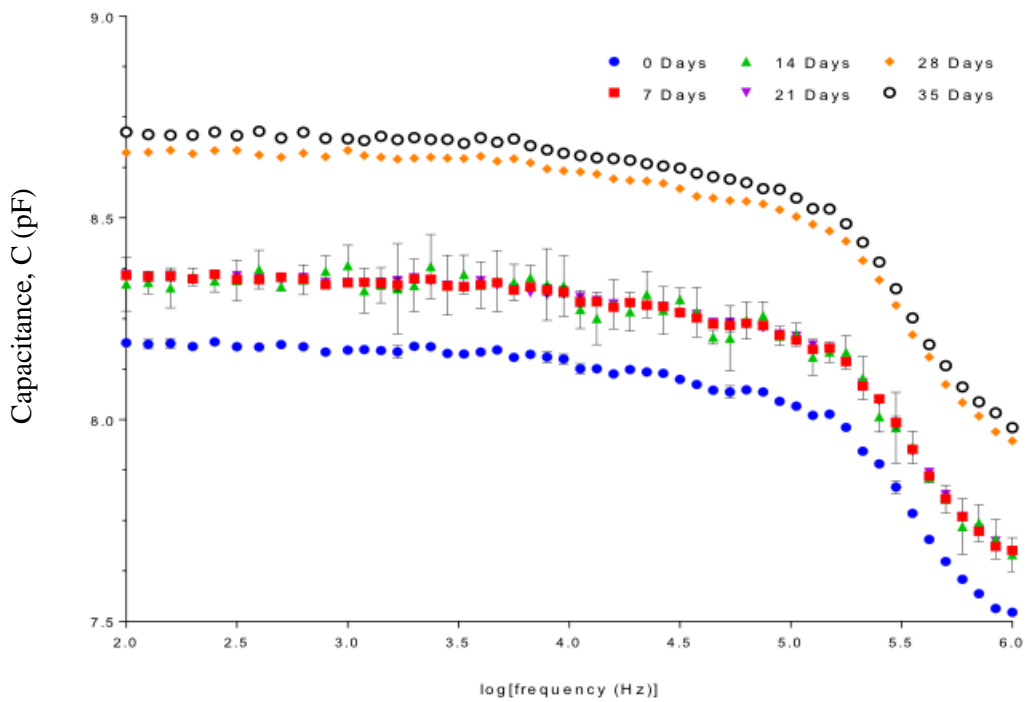


Figure 8-40. Measured capacitance of Okoguard® -Okolon® TS-CPE Type MV-90 2.4kV Nonshielded Power Cable samples insulation, as a function of frequency.

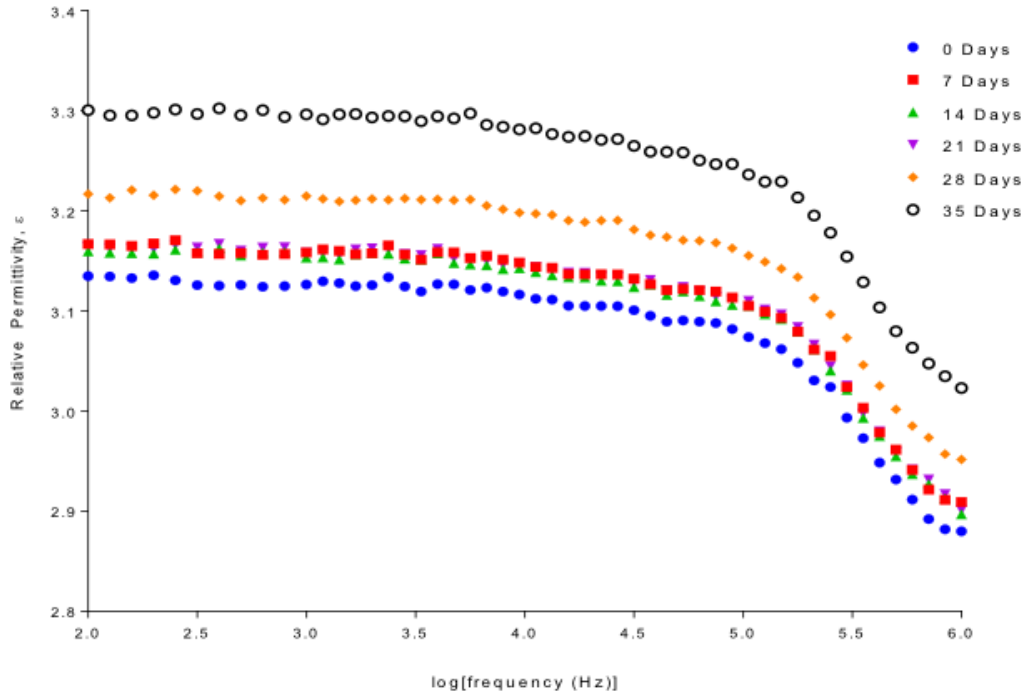


Figure 8-41. Inferred relative permittivity of the EPR insulation of Okoguard® -Okolon® TS-CPE Type MV-90 2.4kV Nonshielded Power Cable samples, as a function of frequency.

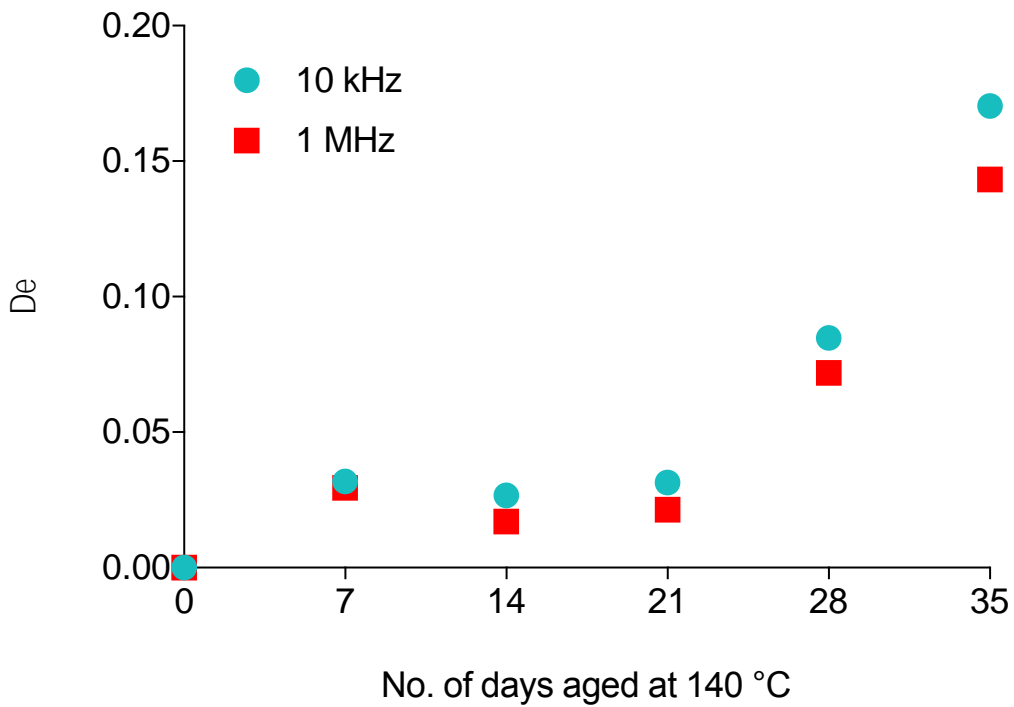


Figure 8-42. Inferred relative permittivity of EPR insulation of Okoguard® -Okolon® TS-CPE Type MV-90 2.4kV Nonshielded Power Cable samples normalized with respect to data for the pristine sample, at select frequencies, as a function of aging time.

## 8.2.4 Discussion

The relative permittivity of CPE jacket measured on the fully-jacketed and part-jacketed sample sets shows good agreement, Figure 8-33 and Figure 8-38. The relative permittivity of CPE jacket increases by approximately 6%, over the 63 days of aging studied on the fully-jacketed sample set, Figure 8-34. The relative permittivity of EPR increases by approximately 6% over 35 days of aging measured on the part-jacketed sample set, Figure 8-41. Change in dissipation factor,  $\Delta D$ , shows a variety of behaviors depending upon the sample material and frequency selected. Figure 8-12 and Figure 8-13 show an increasing trend with aging of EPR for more than ~60 days, against a background of low loss ( $D \sim 0.003$ ). For blackened EPR, dissipation factor shows a much more complex behavior, (Figure 8-19 and Figure 8-20) likely due to the surface modification of the EPR during aging in the presence of CPE. In fact, these characteristics are reflected in the dissipation factor measured upon CPE itself, Figure 8-25, although the magnitude of  $D$  is much higher in the latter case.

The relative % changes in inferred permittivity and dissipation factor from pristine to maximum aged state are collected in Figure 8-43. The general trend shows the dissipation factor to be more sensitive to age-related material changes than inferred permittivity is seen to be. The % change between lower frequency (10 kHz) and higher frequency (1 MHz) data was not obviously different.

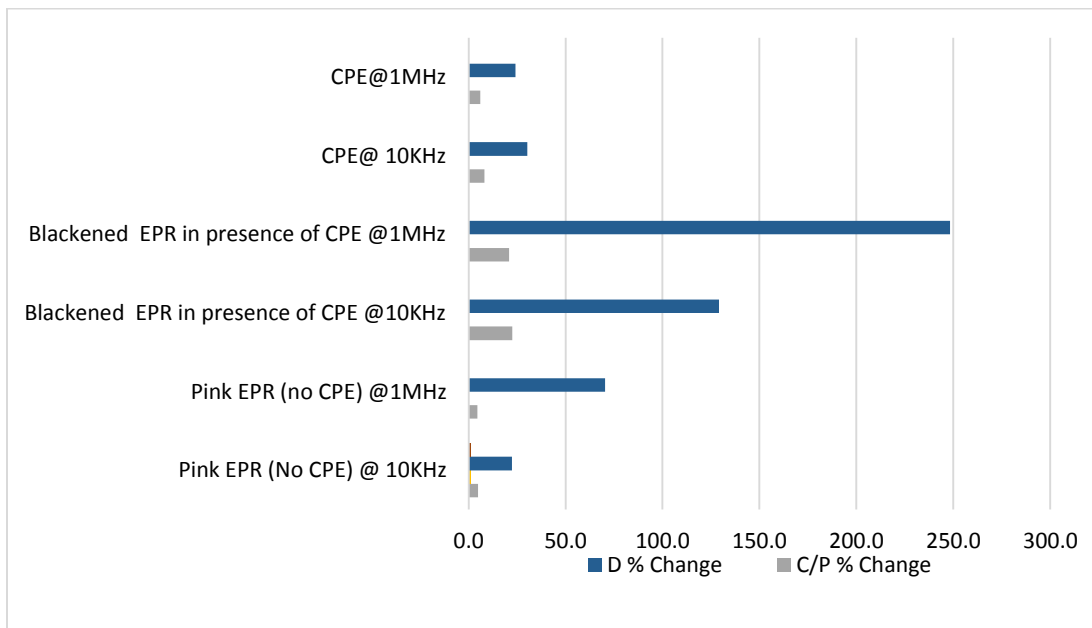


Figure 8-43. % change of dissipation factor ( $D$ ) and relative permittivity and similarly capacitance ( $C/P$ ) for EPR and CPE material of this study between initial and extreme aging points for the materials.

## **8.2.5 Future Work**

### **8.2.5.1 *XLPE samples***

Indenter is known to have difficulties with XLPE polymers (IAEA 2012); EPRI (2011), but IDC measurements are known to be sensitive to water-tree damage in power cables (Liu Yonghong 2015; Liu et al. 2015)—an important damage mechanism in XLPE. Accelerated XLPE thermal and radiation aging is significantly more challenging than EPR accelerated aging requiring months rather than weeks to achieve meaningful degradation. However, exploration of an IDC test for XLPE could fill an important gap.

## 9. CONCLUSIONS

A substantial body of work suggests feasibility to measure cable jacket and insulation conditions using various forms of IDC sensors. Specific measures used in this work are:

- Capacitance and inferred permittivity at relatively low frequency (10 kHz)
- Dissipation factor at relatively low frequency (10 kHz)
- Capacitance and inferred permittivity at relatively high frequency (1 MHz)
- Dissipation factor at relatively high frequency (1 MHz)

The sensitivity to insulation degradation was good for inferred permittivity but the most sensitive indicator for the samples examined was the dissipation factor provided that measurement frequency is selected judiciously.

- FEM models predict sensor behavior and can be used to optimize sensor configurations. In particular, IDC gap width is generally proportional to the field depth and corresponding measurement region for the IDC sensor. This can be exploited to characterize insulation damage as a function of depth from the measurement surface or through a polymer jacket.
- Measured data is consistent with previous measurements on thermally aged EPR-jacketed cable.
- Over the full aging period from pristine samples to those at maximum aging, the correlation between EAB and electrical parameters of dissipation factor and permittivity is weak. This is largely because of the inconsistent trending behavior both metrics early in the aging period.
- Material permittivity and corresponding IDC measurements of capacitance and dissipation factor do correlate with age-related material degradation on the EPR insulation samples and CPE jacket samples examined. These measurements could be developed as a viable field test for local cable condition assessments as an alternate or complementary local measurement such as visual inspection, IM or FTIR/FTNIR.
- The IDC measurement can in principle assess the condition of underlying insulation through an outer jacket material. This ability to assess material condition through the jacket is not possible with other local measurement techniques such as visual inspection, IM or FTIR/FTNIR.



## 10. REFERENCES

- Arvia EM, RT Sheldon, and N Bowler. 2014. "A Capacitive Test Method for Cable Insulation Degradation Assessment." Presented at 2014 IEEE Conference on Electrical Insulation and Dielectric Phenomena (CEIDP 2014), Des Moines, Iowa, 514-17 pp, October 19-22, 2014. IEEE, New York, 10.1109/CEIDP.2014.6995857.
- Bowler N, and S Liu. 2015. "Aging Mechanisms and Monitoring of Cable Polymers." *International Journal of Prognostics and Health Management* 6. doi: [https://www.phmsociety.org/sites/phmsociety.org/files/phm\\_submission/2015/ijphm\\_15\\_029.pdf](https://www.phmsociety.org/sites/phmsociety.org/files/phm_submission/2015/ijphm_15_029.pdf).
- Bowler N, RT Sheldon, and EM Arvia. 2015. "A New Test Method for Cable Insulation Degradation Assessment: Capacitive Sensing." Presented at ANS Topical Meeting on Nuclear Plant Instrumentation, Control and Human-Machine Interface Technologies (NPIC-HMIT) 2015, Charlotte, North Carolina, February 23-26, 2015. American Nuclear Society, La Grange Park, Illinois,
- Chen T, and N Bowler. 2009. "Analysis of Concentric Coplanar Capacitor for Quantitative Dielectrometry." In *Studies in Applied Electromagnetics and Mechanics, Volume 33: Electromagnetic Nondestructive Evaluation (Xiii)*, eds. JS Knopp, et al., 10.3233/978-1-60750-554-9-61, pp. 61-68. IOS Press, The Netherlands.
- Chen T, and N Bowler. 2010. "Analysis of a Concentric Coplanar Capacitive Sensor for Nondestructive Evaluation of Multi-Layered Dielectric Structures." *IEEE Transactions on Dielectrics and Electrical Insulation* 17(4):1307-18. doi: 10.1109/TDEI.2010.5539703.
- Chen T, and N Bowler. 2012a. "Analysis of a Capacitive Sensor for the Evaluation of Circular Cylinders with a Conductive Core." *Measurement Science and Technology* 23(4):045102. doi: 10.1088/0957-0233/23/4/045102.
- Chen T, and N Bowler. 2012b. "A Rotationally-Invariant Capacitive Probe for Materials Evaluation." *Materials Evaluation* 70:161-72. doi:
- Chen T, and N Bowler. 2013. "Design of Interdigital and Concentric Capacitive Sensors for Materials Evaluation." Presented at Proceedings of the 39th Annual Review of Progress in Quantitative Nondestructive Evaluation, Denver, Colorado, 1593-600 pp, July 15-20, 2012. American Institute of Physics, Melville, New York,
- Chen T, N Bowler, and JR Bowler. 2012. "Analysis of Arc-Electrode Capacitive Sensors for Characterization of Dielectric Cylindrical Rods." *IEEE Transactions on Instrumentation and Measurement* 61(1):233-40. doi: 10.1109/TIM.2011.2157573.
- Chen T, JM Song, JR Bowler, and N Bowler. 2011. "Analysis of a Concentric Coplanar Capacitive Sensor Using a Spectral Domain Approach." Presented at Annual Review of Progress in Quantitative Nondestructive Evaluation, Vol. 30B, San Diego, California, 1647-54 pp, July 18-23, 2010. American Institute of Physics, Melville, New York,
- EPRI. 1994. *Low-Voltage Environmentally-Qualified Cable License Renewal Industry Report; Revision 1*. Report No. TR-103841, Electric Power Research Institute (EPRI), Palo Alto, California.
- EPRI. 2005. *Initial Acceptance Criteria Concepts and Data for Assessing Longevity of Low-Voltage Cable Insulations and Jackets*. Report No. TR-1008211, Electric Power Research Institute (EPRI), Palo Alto, California.
- EPRI. 2011. *Plant Engineering: Electrical Cable Test Applicability Matrix for Nuclear Power Plants* Report No. Final Report 1022969, Electric Power Research Institute, Palo Alto, California.
- EPRI. 2015. *Plant Engineering: Evaluation and Insights from Nuclear Power Plant Tan Delta Testing and Data Analysis - Update*. Report No. TR-3002005321, Electric Power Research Institute, Palo Alto, California.
- Fifield LS, Y Shin, and KL Simmons. 2017. "Non-Destructive Evaluation of Polyolefin Thermal Aging Using Infrared Spectroscopy." Presented at Proceedings of SPIE 10169, Nondestructive Characterization and Monitoring of Advanced Materials, Aerospace, and Civil Infrastructure

- 2017, Portland, Oregon, 101690U pp, March 25-29, 2017. SPIE, Bellingham, Washington, 10.1117/12.2261983.
- Fifield LS, MP Westman, A Zwoster, and B Schwenzer. 2015. *Assessment of Cable Aging Equipment, Status of Acquired Materials, and Experimental Matrix at the Pacific Northwest National Laboratory*. Report No. PNNL-24198, Pacific Northwest National Laboratory, Richland, Washington.
- Glass SW AJ, LS Fifield, MR Larche, N Bowler, A Sriraman, WC Palmer 2017. *Interdigital Capacitance Local Non-Destructive Examination of Nuclear Power Plant Cable for Aging Management Programs – Interim Report*. Report No. PNNL-26807, Pacific Northwest National Laboratory, Richland, Washington.
- Glass SW, LS Fifield, G Dib, JR Tedeschi, AM Jones, and TS Hartman. 2015. *State of the Art Assessment of Nde Techniques for Aging Cable Management in Nuclear Power Plants Fy2015*. Report No. M2LW-15OR0404024, PNNL-24649, Pacific Northwest National Laboratory, Richland, Washington.
- Glass SW, LS Fifield, and TS Hartman. 2016. *Evaluation of Localized Cable Test Methods for Nuclear Power Plant Cable Aging Management Programs*. Report No. M3LW-16OR0404022, PNNL-25432, Pacific Northwest National Laboratory, Richland, Washington.
- Glass SW, AM Jones, LS Fifield, TS Hartman, and N Bowler. 2017. *Physics-Based Modeling of Cable Insulation Conditions for Frequency Domain Reflectometry (Fdr)*. Report No. PNNL-26493, Pacific Northwest National Laboratory, Richland, Washington.
- Huang Y, Z Zhan, and N Bowler. 2017. "Optimization of the Coplanar Interdigital Capacitive Sensor." *AIP Conference Proceedings* 1806(1):110017. doi: 10.1063/1.4974695.
- IAEA. 2012. *Assessing and Managing Cable Aging in Nuclear Power Plants*. Iaea Nuclear Energy Series <http://www-pub.iaea.org/books/IAEABooks/8753/Assessing-and-Managing-Cable-Ageing-in-Nuclear-Power-Plants>. International Atomic Energy Agency, Vienna.
- Imperatore MV. 2017. "Dielectric Spectroscopy as a Condition Monitoring Diagnostic Technique for Thermally Aged Pvc/Epr Nuclear Power Plant Cables." University of Bologna, Italy, Electrical Engineering. Masters
- Landau LD, and EM Lifshitz. 1960. *Mechanics, Third Edition, Volume 1 of Course of Theoretical Physics*. Butterworth Heinemann, Oxford.
- Li XB, SD Larson, AS Zyuzin, and AV Mamishev. 2006. "Design Principles for Multichannel Fringing Electric Field Sensors." *IEEE Sensors Journal* 6(2):434-40. doi: 10.1109/JSEN.2006.870161.
- Lindsay P, and S Benson. 2012. *Ageing Management of Cable in Nuclear Generating Stations*. Report No. RSP-0284, 13395-REP-00001 Rev. 0, RCM Technologies, Canadian Nuclear Safety Commission, Canada.
- Liu Yonghong HY, Tang Rui, Wang Beibe. 2015. Application of Interdigital Capacitive Sensors for Detecting Power Cable Insulation Damage. In *Proceedings of International Conference on Mechatronics and Automation*, IEEE, 10.1109/ICMA.2015.7237758
- Mantey A. 2015. "Evaluation and Insights from Nuclear Power Plant Tan Delta Testing and Data Analysis-Update." IEEE, Tuscon, Arizona.
- Matiss I. 2014. "Multi-Element Capacitive Sensor for Non-Destructive Measurement of the Dielectric Permittivity and Thickness of Dielectric Plates and Shells." *NDT & E International* 66:99-105. doi: 10.1016/j.ndteint.2014.05.003.
- Menczel JD, and RB Prime, eds. 2009. *Thermal Analysis of Polymers: Fundamentals and Applications*. Wiley, Hoboken, New Jersey.
- Nassr AA, WH Ahmed, and WW El-Dakhakhni. 2008. "Coplanar Capacitance Sensors for Detecting Water Intrusion in Composite Structures." *Measurement Science and Technology* 19(7):075702. doi: 10.1088/0957-0233/19/7/075702.
- Nassr AA, and WW El-Dakhakhni. 2009. "Non-Destructive Evaluation of Laminated Composite Plates Using Dielectrometry Sensors." *Smart Materials and Structures* 18(5):055014. doi: 10.1088/0964-1726/18/5/055014.

- NRC. 2010. *Condition Monitoring Program for Electric Cables Used in Nuclear Power Plants*. Report No. Draft Regulatory Guide DG-1240, U.S. Nuclear Regulatory Commission, Washington, D.C. <http://pbadupws.nrc.gov/docs/ML1007/ML100760364.pdf>.
- NRC. 2012. *Condition-Monitoring Techniques for Electric Cables Used in Nuclear Power Plants*. Report No. Regulatory Guide 1.218, U.S. Nuclear Regulatory Commission, Washington, D.C. <http://pbadupws.nrc.gov/docs/ML1035/ML103510447.pdf>.
- NRC. 2013. *Expanded Materials Degradation Assessment (Emda), Volume 5: Aging of Cables and Cable Systems*. Report No. NUREG/CR-7153, Vol. 5; ORNL/TM-2013/532, U.S. Nuclear Regulatory Commission, Washington, D.C.
- Olmi R, M Bini, A Ignesti, S Priori, C Riminesi, and A Felici. 2006. "Diagnostics and Monitoring of Frescoes Using Evanescent-Field Dielectrometry." *Measurement Science and Technology* 17(8):2281. doi: 10.1088/0957-0233/17/8/032.
- Orrit-Prat J, R Mujal-Rosas, A Rahhali, M Marin-Genesca, X Colom-Fajula, and J Belana-Punseti. 2011. "Dielectric and Mechanical Characterization of Pvc Composites with Ground Tire Rubber." *Journal of Composite Materials* 45(11):1233-43. doi: 10.1177/0021998310380289.
- Ramuhalli P, LS Fifield, MS Prowant, G Dib, JR Tedeschi, JD Suter, AM Jones, MS Good, SW Glass, and AF Pardini. 2015. *Assessment of Additional Key Indicators of Aging Cables in Nuclear Power Plants -- Interim Status for Fy2015*. Report No. PNNL-24309, Pacific Northwest National Laboratory, Richland, Washington.
- Shao ZH, and N Bowler. 2017. "Capacitive Nondestructive Evaluation of Aged Cross-Linked Polyethylene (XLpe) Cable Insulation Material." Presented at 18th International Conference on Environmental Degradation of Materials in Nuclear Power Systems – Water Reactors, Portland, Oregon, 87-97 pp, August 13-17, 2017. The Minerals, Metals & Materials Society, [https://link.springer.com/chapter/10.1007/978-3-319-68454-3\\_8](https://link.springer.com/chapter/10.1007/978-3-319-68454-3_8)
- Shay IC, and M Zahn. 2005. "Cylindrical Geometry Electroquasistatic Dielectrometry Sensors." *IEEE Transactions on Dielectrics and Electrical Insulation* 12(1):41-49. doi: 10.1109/TDEI.2005.1394014.
- Sheldon RT, and N Bowler. 2013. "An Interdigital Capacitive Sensor for Quantitative Characterization of Wire Insulation." Presented at Review of Progress in Quantitative Nondestructive Evaluation, Vol. 32, Denver, Colorado, 1578-85 pp, July 15-20, 2012. American Institute of Physics, Melville, New York,
- Sheldon RT, and N Bowler. 2014a. "Dielectrometry Sensors for Nondestructive Testing of Glass-Fiber Polymer-Matrix Composites." *Materials Evaluation* 72(11):1421-27. doi:
- Sheldon RT, and N Bowler. 2014b. "An Interdigital Capacitive Sensor for Nondestructive Evaluation of Wire Insulation." *IEEE Sensors Journal* 14(4):961-70. doi: 10.1109/JSEN.2014.2301293.
- Shull PJ, AV Clark, PR Heyliger, JC Moulder, and BA Auld. 1990. "Characterization of Capacitive Array for Nde Applications." *Research in Nondestructive Evaluation* 2(1):11-27. doi: 10.1007/bf01606376.
- Simmons K, P Ramuhalli, D Brenchley, and J Coble. 2012. *Light Water Reactor Sustainability (Lwrs) Program – Non-Destructive Evaluation (Nde) R&D Roadmap for Determining Remaining Useful Life of Aging Cables in Nuclear Power Plants*. Report No. PNNL-21731, Pacific Northwest National Laboratory, Richland, Washington.
- Simmons KL, LS Fifield, MP Westman, JR Tedeschi, AM Jones, MS Prowant, AF Pardini, and P Ramuhalli. 2014. *Determining Remaining Useful Life of Aging Cables in Nuclear Power Plants -- Interim Status for Fy2014*. Report No. PNNL-23624; INL-EXT-14-32505 Rev. 0, Pacific Northwest National Laboratory, Richland, Washington.
- Sun W, R Ding, and N Bowler. 2016. "A Capacitive Sensor for Nuclear Power Plant Cable Monitoring." *Materials Evaluation* 74(10):1467-71. doi:
- The Okonite Company. N.D. *Okoguard/Aerial Jumper Cable*. Accessed on September 7, 2017 at [http://okonite.com/Product\\_Catalog/section6/sheet4.html](http://okonite.com/Product_Catalog/section6/sheet4.html) (last updated
- Verardi L. 2013. "Aging of Nuclear Power Plant Cables: In Search of Nondestructive Diagnostic Quantities." University of Bologna, Italy.